AD-A033 113 TEXAS UNIV AT AUSTIN APPLIED RESEARCH LABS F/G 17/1
THE CORRELATION BEAMFORMER -- A METHOD OF BEAM CONTROL WITHOUT --ETC(U)
OCT 76 D A SMITH N61339-74-C-0031
UNCLASSIFIED ARL-TR-76-2-REV NL

1 OF 3
AD A033113

12
8.5

APPLIED RESEARCH LABORATORIES
THE UNIVERSITY OF TEXAS AT AUSTIN

ARL-TR-76-2 (Rev.)
October 1976

Copy No. 66

THE CORRELATION BEAMFORMER – A METHOD OF BEAM CONTROL WITHOUT THE USE OF TIME DELAY OR PHASE SHIFT NETWORKS

Final Report under Contract N61339-74-C-0031, Task 0003
29 November 1973 - 31 December 1975
Revised October 1976 under Contract N61339-76-D-0014, HR03

David A. Smith

Prepared for NAVAL COASTAL SYSTEMS LABORATORY

UNCLASSIFIED

SECURITY CLASSIFICATION OF THIS PAGE (When Data Entered)

REPORT DOCUMENTATION PAGE

READ INSTRUCTIONS BEFORE COMPLETING FORM

1. REPORT NUMBER: ARL-TR-76-2 (Rev Revised)
2. GOVT ACCESSION NO.
3. RECIPIENT'S CATALOG NUMBER

4. TITLE (and Subtitle): THE CORRELATION BEAMFORMER -- A METHOD OF BEAM CONTROL WITHOUT THE USE OF TIME DELAY OR PHASE SHIFT NETWORKS.

5. TYPE OF REPORT & PERIOD COVERED: final technical rept. 29 NOV 73 — 31 DEC 75

6. PERFORMING ORG. REPORT NUMBER

7. AUTHOR(s): David A. Smith

8. CONTRACT OR GRANT NUMBER(s): N61339-74-C-0031, N61339-76-C-0014

9. PERFORMING ORGANIZATION NAME AND ADDRESS: Applied Research Laboratories, The University of Texas at Austin, Austin, Texas 78712

10. PROGRAM ELEMENT, PROJECT, TASK AREA & WORK UNIT NUMBERS: Task 0003

11. CONTROLLING OFFICE NAME AND ADDRESS: Naval Coastal Systems Laboratory, Department of the Navy, Panama City, Florida 32401

12. REPORT DATE: October 1976

13. NUMBER OF PAGES: 197

14. MONITORING AGENCY NAME & ADDRESS (if different from Controlling Office): 197p.

15. SECURITY CLASS. (of this report): UNCLASSIFIED

15a. DECLASSIFICATION/DOWNGRADING SCHEDULE

16. DISTRIBUTION STATEMENT (of this Report)

APPROVED FOR PUBLIC RELEASE; DISTRIBUTION UNLIMITED.

17. DISTRIBUTION STATEMENT (of the abstract entered in Block 20, if different from Report)

18. SUPPLEMENTARY NOTES

19. KEY WORDS (Continue on reverse side if necessary and identify by block number)

Spatial Processing
Beamforming
Cylindrical Arrays
Shading Coefficients
Pulse Compression
Correlation Beamformer
Beam Control

20. ABSTRACT (Continue on reverse side if necessary and identify by block number)

The classic beamforming algorithm involves the process of "phasing-to-a-plane." This report presents a method of beamforming which does not require the phasing-to-a-plane step, and therefore can be implemented without the use of time delay or phase shift networks. (U)

The study was restricted to cylindrical or circular arrays of equally spaced sensor elements, although the method appears to be equally applicable for other geometries. Since no general closed form solution for the required shading

over

DD FORM 1 JAN 73 1473 EDITION OF 1 NOV 65 IS OBSOLETE

UNCLASSIFIED 404 434

SECURITY CLASSIFICATION OF THIS PAGE (When Data Entered)

LB

20. cont'd

coefficients is available, a set of shading coefficient selection algorithms are developed and presented along with the resulting beam pattern performance. Studies of the bandwidth, elevation beam patterns, and the effects of construction errors, as well as methods of implementing the beamformer, are reported. (U)

The results of the study and the experimental program indicate that substantially equal performance can be achieved with a physically smaller array. In addition, the correlation method is easier to implement. As an example, the Two Degree Array (TDA) was compared to the Cylindrical Transducer (CT) for an experimental sonar. The TDA was only 65% the size of the CT. The TDA contained the same number of elements spaced in the azimuthal direction, although it contained 1/9 as many elements in the elevation direction: the TDA and CT operated at the same frequency and demonstrated essentially equal performance in both the azimuthal and elevation planes. Additional examples of size and cost advantage are given in Appendix C. (U)

The chapter on array rise time and the use of coded pulse transmission to accomplish pulse compression on the array is equally applicable to phase shift beamformers. (U)

The assorted effects of changing the sector of active elements on the cylinder are presented in Appendix A. Appendix B reports the result of comparing the algorithmic approach to an equivalent design by using linear programming as an optimization technique. (U)

Appendix C is a design analysis of the reduction in size and cost savings to be expected by using the correlation beamformer method as applied to three existing sonar systems. Appendix D is a reproduction of a signal-to-noise ratio study comparing the correlation beamformer with a phase shift beamformer. (U)

ARL-TR-76-2 (Rev.)
October 1976

THE CORRELATION BEAMFORMER – A METHOD OF BEAM CONTROL WITHOUT THE USE OF TIME DELAY OR PHASE SHIFT NETWORKS

Final Report under Contract N61339-74-C-0031, Task 0003
29 November 1973 - 31 December 1975

Revised October 1976 under Contract N61339-76-C-0014, HRO 3

David A. Smith

Prepared for NAVAL COASTAL SYSTEMS LABORATORY

APPLIED RESEARCH LABORATORIES
THE UNIVERSITY OF TEXAS AT AUSTIN
AUSTIN, TEXAS 78712

ABSTRACT

The classic beamforming algorithm involves the process of "phasing-to-a-plane." This report presents a method of beamforming which does not require the phasing-to-a-plane step, and therefore can be implemented without the use of time delay or phase shift networks.

The study was restricted to cylindrical or circular arrays of equally spaced sensor elements, although the method appears to be equally applicable for other geometries. Since no general closed form solution for the required shading coefficients is available, a set of shading coefficient selection algorithms are developed and presented along with the resulting beam pattern performance. Studies of the bandwidth, elevation beam patterns, and the effects of construction errors, as well as methods of implementing the beamformer, are reported.

The results of the study and the experimental program indicate that substantially equal performance can be achieved with a physically smaller array. In addition, the correlation method is easier to implement. As an example, the Two Degree Array (TDA) was compared to the Cylindrical Transducer (CT) for an experimental sonar. The TDA was only 65% the size of the CT. The TDA contained the same number of elements spaced in the azimuthal direction, although it contained 1/9 as many elements in the elevation direction: the TDA and CT operated at the same frequency and demonstrated essentially equal performance in both the azimuthal and elevation planes. Additional examples of size and cost advantage are given in Appendix C.

The chapter on array rise time and the use of coded pulse transmission to accomplish pulse compression on the array is equally applicable to phase shift beamformers.

The assorted effects of changing the sector of active elements on the cylinder are presented in Appendix A. Appendix B reports the results of comparing the algorithmic approach to an equivalent design by using linear programming as an optimization technique.

Appendix C is a design analysis of the reduction in size and cost savings to be expected by using the correlation beamformer method as applied to three existing sonar systems. Appendix D is a reproduction of a signal-to-noise ratio study comparing the correlation beamformer with a phase shift beamformer.

TABLE OF CONTENTS

LIST OF FIGURES

LIST OF FIGURES (cont'd)

LIST OF FIGURES (cont'd)

LIST OF SYMBOLS

General - 1) Lower case letters usually stand for dimensioned variables—upper case letters are usually normalized lower case variables where the normalization is to the design wavelength.
example: r = array radius in some unit,
and $R = \frac{r}{\lambda}$ dimensionless radius.

2) The master coordinate system is cylindrical and centered at the center of the cylindrical array. The azimuthal angle is $\emptyset$ or φ interchangeably, the elevation angle is θ, and the range is ρ (see Figs. 3-1 and 4-1).

A - the shading coefficients; a real number or function

A_1, A_2, A_3, A_4 - the several parts or factors of A; introduced p. 7.

Area - resolution area - area = $\Delta x * \Delta y$.

BW - the major lobe beamwidth, usually given in radians measured at the half-power points.

$B(\xi,\eta)$ - a single element beam-pattern descriptor, in element centered coordinates.

$B(\varphi,\theta)$ - a single element beam pattern descriptor, in array centered coordinates.

C - speed of sound in water

CW - a signal description meaning that the carrier signal is constant in frequency over the time slot of interest; that is, it does not exclude pulsed operations.

DMRA - design major response axis

DSLL - design side lobe level; used in Chapter IV in connection with the application of Taylor shading functions (Ref. 2).

$D(\varphi)$ - a computed directivity function.

E* - the complex beamformer output voltage.

$e_n^*(\varphi,\theta,t)$ - the complex voltage from the nth element when insonified with a specified source in the far-field from direction φ and θ and at time t.

FFT - fast Fourier transform; a computer algorithm for performing Fourier transforms.

f - operating frequency

f_c - design center frequency.

G,g - normalized and unnormalized distance from a particular element to the field point.

K - the aperture constant: the product of the subtended aperture in wavelengths and the resulting half power beamwidth in degrees; the units of K are wavelength-degrees, first used p. 24.

k - (Chapter IV.C.) an arbitrary parameter $0 \leq k \leq 1$.

$k = \frac{2\pi}{\lambda}$ - the classic wave number

L - depth of aperture in direction of signal propagation; depth of aperture in the x direction of Fig. 3-1.

LD - largest dimension; used first in Appendix A.

M - total number of elements contributing to a single beam.

MRA - achieved major response axis.

N - the maximum value of the element counting index n; element zero is on the DMRA

$\overline{N}$ - used in Chapter IV in connection with the application of Taylor shading functions (Ref. 2)

PL - pulse length

P - (Chapter IV.C.) the normalized distance along the W line measured from the MRA to the point in question; a variable relating the normalized distance along the W line.

P(g) - the pressure field due to some infinitesimal test projector; $P(g) = \frac{P_o}{g} e^{ikg}$.

P_o - the source pressure of some infinitesimal test projector measured at some appropriate range.

q - number of elements in some distance, used in element density determination, i.e., $\frac{q}{d\alpha}$ = number of elements per unit angle as seen from the array center.

S - the element spacing in wavelength along the arc of the array.

S - (Appendix A) sector of azimuth plane covered with preformed beams.

SENS - the array sensitivity, usually stated in number of effective in-phase elements or contributors.

SLL - side lobe level; usually reported in decibels below the level of the major lobe peak.

$\overline{SLL}$ - average side lobe level; an RMS average of the linear pressure over some angular range.

SLL_p - the peak or largest of the various side lobe peaks; usually given in decibels below the peak value of the major lobe.

$S(\tau)$ - (Chapter V) a signal description.

$s(t)$ - (Appendix B) a signal description.

TDA - Two Degree Array - an experimental array designed to exhibit a 2° beamwidth when operated at 100 kHz with a full sector of elements.

W - the subtended width of the array as seen from a point in the farfield on the DMRA (normalized to the design wavelength); alternately used to designate the line proper, i.e., "the W line".

α_n - the angle in radians that element n makes with the DMRA or element zero measured at the circular array center.

α_N - one-half the total sector of included elements in any one beam; the angle that the end element makes with the DMRA measured at the array center.

δ_n - an amplitude error factor; a random sample from some stated distribution.

Δf - bandwidth.

Δ_n - a phase error; a random sample from some stated distribution.

Δx - range resolution.

Δy - crossrange resolution.

ϵ - excess signal length over that required to cover the array.

λ - wavelength of sound in water.

ρ - distance from array center to field point (some units).

$\tilde{\rho}$ - distance from array center to field point in wavelengths, $\tilde{\rho} = \frac{\rho}{\lambda}$.

φ_o, θ_o, t_o, etc. - design values of the variables.

Ψ - the phase term contained in A_1; the exact phase of the signal on the array at the selected time of maximum response; introduced p. 11.

ω - the angular frequency of a signal in radians per second.

I. INTRODUCTION

In January 1973, a method for forming beams using elements or staves on a cylindrical array without the use of time delays or phase shift networks was discovered. Relatively large arrays were under consideration, that is, cylinders whose radii in wavelengths were greater than about 10. A quick survey of the literature revealed no additional information on the method, and further computer simulation uncovered no apparent problems or serious disadvantages that might result from using the processing scheme.

The Naval Coastal Systems Laboratory was asked to support ARL during a two year study of the beamforming method. This report is the major result of that study.

During the first year, a computer model, which was used throughout the remainder of the study, was developed, and two experiments were performed to validate the model. A partial understanding of the role of the coefficients and their effect upon the beam pattern performance was gained, and the problem of rise time was delineated. In addition, the realization that a beam could be scanned at high speed began to take shape.

During the second year, a study of high speed scanning and its implementation was begun, and other methods of implementing preformed beams were studied. The pulse compression problem was studied and a pulse code was developed which achieves pulse compression. Larger arrays were studied for possible systems applications and for preliminary design of hardware to be used in testing the pulse compression codes. A more complete understanding of the role of the coefficients was obtained.

The purpose of this report is two-fold: (1) to document the essence of the correlation beamforming method and to summarize what was learned during the course of the study, and (2) to serve as a design guide for those who would use the method.

Chapters III and IV of this report describe the fundamental concepts of the correlation beamformer method, and describe "rules-of-thumb" that can be used to design or configure a correlation array. One important appendix is C, which discusses the cost and size advantage to be obtained by the use of the method.

II. BACKGROUND

Beam formation is a well-known process by which the directionality of response of an array of acoustic transducers is controlled. In the general case, the individual transducer elements in an array may be arranged with any spatial distribution, and may have their individual response maxima oriented in any direction.

Beam formation can be accomplished in principle in the general case; however, only in the simplest cases can a closed-form solution for the shading coefficients be obtained. If, for example, the elements are equally spaced along a line and either have no response maxima (omnidirectional), or are all pointed in the same direction, then one can solve for the shading coefficients so that the beam pattern will have specific properties. The literature on beam control is extensive in this case.

Another relatively simple case consists of a set of omnidirectional elements equally spaced on a circle; there is no baffle so that all elements can be seen from all directions. Some literature for this case, which contains solutions for the shading coefficients, is available, such as Ref. 1.

For arrays more complex than the simple ones as, for example, a cylindrical baffle containing finite sized elements pointing in a radial direction, no closed-form solutions for the shading coefficients have been obtained. In such a case, the classical method of "phasing to a plane" is used.

Conventional beamforming or spatial processing is accomplished through a linear weighted combination of the outputs of the elements. That is,

the beamformer output is

$$E^*(\varphi,t) = \sum_{n=-N}^{N} A_n^* \, e_n^*(\varphi,t) \quad , \tag{2-1}$$

where $e_n^*(\varphi,t)$ is the complex voltage developed by the nth element when insonified by the signal $S(t)$ arriving from the angle φ and at time t, and A_n^* is the complex weighting coefficient which accomplishes beam formation (both phasing and shading).

The problem is to select the A_n^* in such a way that the envelope of $E^*(\varphi,t)$ has one maximum value at angle φ_o and t_o, and has controlled low levels at other angles $\varphi \neq \varphi_o$, and other times $t \neq t_o$.

The classic algorithm involves the selection of $A_n^* = A_n \exp(i\beta_n)$ in two parts. First, β_n is selected to "phase-the-element-to-a-plane" or delay its output by some angle β_n, so that the collection of M elements appear to lie in a line or on a plane. For a time delay beamformer, β_n may involve several revolutions. For a phase shift beamformer, β_n is restricted to $\pm\pi$.

The second part of the classic algorithm is the selection of the magnitude of the shading coefficients, the A_n. This operation proceeds according to methods contained in the extensive literature concerning line array shading coefficients (for example, see Refs. 2 through 6), and then computer tests are run to obtain the final result.

In both time delay and phase shift beamforming, the angle β_n is important, and during implementation requires the use of phase shifters or delay lines. In sonar arrays of high resolution covering a wide sector, such devices preclude scanning a single beam because of the restricted data rate, and can become a major expense item when many preformed beams are implemented in order to meet the data rate requirements.

During late 1972, while performing work on the suppression of grating lobes in the case of widely spaced elements on cylindrical arrays, it was discovered that beams could be formed without the "phasing-to-a-plane" step. If useful beams could be formed and controlled without the phase shifters or delay lines, then arrays of smaller size at less expense could be constructed. Therefore, a proposal to study the "method of beamforming without the use of time delay or phase shift networks" was submitted and accepted. This report is the result of that study.

The cylindrical array was chosen for study because of its azimuthal symmetry; many beams can be formed by applying the same set of shading coefficients to a different set of elements.

The method of "forming beams without the use of time delay or phase shift networks" or "forming beams by the use of real shading coefficients" has finally come to be called a "correlation beamformer," primarily because of the way the coefficients are selected. However, the new method does not simplify the mathematics of beam formation; therefore, as before, no closed-form solution is available.

The solution to the problem of finding shading coefficients for the correlation beamformer on a cylindrical array has been to develop a set of rules or algorithms to determine the coefficients; then a computer implemented mathematical model is exercised to evaluate the predicted results. By this process, the heuristically derived coefficient selection algorithms have been proved, and array scaling rules have been determined.

Chapters III and IV discuss the array performance in relation to the coefficient selection algorithms. The array fill time problem and two proposed solutions are discussed in Chapter V. Chapters VI, VII, and VIII of the report include methods of implementing either scanned or preformed beams, some technological fallout of the study, and experimental verification, respectively. Chapter IX gives the study conclusions and recommendations for further work.

Although this study was aimed at the correlation beamformer for cylindrical arrays, the correlation method is equally applicable to other array geometries (for example, lines and planes or volume arrays). The coefficient selection algorithms are unchanged for other geometries. Also, some of the performance results determined in this study apply equally well to phase shift or time delay beamforming methods.

III. THE DESIGN AND PERFORMANCE OF THE REFERENCE CYLINDRICAL ARRAY--THE SIMPLE CASE

A. The Role of the Shading Coefficients

In this chapter, the study of the design and performance of the correlating beamformer will be restricted to the simplest possible case: point elements, equally spaced one-half wavelength apart on the front half of a cylindrical baffle of radius R wavelengths. The coefficient selection algorithm will be described, and the beam performance and scaling rules developed.

Figure 3-1 shows the assumed geometry. For the present, the test probe will be assumed to be in the farfield and will emit a simple CW signal $\sin(\omega t)$. The baffle will be assumed to be opaque but otherwise does not affect the element's pattern; that is, an element's response is constant and independent of angle if it is in the line of sight of the test probe; the output is zero otherwise.

The beamforming operation will be

$$E^*(\varphi,t) = \sum_{n=-N}^{N} A_n \, e_n^*(\varphi,t) \quad , \tag{3-1}$$

where the * denotes a complex number and e_n^* is the output voltage from the nth element at some time t when the test probe is at angle φ.

The set of real numbers A_n are discrete samples of the continuous function A(n) or $A(\alpha_n)$ which will be developed in parts, each part playing a specific role in the beamforming operation. The separate parts of A(n) are

$$A(n) = A_1(n) * A_2(n) * A_3(n) \tag{3-2}$$

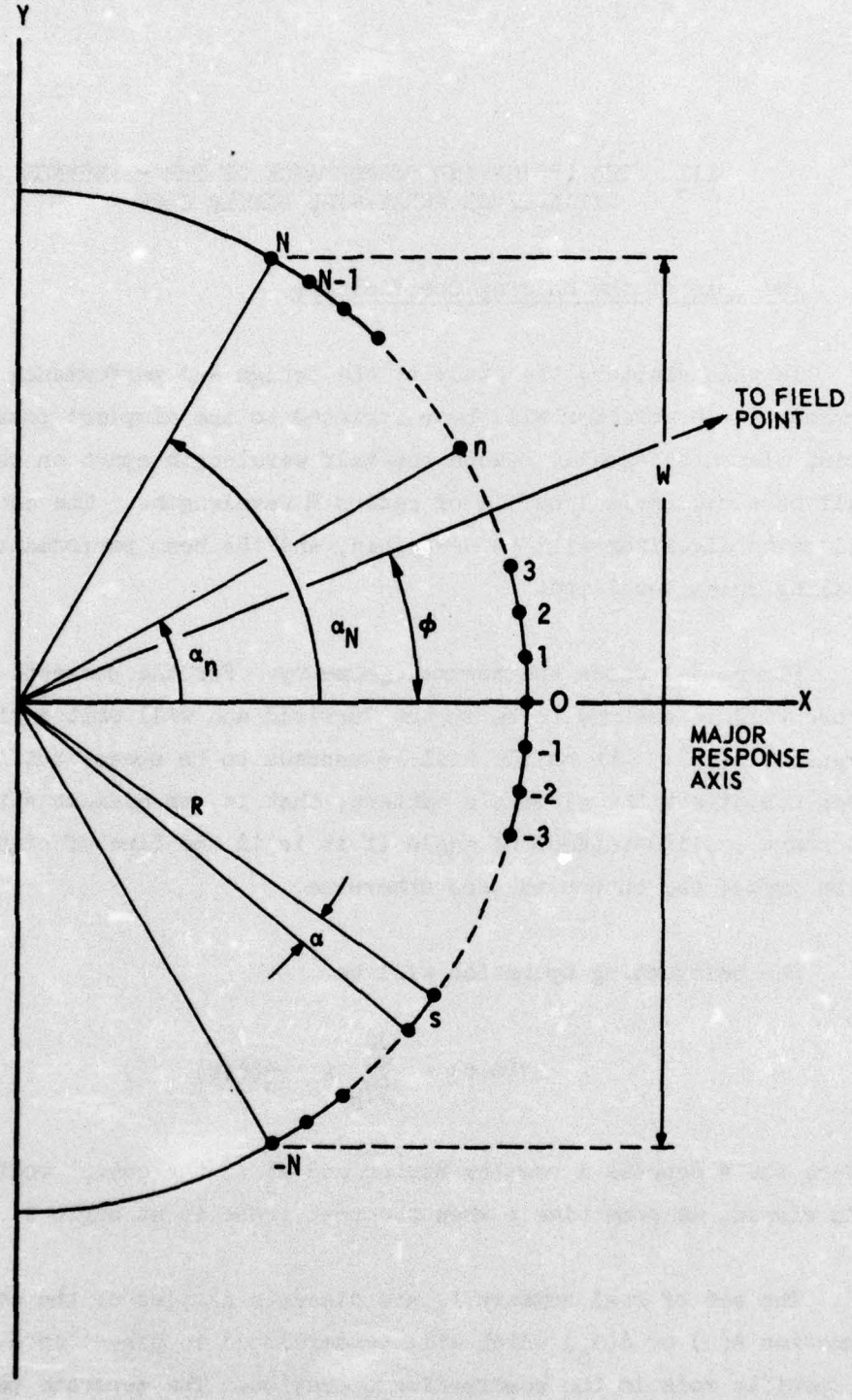

FIGURE 3-1
ASSUMED GEOMETRY

ARL - UT
AS-74-1701
DAS - DR
5 - 23 - 74

where

$A_1(n)$ is the signal replica factor,
$A_2(n)$ is the sensor density corrector, and
$A_3(n)$ is the aperture window function.

1. The Signal Replica Factor

Consider a cylinder whose radius is 15 wavelengths. Further, assume the n=0 element is in the direction of the major response axis (MRA) (the X axis in Fig. 3-1). If the test probe is at φ=0 and the array sensitivity is measured, the result will be one apparent element. As additional elements are added in pairs, n=±1,±2, etc., the array sensitivity will grow until the additional elements lie outside the first Fresnel zone on the cylinder. As elements are added into the second Fresnel zone, the array sensitivity will decrease, making the apparent number of elements on the array decrease. The dotted curve in Fig. 3-2 illustrates this behavior.

If phase shift or time delay beamforming were used, the elements would be moved electrically so that they all would add coherently, and the dashed curve would result. One can see from the dotted curve that the addition of the pair of elements marked 15 will cause the overall sensitivity of the array to decrease because these added elements exist in the second Fresnel zone. If one were to reverse their signs before adding, the solid curve would result. That is, the solid curve is the result of weighting by +1 those elements in the odd numbered zones, and weighting by -1 those elements in the even numbered zones.

The choice of $A_1(n)=\pm 1$ does result in a narrow major lobe with good sensitivity, but with unacceptable side lobe performance. The concept of a replica correlator suggests that the factor $A_1(n)$ be selected to more accurately replicate the signal at an element location.

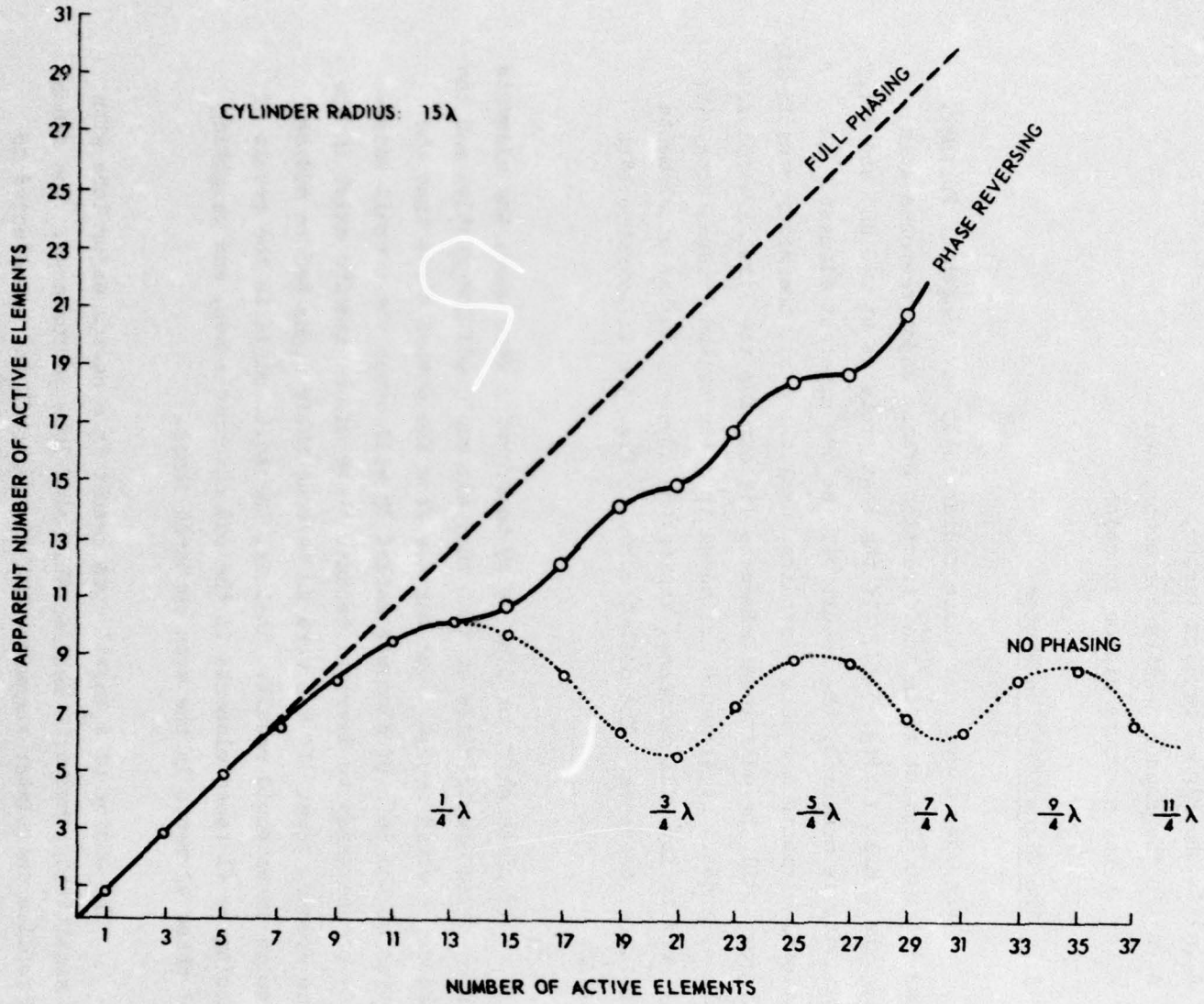

FIGURE 3-2
ARRAY SENSITIVITY VERSUS NUMBER OF ELEMENTS

ARL - UT
AS-73-380
DAS - DR
5 - 9 - 73

Figure 3-3 shows a long CW signal insonifying an array of elements. In order to define a signal replica, we must know the signal type, the proposed direction, and the proposed times at which a peak positive beamformer output is desired. For example, assume a simple sine wave arriving from $\varphi=0$, and require a peak output at the instant when the signal is a cosine wave on the array as shown in Fig. 3-3. The nth element at angle α_n from the MRA or signal matching direction is shown. The nth element is R-R cos α_n wavelengths behind the n=0 element in the direction of signal propagation. So

$$2\pi R(1 - \cos \alpha_n) \tag{3-3}$$

represents the distance in radians beyond the zeroth element. Thus, the impressed instantaneous signal at element n is

$$\cos[2\pi R(1 - \cos \alpha_n)] \tag{3-4}$$

provided

$$|\alpha_n| \leq \pi/2 \quad . \tag{3-5}$$

If the signal replica is modified with a phase term ψ, such that

$$A_1(\alpha_n) = \cos[2\pi R(1 - \cos \alpha_n) - \psi] \quad , \tag{3-6}$$

then it can be made to represent any desired signal phase shift before matching. For the simple case under consideration, however, $\psi=0$, as shown in Fig. 3-3, and the signal replica factor is

$$A_1(\alpha_n) = \cos[2\pi R(1 - \cos \alpha_n)] \quad . \tag{3-7}$$

Chapter IV contains a section devoted to the more general case of arbitrary ψ.

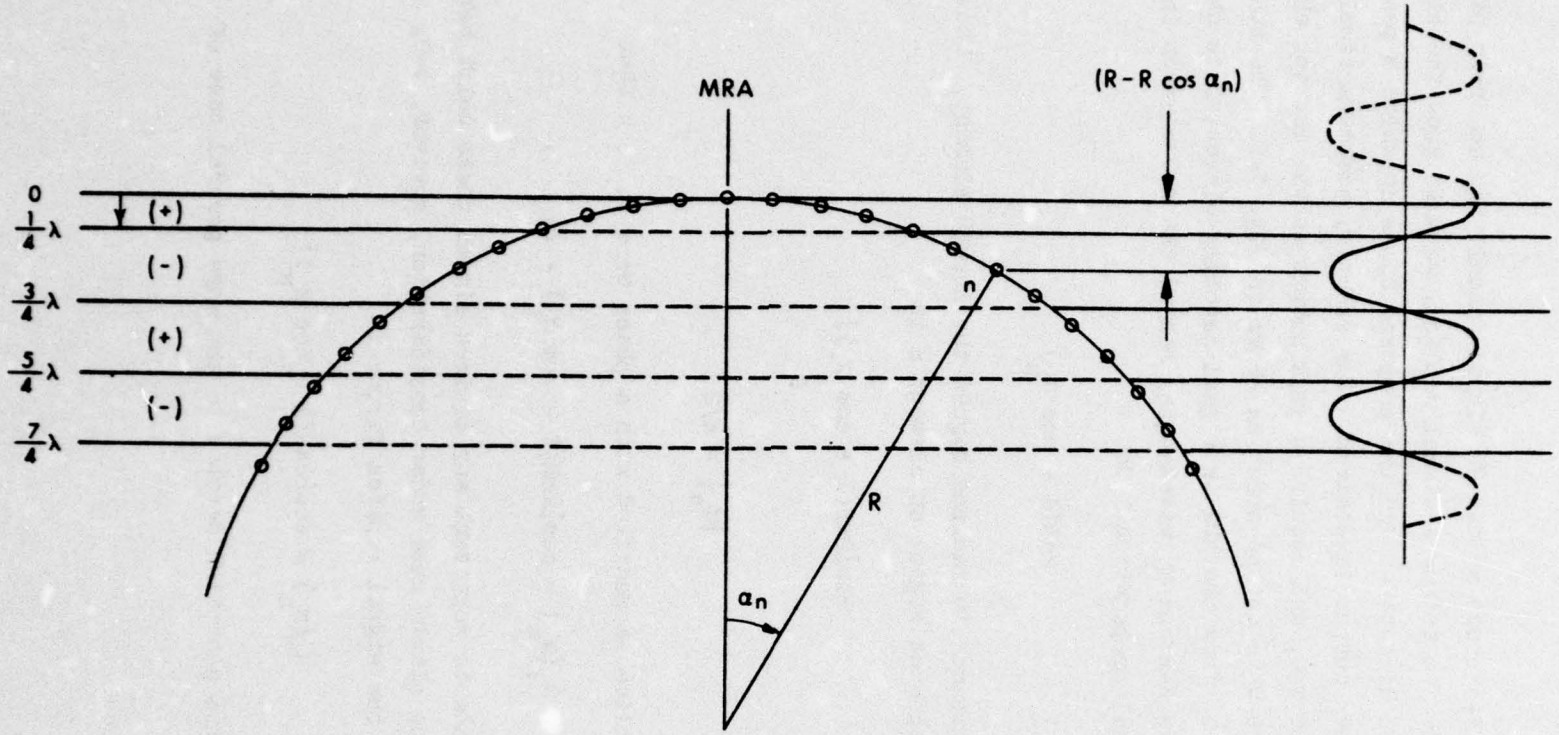

FIGURE 3-3
POSITIONS OF ELEMENTS IN A MONOCHROMATIC PLANE WAVE FIELD

ARL - UT
AS-73-381
DAS - DR
5 - 9 - 73

2. Sensor Density Corrector

If the coefficient factor $A_1(n)$ only is used, and a signal is applied to the array, one would in general find a varying sensitivity over the aperture W shown in Fig. 3-1. Of course, the varying sensitivity over the W aperture, called the aperture window function, is usually used to control side lobe levels in line or plane arrays. This window function must have special characteristics if it is to be useful in controlling side lobe levels. Our approach to this problem is in two parts: (1) a function $A_2(n)$ which will make the $A_1(n) * A_2(n)$ aperture window function look uniform, and (2) a function $A_3(n)$ which independently applies the required shading for side lobe control.

The method of selecting $A_2(n)$, the sensor density corrector, is to first evaluate the apparent sensitivity over the W aperture when $A_1(n)$ only is applied. One of the main contributors to the aperture function is the apparent density of sensors when they are projected to the W line. Other contributors can be the envelope of A_1 or the envelope of the signal. We are not interested in the cyclic nature of A_1 or the carrier of the signal over the aperture, only the average sensitivity per unit length on W; therefore, only the envelopes are used.

As an example, consider some unit width on W near the center of the array. The signal strength there is unity. Also, the envelope of $A_1(\alpha)$ is unity. Further, the projected sensor density is about the same as the density on the cylinder, which is two elements per wavelength. Now, consider the situation near the end of W. Again, the signal and A_1 envelopes are unity, but the projected sensor density near the edge of the array is very large. The aperture window function is therefore larger toward the edges of the aperture, and $A_2(\alpha)$ should be chosen to correct this effect.

In Fig. 3-1, let the distance along the W line be Y, with Y=0 at the center of the W line. An element at α_j on the cylinder is

projected onto the W line at Y_j, where

$$Y_j = R \sin \alpha_j \quad . \tag{3-8}$$

If the element density on the cylinder is

$$\frac{q}{d\alpha} = \frac{\text{number of elements}}{\text{unit angle}} \quad , \tag{3-9}$$

then the projected density on W is

$$\frac{q}{dY} = \frac{q}{d\alpha} \frac{1}{R \cos \alpha} \quad . \tag{3-10}$$

Since $q/Rd\alpha$ is a constant, the functional dependence of element density on the W line is $1/\cos \alpha$. The obvious choice for the density corrector, then, is $A_2(\alpha)=\cos \alpha$, since the aperture function for the product $A_1(\alpha) * A_2(\alpha)$ will be

$$\frac{q}{dY} = \frac{q}{d\alpha} \frac{1}{R \cos \alpha} \cos \alpha = \text{constant} \quad . \tag{3-11}$$

If the signal envelope had varied over the array, then $A_1(\alpha)$ would have varied, and these effects would have been incorporated in the calculation. In fact, in Chapter V, a triangular envelope signal will be used and $A_2(\alpha)$ calculated for that case.

3. The Aperture Window Function

This part of the coefficient selection algorithm is based on the approximation that, for beam pattern properties near the major lobe (beamwidth, first side lobe level, sensitivity), the array aperture function appears to be approximately independent of field angle φ. It is further assumed that, for angles near the MRA, the Fourier transform relationship exists between the array illumination function and the farfield directional response, as it does for a line array.

Now, we have a signal replica A_1 and an A_2 selected so that the window function is uniform. Line array theory would predict a first side lobe level of -13 dB//major lobe level. If we contrive by the factor $A_3(\alpha)$ to make the aperture function on W some function, say F(Y), then by analogy with line arrays, the farfield directivity pattern should be described by the Fourier transform of F(Y).

For example, let $A_3(\alpha)$ be arbitrarily selected as

$$A_3(\alpha) = \cos \alpha \quad . \tag{3-12}$$

The projection of this function on the W line can be found by noting that

$$Y = R \sin \alpha \quad , \tag{3-13}$$

or

$$\alpha = \arcsin \frac{Y}{R} \quad . \tag{3-14}$$

If

$$A_3(\alpha) = \cos \alpha \quad , \tag{3-15}$$

then

$$A(Y) = \cos(\arcsin \frac{Y}{R}) \tag{3-16}$$

or

$$A(Y) = \sqrt{1 - \frac{Y^2}{R^2}} \quad . \tag{3-17}$$

The normalized modulus of the Fourier transform of the A(Y) can be shown to be

$$D(\varphi) = \frac{2 J_1(x)}{x} \quad , \tag{3-18}$$

where $x = 2\pi R \sin \varphi$ and J_1 is a Bessel function of the first kind of order one. (See Ref. 7.)

The $A_3(\alpha)$ algorithm states that the function $D(\varphi)$ above should be descriptive of the beamwidth and first side lobe level if the A_3 conjecture is nearly true. The function $D(\varphi)$ is well known and is the same as the response of a broadside circular piston of radius R wavelengths. The half-power beamwidth of the function is

$$BW = 2 \arcsin \frac{1.616}{2\pi R} \text{ (radians)} \quad , \tag{3-19}$$

and the first side lobe is suppressed 17.8 dB below the level of the major lobe.

A simple development of the Fourier transform relationship for line and plane arrays is given in Ref. 7 and an excellent treatment of Fourier integral methods in beam pattern analysis is given in Ref. 4.

The final shading coefficients $A(\alpha_n)$, represented by the product of its factors as shown in Eq. (3-2) for the simple reference array, are

$$A(\alpha) = \cos^2 \alpha \cos[2\pi R(1 - \cos \alpha)] \quad . \tag{3-20}$$

This continuous function of α is sampled at the locations of each element α_n to arrive at the list of discrete shading values to be used in the beamformer.

Figure 3-4 shows plots of Eq. (3-20) for two small values of R. The figure should help visualize the shape of the shading coefficients and their dependence on the radius parameter R.

B. The Performance of the Array

The reference array is an array of point sensors spaced $\lambda/2$ apart, covering the front half of the surface of a cylindrical, opaque baffle of radius R wavelengths. The test signal is an infinitely long CW signal, $\sin(\omega t)$, emitted from a probe in the very farfield at angle φ. The

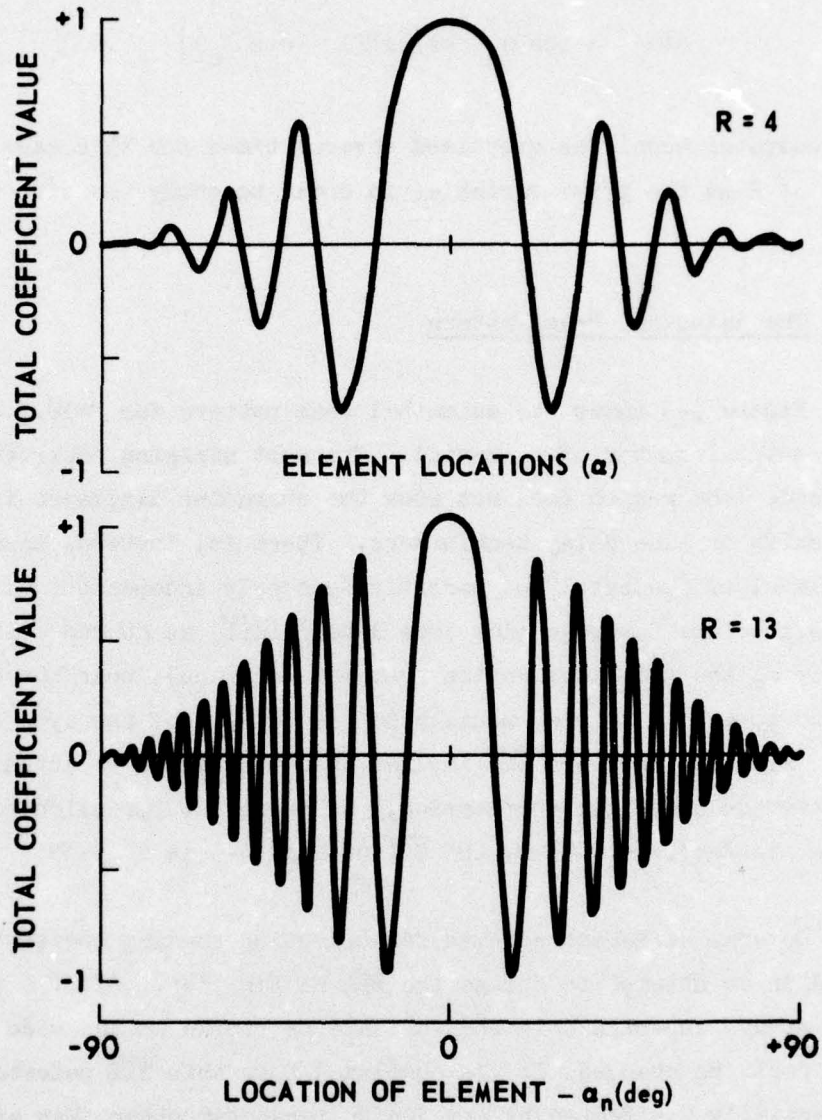

FIGURE 3-4
SHADING VALUE DEPENDENCE ON ELEMENT LOCATION IN ARRAY

ARL - UT
AS-75-376-S
DAS - DR
3-19-75

selected shading coefficients are, as developed in the previous sections,

$$A(\alpha_n) = \cos^2\alpha_n \cos[2\pi R(1 - \cos \alpha_n)] \quad . \qquad (3\text{-}21)$$

The computer model was exercised several times for this case, using the value of R as the prime variable, in order to study the effects of scaling.

1. The Azimuthal Beam Pattern

Figure 3-5 shows the azimuthal beam pattern for R=12.3 and N=38(2N+1=M=total number of elements). The most striking observation is that the side lobe region does not show the character displayed in patterns of phase shift or time delay beamformers. There is, instead, an almost constant level or "pedestal" of sensitivity nearly independent of angle. We have defined the "average side lobe level" ($\overline{SLL}$) as an rms average sensitivity of the side lobe region from the first null near the major lobe out to some final angle, usually 60° in pattern of the type shown in Fig. 3-5. Although the term $\overline{SLL}$ implies absolute level, we actually present "average side lobe suppression," an average suppression below the major lobe, in decibels. Thus, the $\overline{SLL}$ of Fig. 3-5 is 18.9 dB.

Several different schemes for selecting shading coefficients were tried in an attempt to change the $\overline{SLL}$ of Fig. 3-5. After a rather extensive study, in which only the variance or ripple of the side lobe structure could be changed, it was concluded that this $\overline{SLL}$ pedestal appears to be essentially unaffected by any design parameter other than array size R.

This constant side lobe level or pedestal behavior has been noted by Steinberg (Ref. 8) for line arrays of randomly spaced elements. His explanation for line arrays is simply that, on-axis, all elements see the same pressure, and hence the summation in the processor (adder) is a coherent addition. As more elements are added to the array, the on-axis

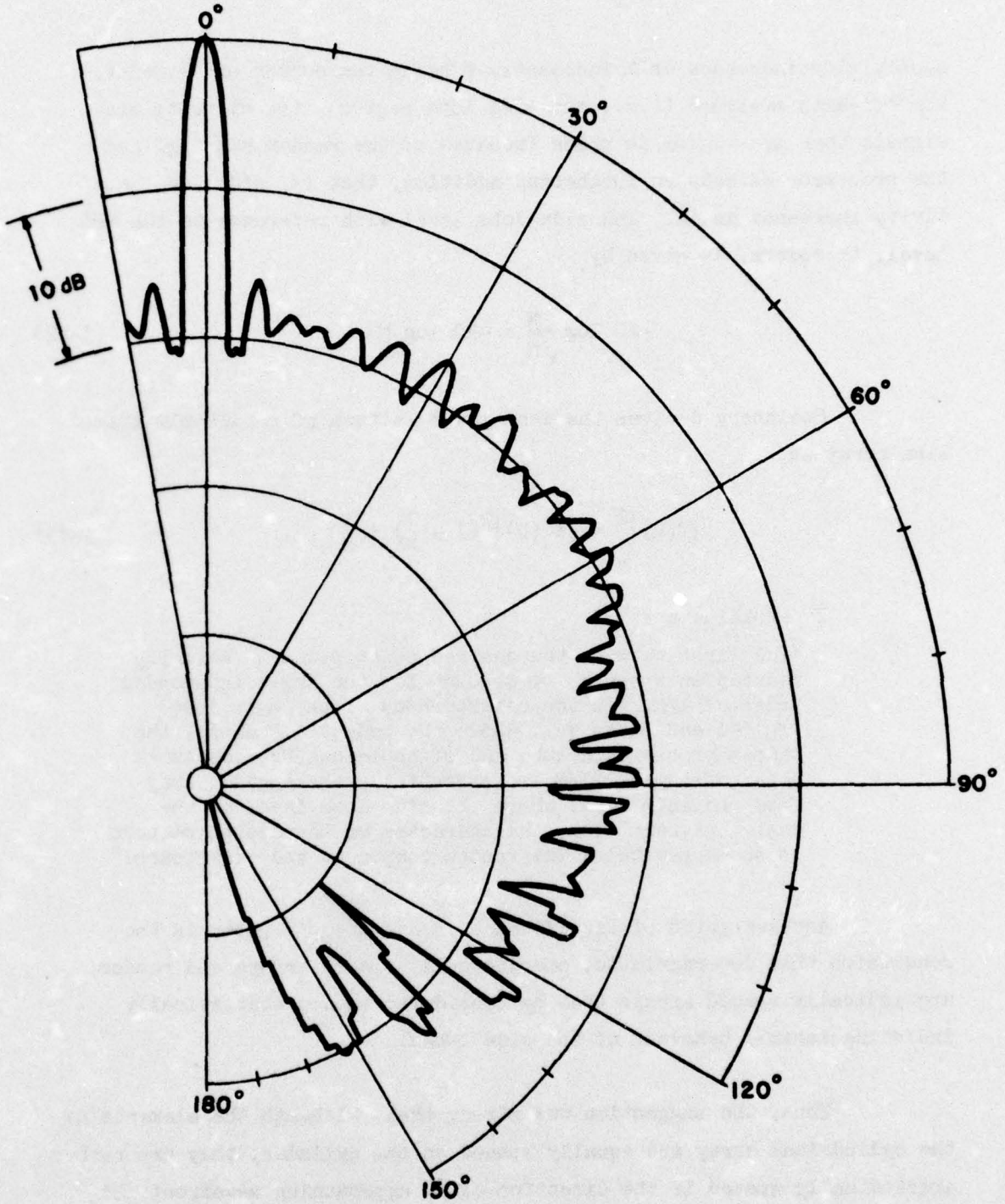

FIGURE 3-5

AZIMUTHAL BEAM PATTERN
POINT ELEMENTS
R = 12.3 N = 38

AS-74-1702
DAS-0031-3

sensitivity increases as M increases, M being the number of elements. For off-axis pressure (i.e., the side lobe region), the elements see signals that are random in phase (because of the random spacing) and the processor effects an incoherent addition, that is, side lobe sensitivity increases as $\sqrt{M}$. The side lobe level with reference to the MRA level, therefore, is given by

$$-20 \log \frac{M}{\sqrt{M}} = -10 \log M \quad . \tag{3-22}$$

Steinberg derives the mean power pattern of a randomly spaced line array as

$$|f(U)|^2 = |f_o(U)|^2(1 - \tfrac{1}{M}) + \tfrac{1}{M} \quad . \tag{3-23}$$

He explains that

> "The first term is the desired power pattern* slightly reduced in strength to account for the angle independent pedestal 1/M. In the neighborhood of the main lobe $|f_o|^2 \approx 1$ and rises well above the pedestal. Hence, the shapes of the main lobe and of those nearby side lobes whose strength $\gg 1/M$ are essentially unchanged. Away from the main lobe, where the side lobe level of the design pattern $< 1/M$, the character of the design pattern is submerged below the random component and disappears."

Another point of significance in Steinberg's paper is the conclusion that deterministic, aperiodically spaced arrays and random, aperiodically spaced arrays that he considered showed statistically indistinguishable behavior of the side lobes.

Thus, the suggestion was strong that, although the elements of the cylindrical array are equally spaced on the cylinder, they are rather aperiodically spaced in the direction of an approaching wavefront and might therefore meet one of Steinberg's conditions.

---

*f_o, we think, is controlled by $A_3(\alpha)$.

Further, the beam patterns that result with the cylinder are rather well described by the Steinberg approach. For example, the Steinberg pedestal should be 10 log M below the level of the MRA. Since the cylindrical array of radius R wavelengths has a circumference of $2\pi R$, and since there are elements spaced each $\lambda/2$ on one-half the array, then there are $2\pi R$ elements in each aperture.

This conjecture was tested for arrays with R=12 to R=407 in steps of approximately a factor of two. In every case,

$$\overline{SLL} = -10 \log 2\pi R \tag{3-24}$$

described the resulting average side lobe suppression to within 1 dB. Figure 3-6 is an example of a beam pattern plot with R=100. The predicted $\overline{SLL}$ is -28 dB.

Steinberg's average side lobe level was derived assuming equal strength elements, that is, no shading, or A(y)=1. If the elements were shaded, for example, $A_i \neq 1$, then the on-axis sensitivity would become

$$\sum_{i=1}^{M} A_i \quad , \tag{3-25}$$

not

$$\sum_{i=1}^{M} 1 = M \quad , \tag{3-26}$$

and the incoherent addition in the side lobe region would become

$$\sqrt{\sum_{i=1}^{M} A_i^2} \quad , \tag{3-27}$$

not

$$\sqrt{\sum_{i=1}^{M} 1^2} = \sqrt{M} \quad . \tag{3-28}$$

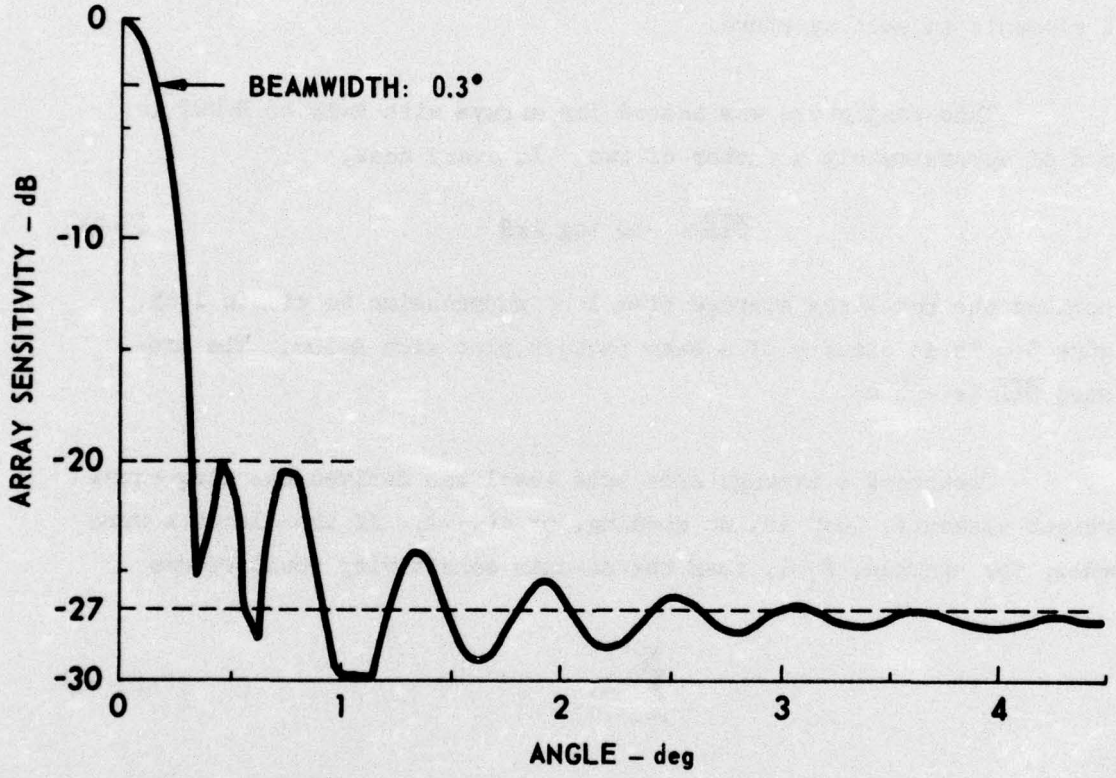

FIGURE 3-6
AZIMUTHAL BEAM PATTERN
— POINT ELEMENTS —
R = 100

ARL - UT
AS-73-403-S
DAS - DR
5 - 10 - 73
REV 3-19-75

In spite of these differences, which have so far remained unexplained, the prediction

$$\overline{SLL} = -10 \log 2\pi R = -10 \log M \qquad (3\text{-}29)$$

appears to be good.

In the Steinberg quote on a previous page, the statement that "those features of the desired pattern whose strength is much greater than 1/M are not changed by the presence of the pedestal" would suggest that the beamwidth (BW) of the pattern should be determined by the $D(\varphi)$ function, derived from the transform of the $A_3(Y)$.

Now, when

$$A_3(\alpha) = \cos \alpha \quad , \qquad (3\text{-}30)$$

then

$$A_3(Y) = \sqrt{1 - \frac{Y^2}{R^2}} \quad , \qquad (3\text{-}31)$$

and

$$D(\varphi) = \frac{2 J_1(x)}{x} \qquad (3\text{-}32)$$

where

$$x = 2\pi R \sin \varphi \quad . \qquad (3\text{-}33)$$

Solving for $\varphi_o = BW/2$ in the equation

$$D(\varphi_o) = \frac{1}{\sqrt{2}} \qquad (3\text{-}34)$$

leads to the result that

$$BW = 2 \arcsin \frac{1.616}{2\pi R} \text{ (radians)} \quad . \qquad (3\text{-}35)$$

Again, this prediction was compared to the "measured" beamwidth of the computed pattern from R=12 to R=407, with the result that Eq. (3-35) predicts beamwidth to within 2%.

Another result of the beamwidth computations is that the "beam spreading" is less than 20%. Beam spreading is defined as the percentage increase in resulting beamwidth over that beamwidth which can be expected with a uniformly illuminated aperture of the same length (2R). It is a measure of beam spreading caused by the application of some shading function. For example, cosine squared shading on a line array spreads the beamwidth 64% over that attainable on the same aperture with uniform shading. The 20% figure obtained with the present method indicates a rather large utilization of available aperture.

Given a shading function, in this case $A_3(\alpha)=\cos\alpha$, one can define an aperture constant K, which is the product of the number of wavelengths in the aperture times the resulting half-power beamwidth in degrees, provided the BW is not too large. Thus

$$K = 2R \cdot BW \text{ (degrees} \cdot \text{wavelengths)} \quad . \tag{3-36}$$

In the present case (the reference array)

$$K = 2R \cdot \frac{180}{\pi} \cdot 2 \arcsin \frac{1.616}{2\pi R} \quad . \tag{3-37}$$

When R>10, BW(deg)<3°, and $\sin \varphi_o \approx \varphi_o$ to within less than 0.1%, Eq. (3-37) can be approximated by

$$K = \frac{360 \cdot 1.616}{\pi^2} \approx 59(\text{wavelength} \cdot \text{degrees}) \quad . \tag{3-38}$$

An additional observation concerns the behavior of the first side lobe, usually the largest lobe, which is indicated by SLL_p. Recall that since $A_3(\alpha)=\cos\alpha$, the predicted coherent beam pattern is $D(\varphi)$ as given in Eqs. (3-32) and (3-33). The suppression of the first side lobe

of this function is 17.8 dB, independent of array size. However, the incoherent pattern or random pedestal, which does depend on array size, may add or subtract from the predicted peak side lobe level. In Fig. 3-5 the random pedestal is at about -19 dB. The resulting lobe, considering the addition or subtraction of the two components with unknown phase, could range from a high of -12 dB to a low of -36 dB. So it is not surprising that the peak lobe in Fig. 3-5 does not measure -17.8 dB. The same argument can be applied to Fig. 3-6. The range of values of peak side lobe level that should not be surprising in Fig. 3-6 are from a high of -15.2 dB to a low of -21.5 dB. The main point concerning the peak side lobe SLL_p is that it is fruitless to choose an $A_z(Y)$ which predicts a side lobe less than -10 log $2\pi R$, since it would just disappear below the random component.

2. The Elevation Beam Pattern

Figure 3-7 shows the elevation beam pattern for two sizes of the reference case array. Several such plots were studied, and all behaved as shown. The half-power beamwidth decreases with the inverse square root of size, much like the beamwidth of an end-fire array. In fact, the measured beamwidth from computer runs can be predicted from the end-fire array directivity function if one uses a length of 0.55 R. For the reference case, the beamwidth can be calculated from

$$BW(\theta) = \frac{145}{\sqrt{R}} \text{ (deg)} \quad . \tag{3-39}$$

This, of course, depends heavily upon the shading coefficients and especially the sector of active elements, in this case $2\alpha_N = 180°$.

The side lobe region shown in Fig. 3-7 is very unlike an end-fire array, however. No clear explanation of the smooth behavior in Fig. 3-7 is available. The sensitivity at $\theta = 90°$, that is, with the cylindrical array seen end on, is a measure of the average value of the coefficients. This is because, at this angle, the signal insonifying the array is in

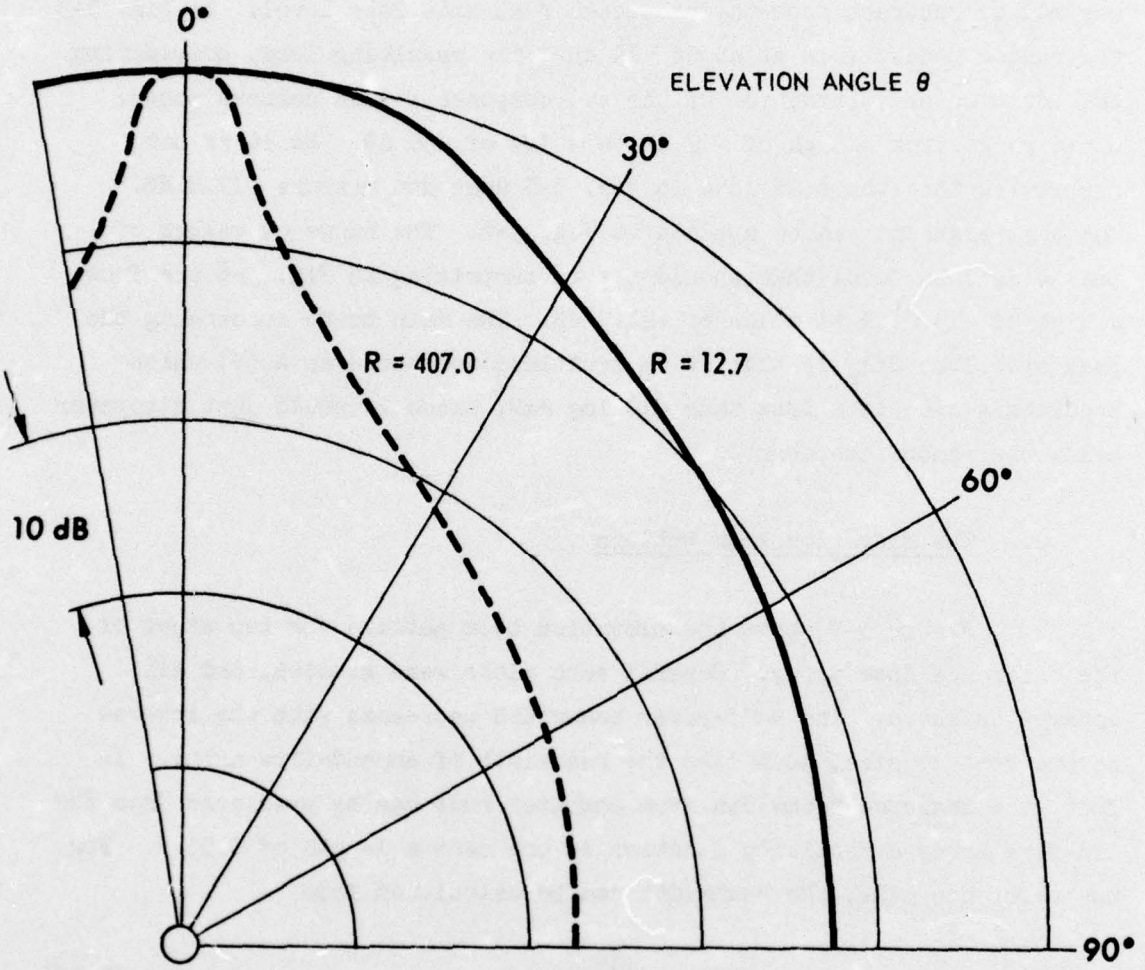

FIGURE 3-7
ELEVATION BEAM PATTERN
DUE TO ARRAY ONLY
— POINT ELEMENTS —

ARL - UT
AS-75-378-S
DAS-DR
3-19-75

phase at each element. The suppression at $\theta=90°$ has been found empirically to be roughly described by

$$-10 \log R\sqrt{2} \quad \text{dB//major lobe level} \quad . \quad (3\text{-}40)$$

3. Bandwidth--Frequency Response

Again, because the array has depth in the direction of signal propagation, signal detection is expected to be a rather narrowband process. During the matching operation, that is, during the selection of the $A_1(\alpha_n)$ coefficients, R cycles of the signal must be known. If, for example, during operation of the array, the center frequency was changed so that R+1/2 cycles of the signal occurred in the original radius of the array, then, when the front edge of the array was insonified by the start of a cosine wave, the back of the array would be insonified by a signal exactly out-of-phase with what was expected.

In order to test the array bandwidth behavior, the computer model was run for several operating frequencies for an R=12.3 array chosen to operate at 100 kHz. Figure 3-8 is a summary of these runs, and shows how the various pattern parameters change with operating frequency.

If the bandwidth is considered as "that frequency range over which the array sensitivity has deteriorated no more than 3 dB," then the bandwidth is 14.5 kHz. However, over this range, the beamwidth increases by a factor of two! If the bandwidth is restricted to that range of frequencies over which the beamwidth does not increase beyond 25%, then the operating bandwidth becomes 7.3 kHz. If the bandwidth is defined as "the range of operating frequency over which the half-power beamwidth increases no more than 25%," then the useful bandwidth can be stated as

$$\Delta f = \frac{f}{1.12\ R} \quad . \quad (3\text{-}41)$$

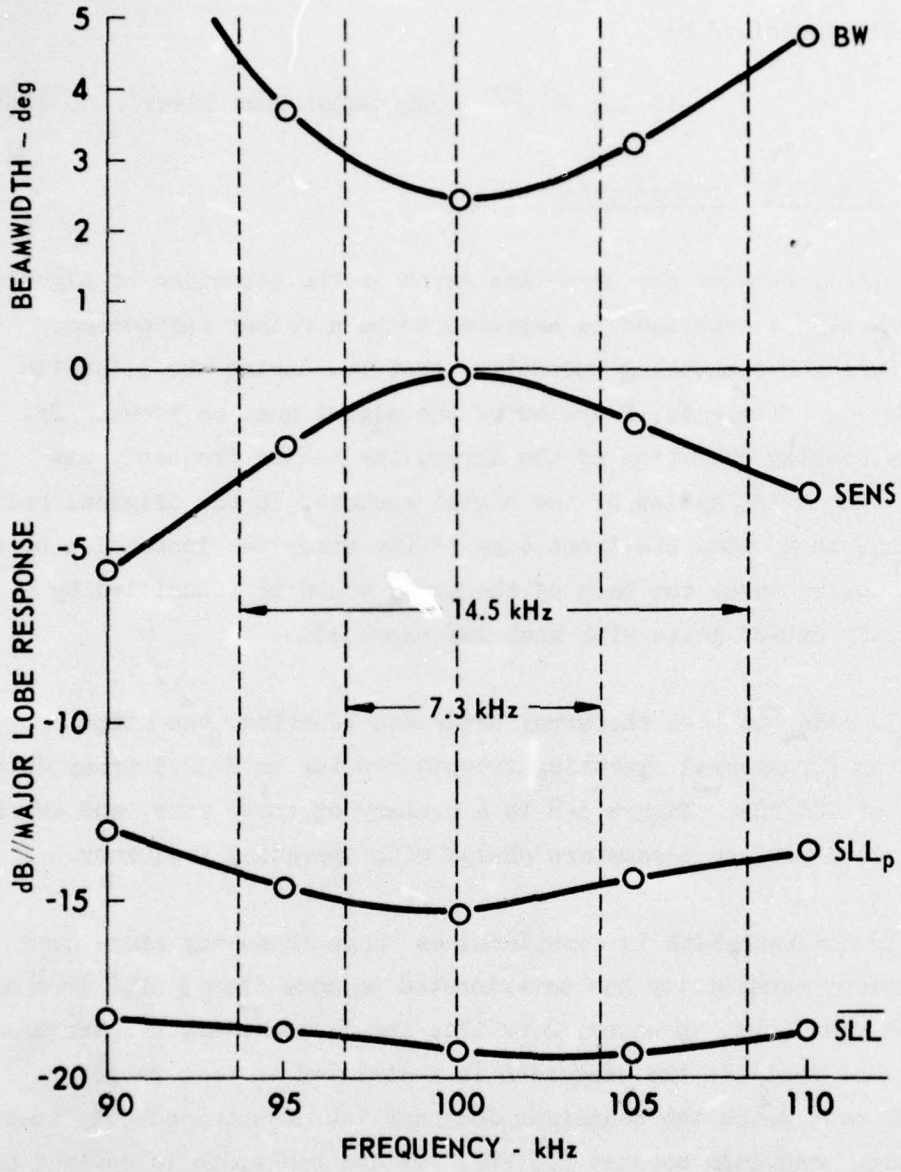

FIGURE 3-8
EFFECTS OF OPERATING FREQUENCY
ON AZIMUTHAL PATTERN PARAMETERS
R = 12.3

ARL - UT
AS-74-1709-S
DAS - DR
3 - 19 - 75
REV 3-19-75

If the half-power sensitivity bandwidth is used, then

$$\Delta f = \frac{f}{0.56\ R} \quad . \tag{3-42}$$

One should note that the present "bandwidth" considerations are not related to the system rise time, or to the bandwidth of the electro-acoustic sensor channels which deliver the voltages $e_n^*(\varphi,t)$ in Eq. (3-1). The present consideration is more closely related to correlator mismatch error between the assumed and operating wavelength of the signal at the array face.

The effects of changes in the operating wavelength are more complicated than what has been presented here. For example, if the shape of the major lobe, not just the -3 dB width or the sensitivity deterioration, is considered, then a more complicated and uncertain prediction of behavior results. This effect will be described and methods of reducing the effect will be considered in the following chapter.

4. Sensitivity--Array Gain

The prediction of the absolute receiving sensitivity of an array (in volts/plane wave μbar) is very difficult because of its dependence upon several factors, such as the absolute sensitivity of the elements, or the gain of the preamplifiers. Of more interest here is the relative gain of the correlation beamformer when compared to, say, phase shift or time delay type beamformers.

In general, the main difference between the correlation method and phase shift or delay line methods in terms of sensitivity is that, where the two latter methods move each element electrically so that all element voltages are in phase and sum to M (the number of contributors), the correlation method adds element voltages without first bringing them into phase coherence.

If the collection of instantaneous samples of element voltages is e_n, then the signal replica factor $A_1(n)$ will be equal to e_n. If this effect alone is considered, then the output voltage would be

$$E = \sum_{n=1}^{M} A_1(n)\, e_n \quad , \tag{3-43}$$

or, since

$$A_1(n) = e_n \quad , \tag{3-44}$$

$$E = \sum_{n=1}^{M} e_n^2 \quad . \tag{3-45}$$

Now, if the array is large, then e_n is a collection of samples of a cosine wave uniformly distributed throughout the cycle, so that E might be approximated by

$$E \approx \frac{M}{2\pi} \int_0^{2\pi} \cos^2\varphi \, d\varphi \tag{3-46}$$

or

$$E = \frac{M}{2} \quad , \tag{3-47}$$

whereas, the phase shift or time delay operation results in

$$E = M \quad . \tag{3-48}$$

The general result then is that the sensitivity of an array with a correlation beamformer is at least 6 dB lower than coherent processors, all other factors being equal. Of course, given a geometry and a beam pattern specification, the other shading factors will, in general, be the same.

Another item of interest is the processing gain against thermal noise. Appendix D contains a detailed comparison between a correlation

processor and a phase shift processor which were designed to accomplish equivalent beam pattern performance. The signal-to-thermal noise ratios were within 0.5 dB of each other.

Methods for computing sensitivity and S/N ratio are outlined in Appendix D and can be applied to individual problems as the need arises.

IV. THE DESIGN AND PERFORMANCE OF MORE REALISTIC CYLINDRICAL ARRAYS

In the previous chapter, the simplest possible cylindrical array was developed in order to convey the beamformer concept, to show the coefficient selection algorithms, and to outline the performance and scaling rules. This array was called the reference array.

In this chapter, we will consider modifications to the reference array that are required to make the array assumptions more realistic and the analysis more flexible.

Figures 4-1 and 4-2 show the coordinate system used in this and the remaining chapters of this report. Figure 3-1 will not be repeated here, but is applicable as well.

A. Finite Size Array Sensors

1. Azimuthal Effects

One of the first modifications to the reference array required to make the analysis more realistic is the inclusion of finite size elements or staves. Such elements exhibit directional response individually, and, since they are assumed to be mounted on the cylindrical baffle and point radially outward, the effect is difficult to analyze. Intuition indicated that the element beam pattern (azimuthal) should be accounted for in the direction of the array major lobe, since such accounting can only be done in one direction. The computer model was then exercised to evaluate the array pattern performance.

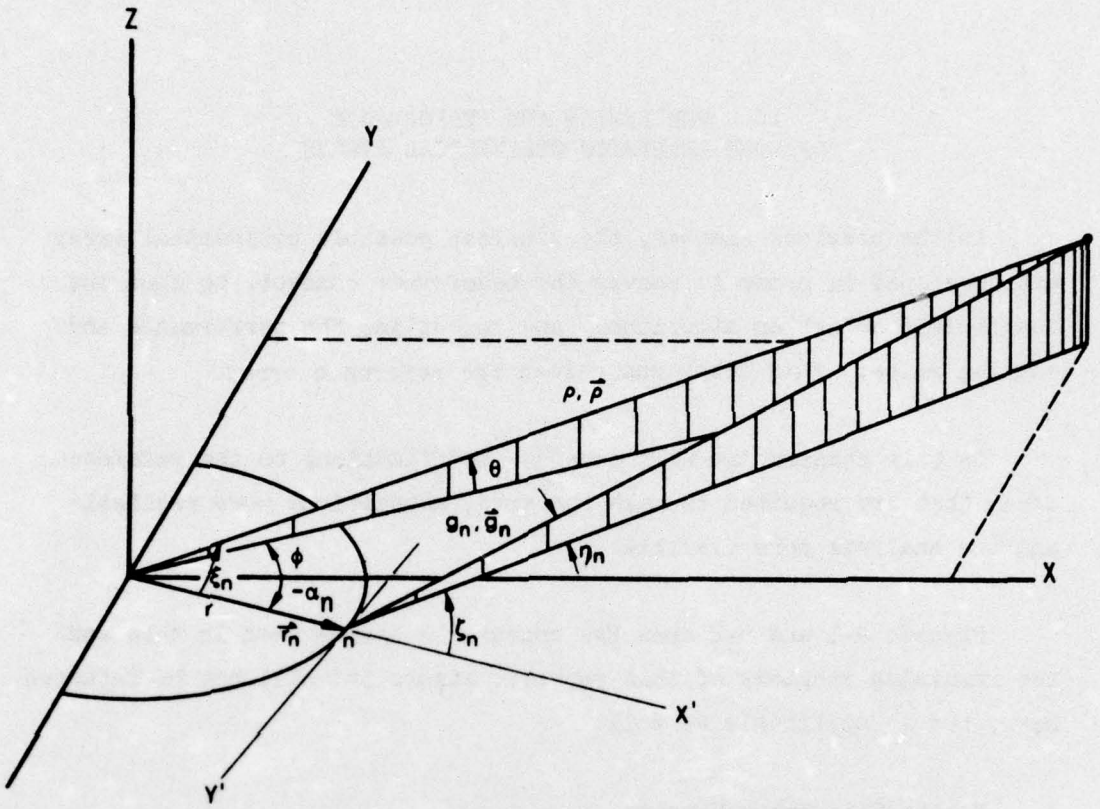

FIGURE 4-1
MASTER COORDINATE SYSTEM

AS-74-1699
DAS-0031-3

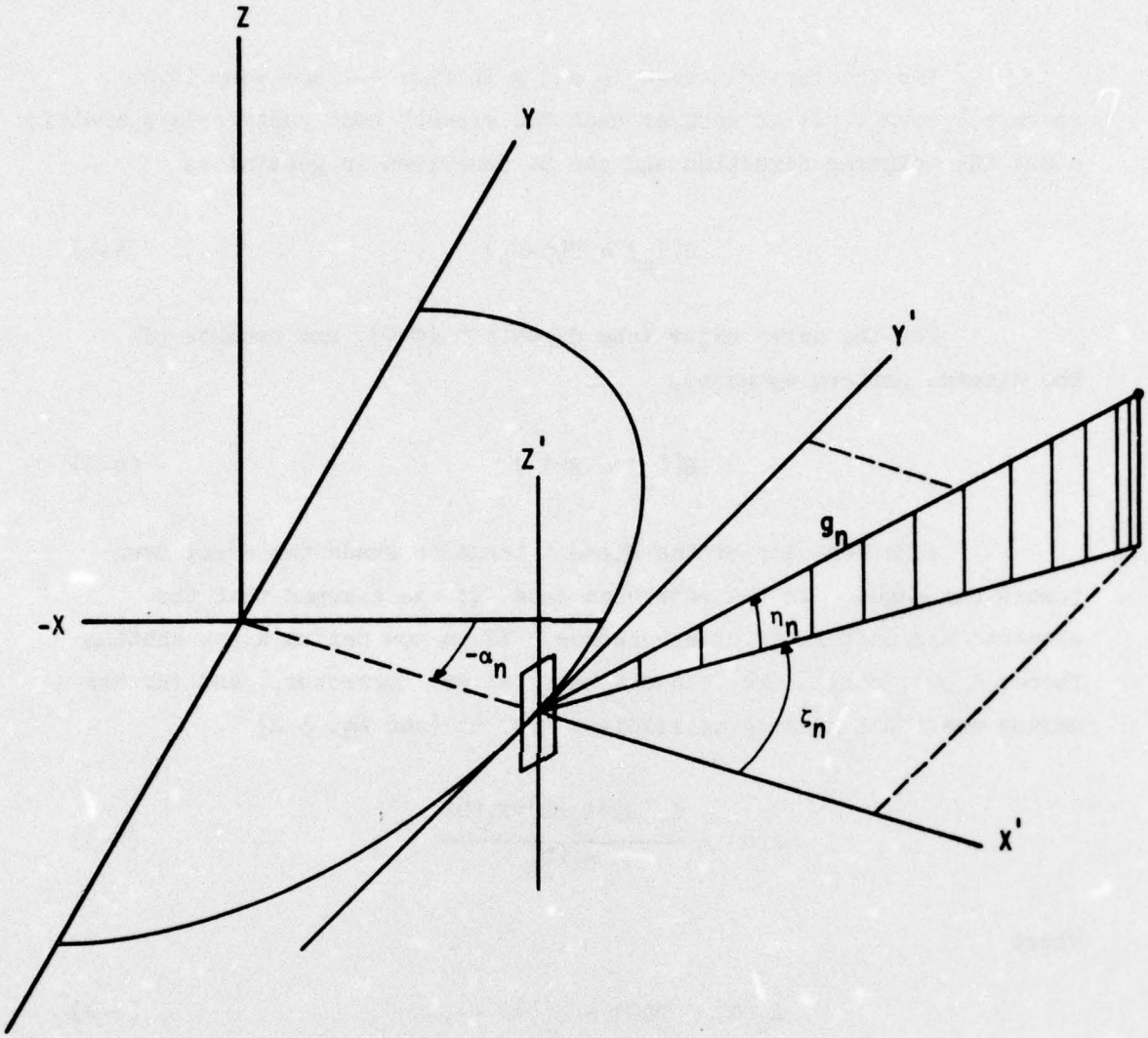

FIGURE 4-2
ELEMENT DETAIL

AS-74-1700
DAS-0031-3

For the farfield case, ρ and g in Fig. 4-1 are very large so that $\zeta_n = \varphi - \alpha_n$. It is assumed that the element beam pattern is symmetric about its pointing direction and can be described in general by

$$B(\zeta_n) = B(\varphi - \alpha_n) \quad . \tag{4-1}$$

For the array major lobe direction ($\varphi=0$), and because of the element pattern symmetry,

$$B(\zeta_n) = B(\alpha_n) \quad . \tag{4-2}$$

Such behavior of the element tends to shade the array down toward the edges. In the reference case, it was assumed that the elements had uniform angular response. If we now define a new shading factor $A_4(\alpha)$, called the "element beam pattern corrector," and further define the total shading coefficient $A(\alpha)$ as (see Eq. 3-2)

$$A(\alpha) = \frac{A_1(\alpha) * A_2(\alpha) * A_3(\alpha)}{A_4(\alpha)} \quad , \tag{4-3}$$

where

$$A_4(\alpha) = B(\alpha) = B(\zeta) \quad , \tag{4-4}$$

then we will have raised the coefficient value at an angle α_n in such a way as to account for that element's pattern loss in the direction of the array major lobe. The resulting performance should be nearly the same as that of the point element case for pattern parameters near the major lobe.

Before exercising the computer model, a specific functional form for the $B(\alpha)$ was needed. Prior experience with small width elements (less than 0.5 λ wide) on rather large cylindrical baffles (R>10) indicated that the pattern could be adequately described by

$$B(\alpha) = \left(\frac{1 + \cos \alpha}{2}\right)^x \qquad (4\text{-}5)$$

where x is a constant selected to make B fit a measured element pattern.

For the computer runs investigating the performance of finite size elements, several values of x were used. Figure 4-3 shows the beam pattern obtained when x=3, and should be compared with Fig. 3-4, the point element counterpart. The sensitivity, beamwidth, and peak side lobe levels are identical. The average side lobe level for the finite size element case is slightly lower because of the pattern smoothing evident in Fig. 4-3.

In summary then, one can design arrays using the point element assumptions and scaling rules. During construction of a real array, element patterns can be measured and a functional form determined. Then $A_4(\alpha)$ can be selected and incorporated in the shading coefficients as shown in Eq. (4-3) without affecting the point element performance prediction.

2. Elevation Effects

In Chapter III we presented the elevation beam pattern of the point element array (Fig. 3-7) and the scaling rules for that effect. When finite size elements are utilized and the element elevation pattern is $B(\eta)$ (it is assumed throughout that $B(\zeta,\eta)=B(\zeta)*B(\eta)$), it was found that the composite array elevation pattern through the $\varphi=0$ plane was very closely described by the product of the element pattern $B(\eta)$ and the point element array pattern (recall the line array product theorem).

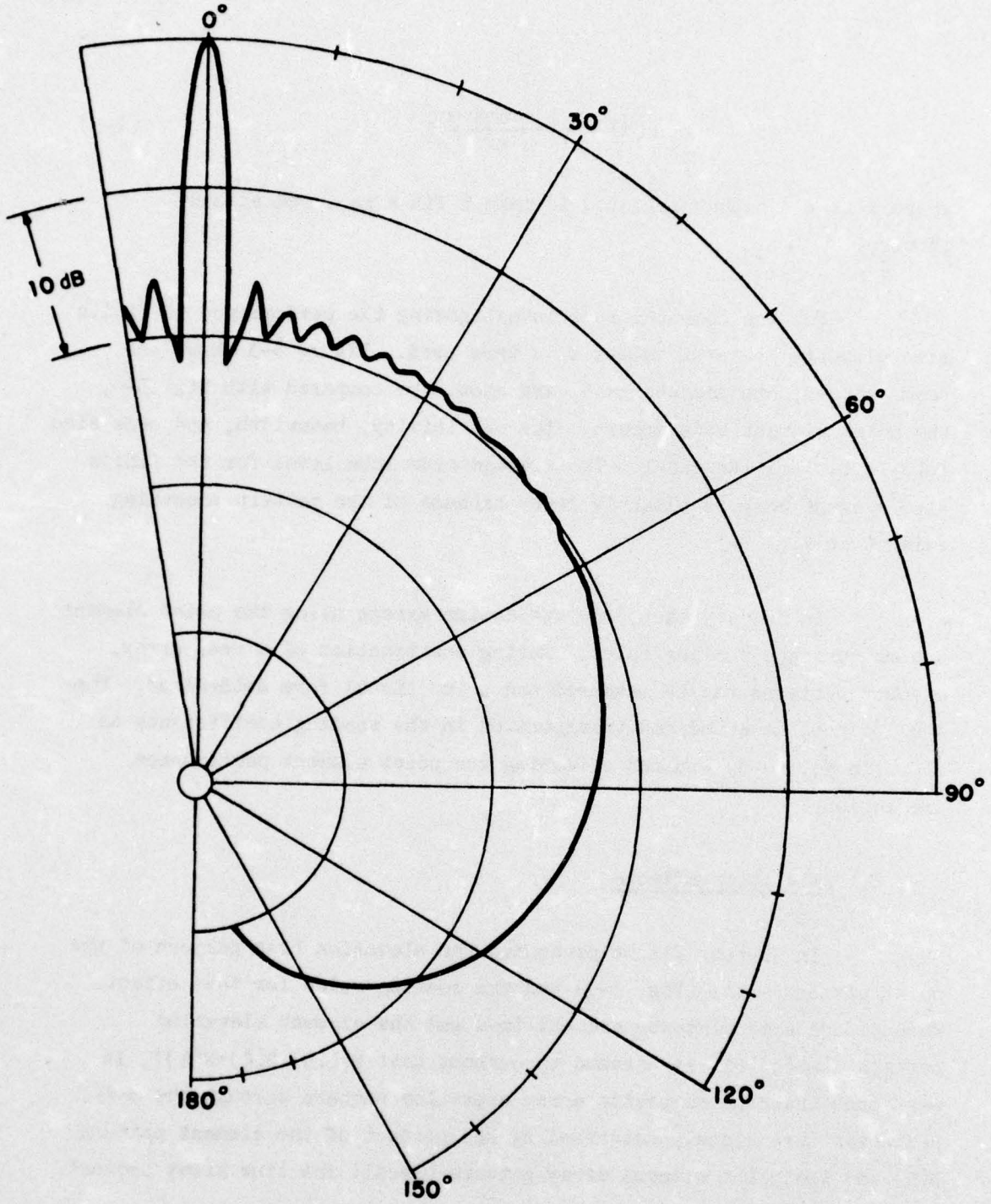

FIGURE 4-3

AZIMUTHAL BEAM PATTERN
FINITE-SIZE ELEMENTS (≈0.5 λ WIDE, NO LENGTH)
R = 12.3 N = 38

AS-74-1706
DAS-0031-3

Figure 4-4 shows a composite elevation pattern with element length 3.39 λ. Such an element alone should have a sin x/x beamwidth of 15° and first side lobe level of -13.5 dB. The comparable point element array elevation pattern is the solid curve in Fig. 3-7. The composite in Fig. 4-4 has a 14.8° beamwidth (not much affected) and a first side lobe of -16.5 (a reduction of 3 dB due to the array response). More will be said about this effect in Chapter VIII where experimental validation of the theory is discussed.

B. The Effects of Element Spacing

In order to determine the effects of various element spacings, the computer model was exercised for element spacings from 0.1 λ to 0.8 λ, holding the cylinder radius constant at R=12.3. The elements were points and only azimuthal patterns were obtained. Figure 4-5 shows one such pattern with a spacing of 0.6 λ.

One effect that can be seen in Fig. 4-5 is the growth of the classic "grating lobe" at about 120°. As the spacing grows larger, this lobe becomes larger in amplitude and moves toward the major lobe at 0°. The grating lobe behavior is identical to that of a phase shift or time delay beamformer.

The second and more important effect seen in Fig. 4-5 is the breakup of the usual uniform side lobe region. As the element spacing increases beyond 0.5 λ, the peak side lobe grows rapidly. A summary of the effect is shown in Fig. 4-6 for an R=12.3 array. The effects shown here indicate that when side lobe level is important (as it almost always is) one must space elements on the cylinder at less than 0.55 λ. and preferably at 0.5 λ.

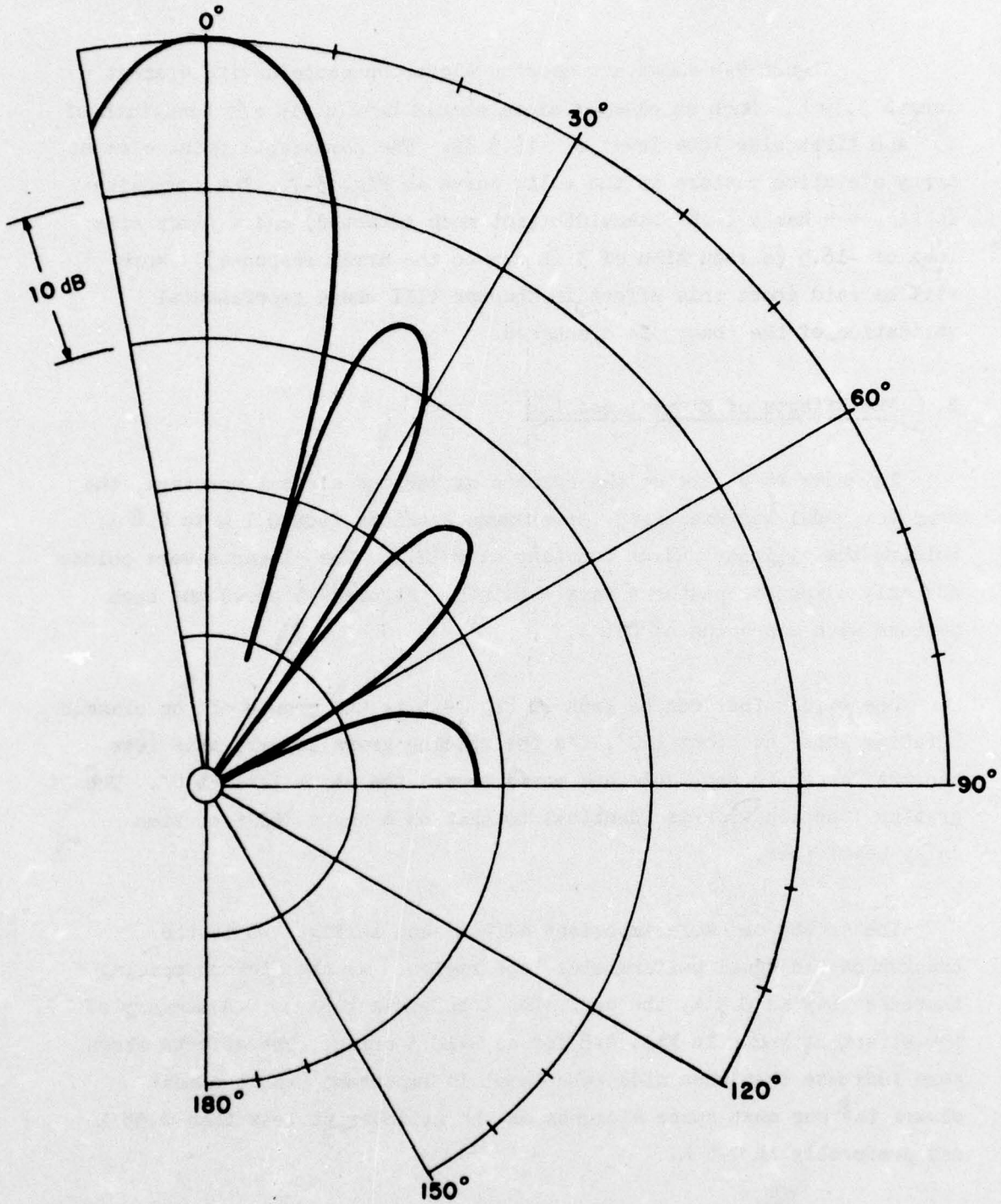

FIGURE 4-4

ELEVATION BEAM PATTERN
FINITE-SIZE ELEMENTS (≈0.5 λ WIDE, 3.39 λ LONG)
R = 12.3 N = 38

AS-74-1708
DAS-0031-3

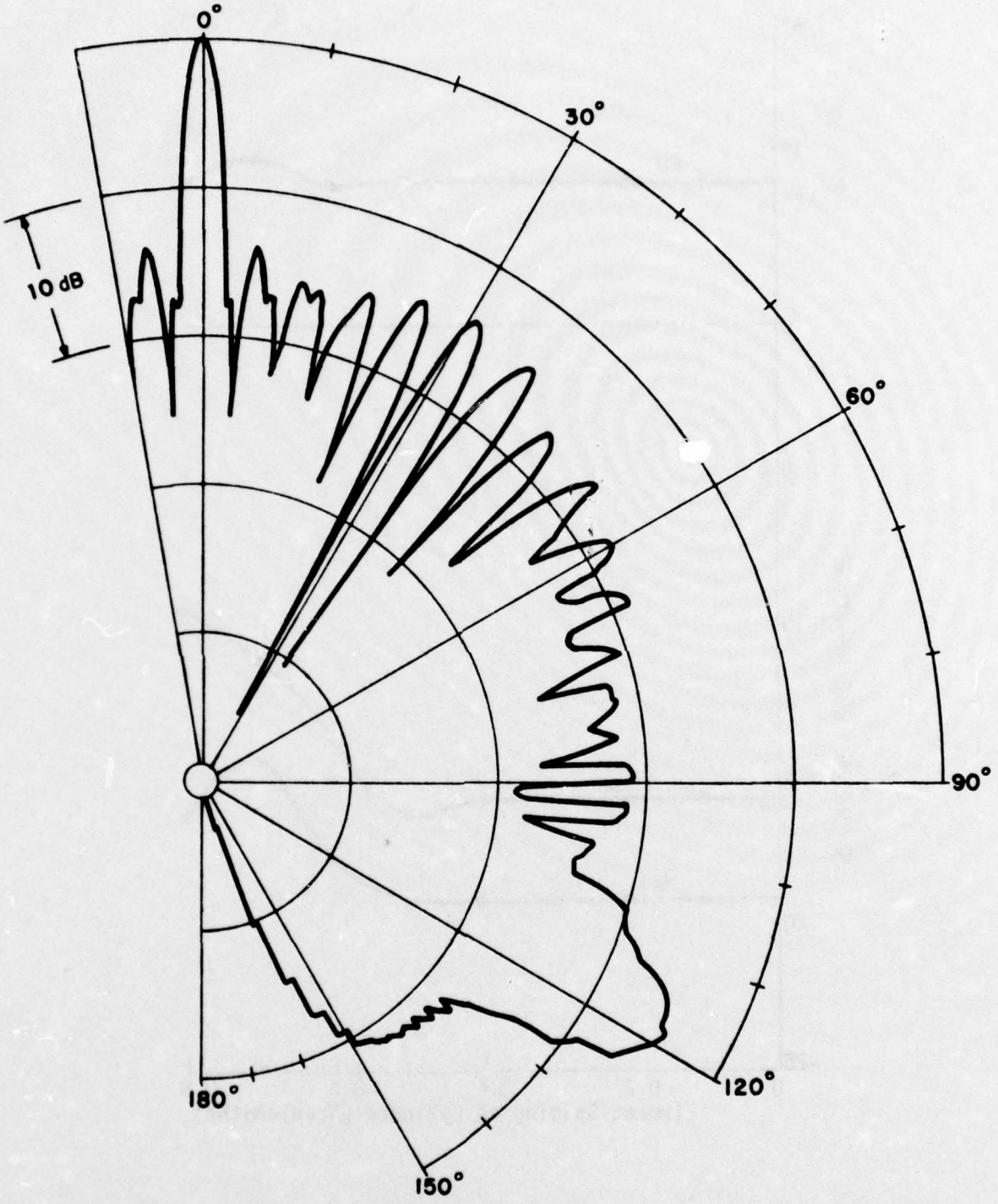

FIGURE 4-5

AZIMUTHAL BEAM PATTERN
POINT ELEMENTS SPACED 0.6 λ
R = 12.3 N = 31

AS-74-1704
DAS-0031-3

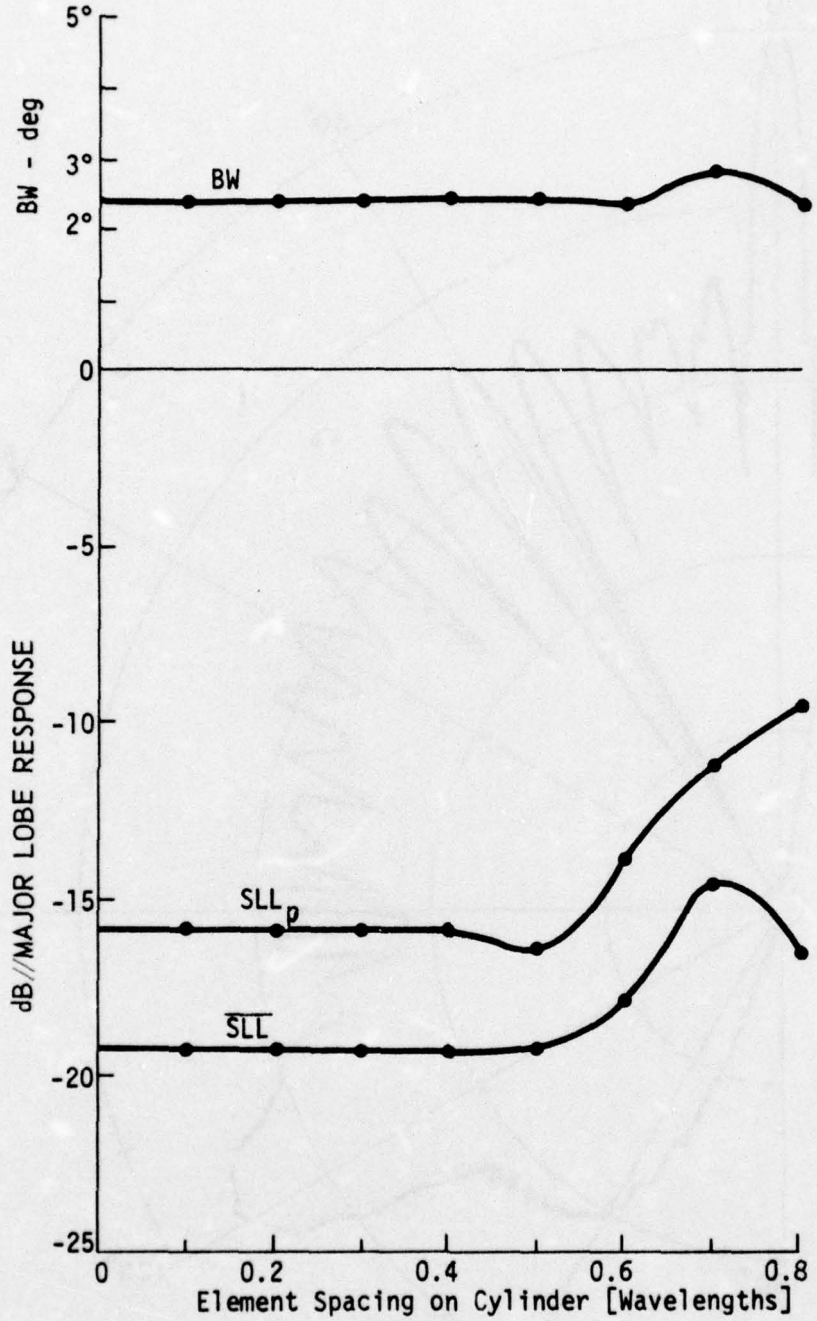

FIGURE 4-6

EFFECTS OF ELEMENT SPACING ON AZIMUTHAL PATTERN PARAMETERS
R = 12.3

AS-74-1696
DAS-0031-3

C. Effects of A_3 on Beamwidth and Side Lobe Level

Variations in azimuthal beam pattern performance of the correlation array were investigated by application of different line aperture illumination functions (A_3). References 2 through 6 discuss such functions and their application to line apertures. Selected amplitude weighting of the element outputs produced changes in beamwidth and peak and average side lobe level.

The study involves the application of the named line shading functions to the equivalent line aperture of the array (the W line). The function is then projected back to the cylinder, where the A_3 coefficient factor is evaluated. The computed patterns involve the total composite coefficient $A(\alpha)=A_1(\alpha)*A_2(\alpha)*A_3(\alpha)$ as defined and used previously. The A_3 used in the reference array was a cosine on the cylinder, which results in a "house top" or "triangle" on the W line.

The effects of each weighting function were evaluated by a computer program which implements a mathematical model of the cylindrical array response to a point source in the farfield. In all cases the array had a diameter of 100 λ, and the elements were separated by $\lambda/2$, thus resulting in 628 elements on a 180° aperture. Following is a list of the line array weighting functions which were considered:

1) Uniform
2) Triangle Functions
3) $\cos(\pi p/2)$
4) $k + (1-k)\cos(n\pi p/2)$ where $0 \leq k \leq 1$ and $0.5 \leq n \leq 3$
5) $k + (1-k)\cos^2(n\pi p/2)$ (Hamming Function) where $0 \leq k \leq 1$ and $0.5 \leq n \leq 3$
6) Taylor Functions

where p is the normalized distance from the W line center to the subtended array edge, that is, $0 \leq p \leq 1$.

Figure 4-7 shows the results of applying some of the more useful shading functions. The bars connect the peak side lobe point with the corresponding average side lobe point. Since this test was conducted on an R=100 array, the resulting beamwidth numbers can be connected to K (the aperture constant) by multiplying by 200. The point to be emphasized in Fig. 4-7 is the very rapid loss in the aperture constant as the peak side lobe is pushed down.

Equal weighting of the line aperture produces the narrowest beamwidth (0.252°) and a very low average side lobe level (-26.2 dB), but with a poor peak side lobe of -14.56 dB. Weighting the line aperture with a simple triangle function improves the response to a beamwidth of 0.296°, the average side lobe level of -26.9 dB, and a peak side lobe of -20 dB (the standard $A_3=\cos\alpha$). Other often used line weighting functions, such as cosine and Hamming, decrease the peak side lobes to -22.4 dB and -23.4 dB, but with a subsequent growth in beamwidth to 0.345° and 0.38°. respectively. Of the functions tested, the Taylor functions (Ref. 2) produce the best compromise between beamwidth and side lobe level.

D. Effects of ψ Changes in $A_1(\alpha)$

The reference array discussed in Chapter III assumed the signal to be positioned on the array so that a cosine wave existed at t=0 (see Fig. 3-3). Then $A_1(\alpha)$ was chosen to be a replica of that signal at t=0. Equation (3-6) suggests that other times could be chosen for peak response by using the cosine phase shift ψ in the reference signal. If $A_1(\alpha)$ is then matched to the phase shifted signal, it becomes

$$A_1(\alpha) = \cos\left[2\pi R(1 - \cos\alpha) - \psi\right] . \qquad (4\text{-}6)$$

Now the major effect of changes in ψ is the shift of the acoustic center of the array; however, the shift is not in direct proportion to changes in ψ. The explanation can be found in the shift in "center of mass of the coefficients."

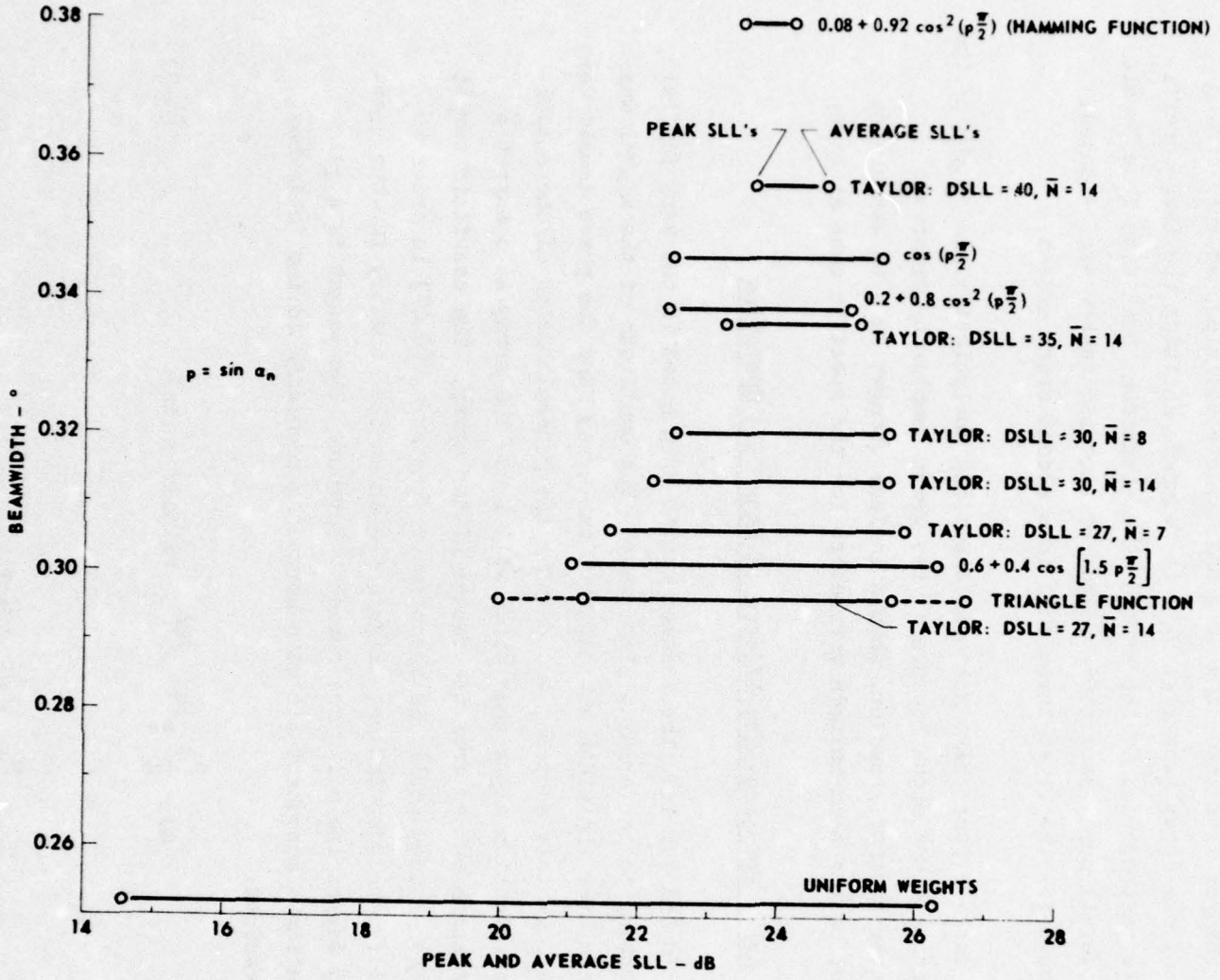

FIGURE 4-7
BEAMWIDTH VERSUS PEAK AND AVERAGE SLL ON A CYLINDRICAL ARRAY

ARL - UT
AS-76-50
DAS - DR
1 - 20 - 76

As Ψ changes from zero, the original large coefficient at the leading edge of the array (see Fig. 3-4) is reduced, shifting the large coefficients farther back in the array. The beamwidth, peak side lobe level, the overall array sensitivity, and the acoustic center are affected, although for the first three this is a second order effect.

These effects have not been explained analytically and graphs of the effects are not shown because of the great complexity involved. Computer designs, however, should include changes in Ψ to assess the effect on the beam pattern parameters for the specific case at hand.

E. Array Focusing--The Effects of Nearfield Operation

In Chapter III, the assumed signal originated in the very farfield, presenting to the array a plane wave. The amplitude of the signal was uniform over the width and depth of the array, and the phase fronts were plane. In this section, we consider the generalization of the coefficient selection algorithms which will focus the array at a target $\tilde{\rho}$ (wavelength units) from the center of the array. The nearfield target will be assumed to lie in the plane of the array (θ=0°) in order to simplify the description. Figure 4-8 shows the geometry for the nearfield target including the curved wavefront. The target is a point radiating a monochromatic wave spreading according to the following expressions.

$$P(g) = \frac{P_o}{g} e^{ikg} e^{i\omega t} \quad \text{(linear units)} \quad , \tag{4-7}$$

or

$$P(G) = \frac{P_o}{G} e^{j2\pi G} e^{j2\pi cT} \quad \text{(wavelength units)} \quad . \tag{4-8}$$

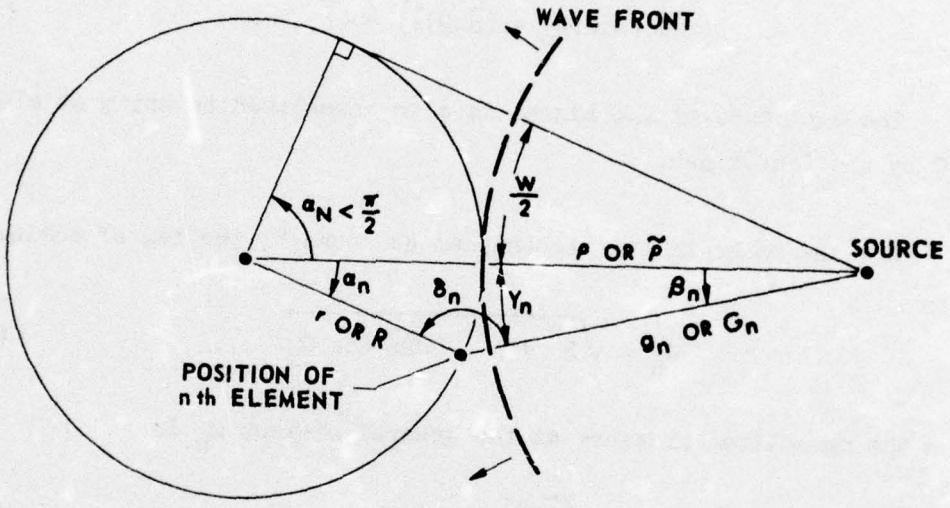

FIGURE 4-8
ARRAY GEOMETRY FOR A POINT
TARGET IN THE NEAR FIELD

ARL - UT
AS-76-49
DAS - DR
1 - 20 - 76

The coefficient factor $A_1(\alpha_n)$ is the signal replica factor. That is

$$A_1(\alpha_n) = \text{Real Part } [\text{Sig}(\varphi=0, t=t_o)] \tag{4-9}$$

where $\varphi=0$ is the beamforming direction and t_o is a time selected to cause the n=0 element at $\alpha_o=0$ to see a peak positive pressure. That is, t_o is such that

$$\cos\left(2\pi[ft_o - (\tilde{\rho}-R)]\right) = +1 \quad . \tag{4-10}$$

The amplitude of the signal is also normalized to unity at element n=0 by the factor $\tilde{\rho}-R$.

Now the range to any element can be found by the law of cosines as

$$G_n = \sqrt{R^2 + \tilde{\rho}^2 - 2R\tilde{\rho}\cos\alpha_n} \quad , \tag{4-11}$$

and the normalized pressure at the general element α_n is

$$P(\alpha_n) = \frac{(\tilde{\rho}-R)}{G_n}\cos[2\pi(ft_o - G_n)] \quad , \tag{4-12}$$

or

$$P(\alpha_n) = \frac{\tilde{\rho}-R}{G_n}\cos[\tilde{\rho}-R-G_n] \quad . \tag{4-13}$$

Equations (4-12) and (4-13) describe the normalized signal pressure at each element, and as usual, we set

$$A_1(\alpha_n) = P(\alpha_n) \quad . \tag{4-14}$$

Now $A_2(\alpha)$ is the sensor density corrector. It was computed for the plane wave used in Chapter III.A.2. The same algorithm will be

used here, but with different geometry as shown in Fig. 4-8. In this case, the W line is curved and the relationship between the apparent element position on the W curve (Y_i) and the element position in the array (α_i) is

$$Y_i = (\tilde{\rho}-R)\beta_i \quad , \tag{4-15}$$

where β_i can be found by the law of sines, resulting in

$$\beta_i = \arcsin\left[\frac{R}{G_i}\sin\alpha_i\right] \quad , \tag{4-16}$$

or

$$Y_i = (\tilde{\rho}-R)\arcsin\left[\frac{R}{G_i}\sin\alpha_i\right] \quad . \tag{4-17}$$

Now, following the outline in Chapter III.A.2., if the element density on the cylinder is $q/d\alpha$, then the apparent density on the W curve is q/dY. The derivative of Eq. (4-17) with respect to α, remembering that G is a function of α also, will allow the evaluation of q/dY in terms of $q/d\alpha$. In addition to this density term, the envelope of both the signal and $A_1(\alpha)$ should be included. The normalized signal strength at the nth element is

$$\frac{\tilde{\rho} - R}{G_n - \tilde{\rho} + R} \quad , \tag{4-18}$$

and A_1 was chosen to have the same envelope (Eq. 4-14). So, although the apparent element density near the edge of the W curve increases, the signal and A_1 envelopes decrease. Thus, $A_2(\alpha)$ should be chosen to make

$$A_2(\alpha)\left[\frac{\tilde{\rho} - R}{G_n - \tilde{\rho} + R}\right]^2 \frac{q}{dY} = \text{constant} \quad . \tag{4-19}$$

Now, $A_3(\alpha)$ is the aperture window function and should be applied to the W curve. Its value at each element can be evaluated using Eq. (4-17) to relate α to Y.

Also, $A_4(\alpha)$ (the element beam pattern corrector) should be modified slightly to include the effect of parallax. As can be seen in Fig. 4-8, the correction to the element pointing angle is simply β_i, so that $A_4(\alpha+\beta)$ is the element beam pattern corrector where β is given in Eq. (4-16).

Experiments and computer modeling indicated that, if the coefficient selection algorithms described above are utilized, then the performance of a focused beam with a target at the focused range is essentially the same as the performance of the unfocused reference beam of Chapter III with a target in the farfield.

F. Frequency Response

In Chapter III.B.3., the bandwidth of the reference array was discussed. The array sensitivity, half-power beamwidth, and the peak and average side lobe changes due to changes in operating frequency were shown. A more stringent requirement on the operating frequency may be the change in shape, or in form factor, of the major lobe.

In order to study this effect, a large array (R=136) was chosen. Figure 4-9 is a plot of the beamwidths measured at different levels on the major lobe as a function of operating frequency. The array was designed to operate at 224 kHz. The sector of elements covers $2\alpha_N=120°$, so the array depth ($R(1-\cos\alpha_N)=68$) is 68 wavelengths. Eq. (3-41) would indicate a 2.94 kHz operating band in which the -3 dB beamwidth would not grow beyond 25%. This estimate is confirmed in Fig. 4-9. However, over this band, the -15 dB beamwidth is seen to grow by about 45%. In some cases, it may be necessary to restrict the operating bandwidth further to control the major lobe shape. If the

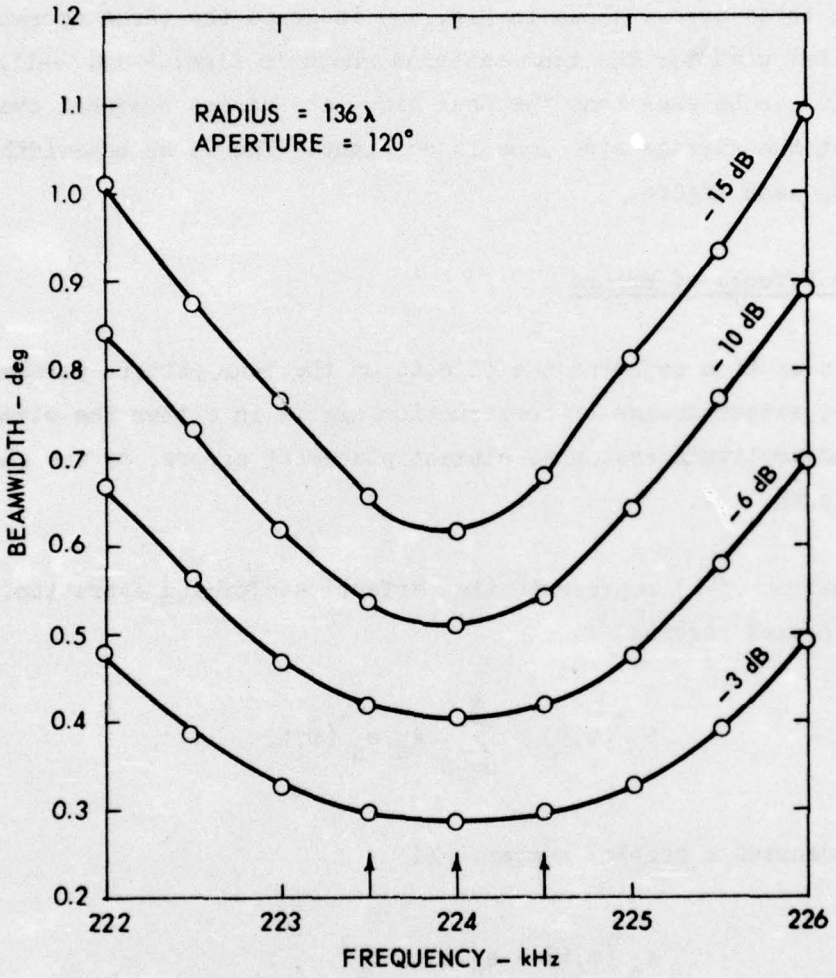

FIGURE 4-9
BEAMWIDTH vs FREQUENCY

ARL - UT
AS-75-1210
KM - ORS
9 - 3 - 75

operating band is restricted to one-half that predicted by Eq. (3-41) (≈1.5 kHz), then even the -15 dB beamwidth grows less than 20%.

The three arrows shown in Fig. 4-9 indicate the three operating frequencies used for the beam patterns shown in Figs. 4-10, 4-11, and 4-12. It can be seen that the peak side lobe varies somewhat over the band, but the average side lobe is constant. The -3 dB beamwidths are listed on each figure.

G. The Effects of Errors

This section concerns the effects on the beam pattern parameters caused by either design or construction errors in either the element phase and amplitude response, element placement errors, or the shading coefficients.

Equation (3-1) represents the perfect beamforming operation. It is repeated here as

$$E_o^*(\varphi,t) = \sum_{n=-N}^{N} A_n \, e_n^*(\varphi,t) \quad , \tag{4-20}$$

where * denotes a complex number. If

$$e_n^*(\varphi,t) = e_n \exp[i\beta_n] \quad , \tag{4-21}$$

and all possible amplitude errors are grouped in δ_n, and all phase errors are grouped in Δ_n, then the imperfect beamformer operation can be written as

$$E_e^* = \sum_n A_n \, e_n \, \delta_n \exp[i(\beta_n - \Delta_n)] \tag{4-22}$$

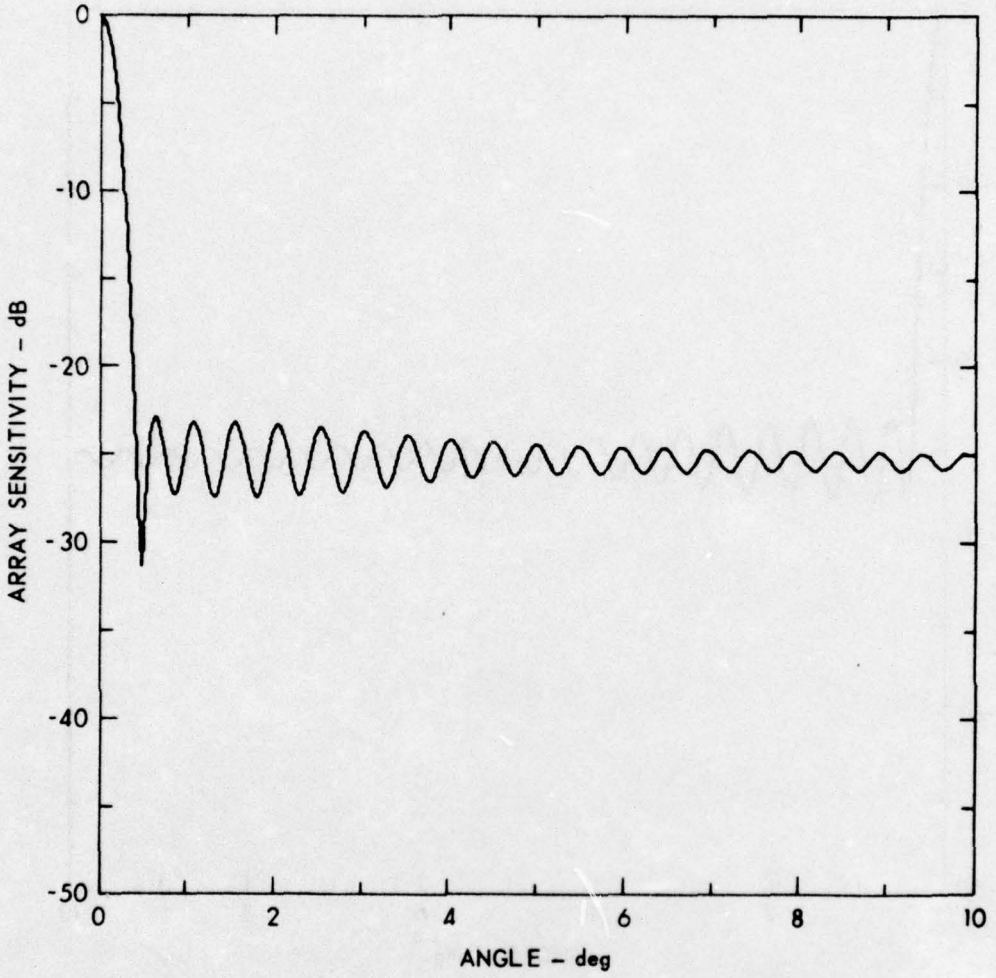

RADIUS = 136.55 λ
RADIUS = 91.44 cm
FREQUENCY (DESIGN) = 224.0 kHz
FREQUENCY (OPERATE) = 223.5 kHz

BEAMWIDTH = 0.2962°
PEAK SLL = –23.0 dB
AVERAGE SLL = –25.3 dB

FIGURE 4-10
BEAM PATTERN AT 223.5 kHz

ARL - UT
AS-75-1211
KM - ORS
9 - 3 - 75

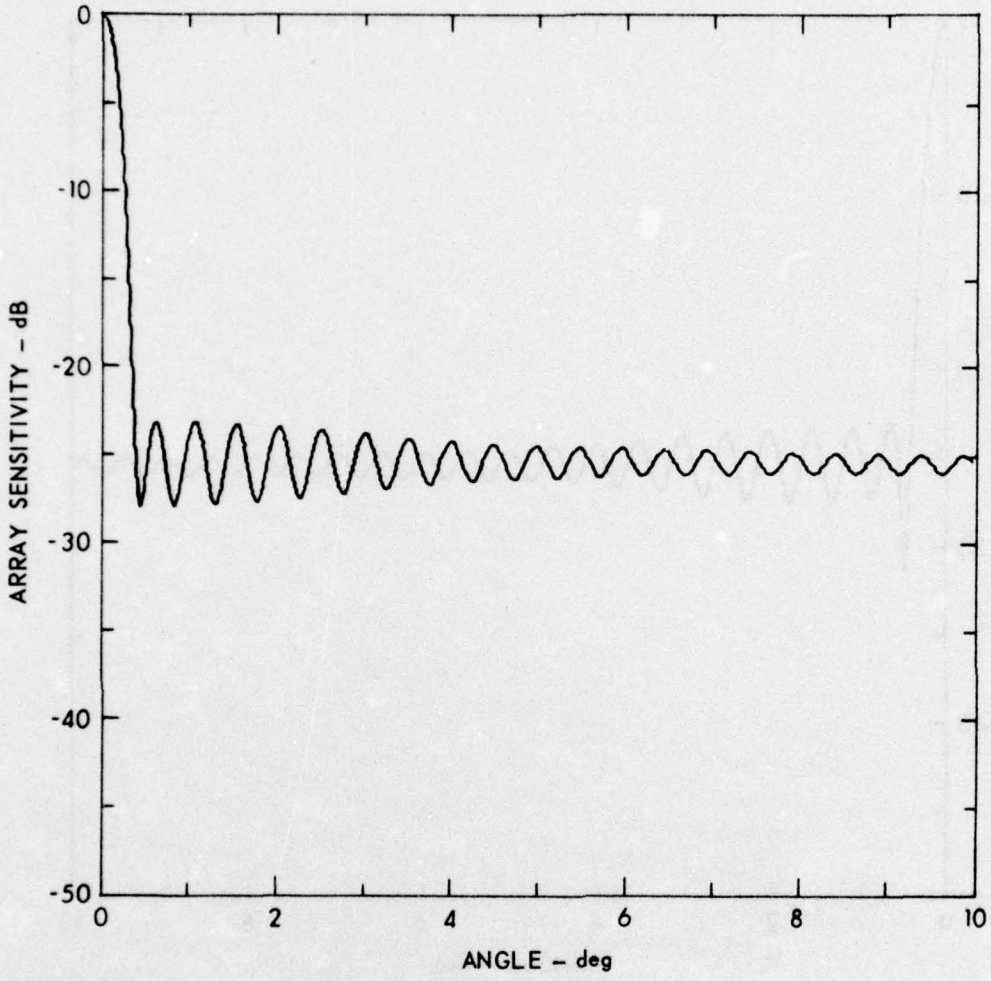

RADIUS = 136.55 λ
RADIUS = 91.44 cm
FREQUENCY (DESIGN) = 224.0 kHz
FREQUENCY (OPERATE) = 224.0 kHz

BEAMWIDTH = 0.2873°
PEAK SLL = – 23.2 dB
AVERAGE SLL = – 25.3 dB

FIGURE 4-11
BEAM PATTERN AT 224 kHz

ARL - UT
AS-75-1212
KM - ORS
9 - 3 - 75

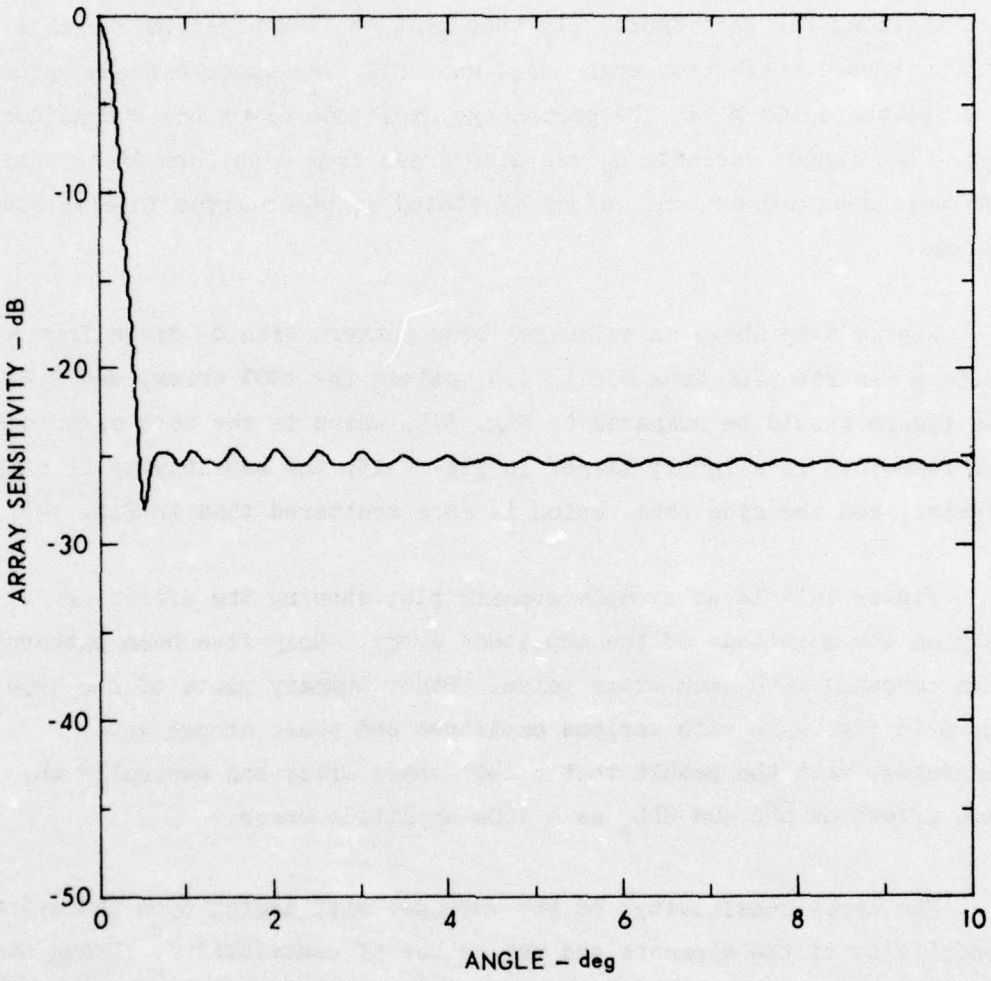

RADIUS = 136.55 λ
RADIUS = 91.44 cm
FREQUENCY (DESIGN) = 224.0 kHz
FREQUENCY (OPERATE) = 224.5 kHz

BEAMWIDTH = 0.2961°
PEAK SLL = –24.6 dB
AVERAGE SLL = –25.3 dB

FIGURE 4-12
BEAM PATTERN AT 224.5 kHz

ARL - UT
AS-75-1213
KM - ORS
9 - 3 - 75

The first test of the effects of error was performed with uniform distributions for the errors. In that test, δ_n was a random variable with uniform distribution whose mean was unity and whose extreme values were 1±X where 100 X was the percentage amplitude error under consideration. The random variable Δ_n was also drawn from a uniform distribution with zero mean and extreme values ±Y stated as phase error in electrical degrees.

Figure 4-13 shows an azimuthal beam pattern with δ_n drawn from a uniform distribution from 0.6 to 1.4, called the ±40% error, and $\Delta_n \equiv 0$. The figure should be compared to Fig. 3-5, which is the zero error case. The beamwidth is slightly larger in Fig. 4-13, the sensitivity is slightly greater, and the side lobe region is more scattered than in Fig. 3-5.

Figure 4-14 is an example summary plot showing the effect of varying the magnitude of the amplitude error. Only five beam patterns were computed with each error value. Other summary plots of the type shown in Fig. 4-14 with various amplitude and phase errors were generated, with the result that a ±40° phase error had generally the same effect on $\overline{SLL}$ and SLL_p as a ±60% amplitude error.

The array sensitivity, on the average, will depend upon the average sensitivity of the elements and the number of contributors. Using the same arguments, the average side lobe level depends upon the incoherent addition of the element's contributions. The variance of the side lobe level grows with element amplitude error but decreases with the number of contributors. The average side lobe level decreases with an increase in the number of contributors. To the first order, then, the variance of the average side lobe level depends only upon the element error, not upon the size, number of elements, or the absolute side lobe level. This statement is demonstrated in Fig. 4-15, which shows two patterns with different numbers of elements (and hence different average side lobe levels) but with the same element error. One can see the side lobe

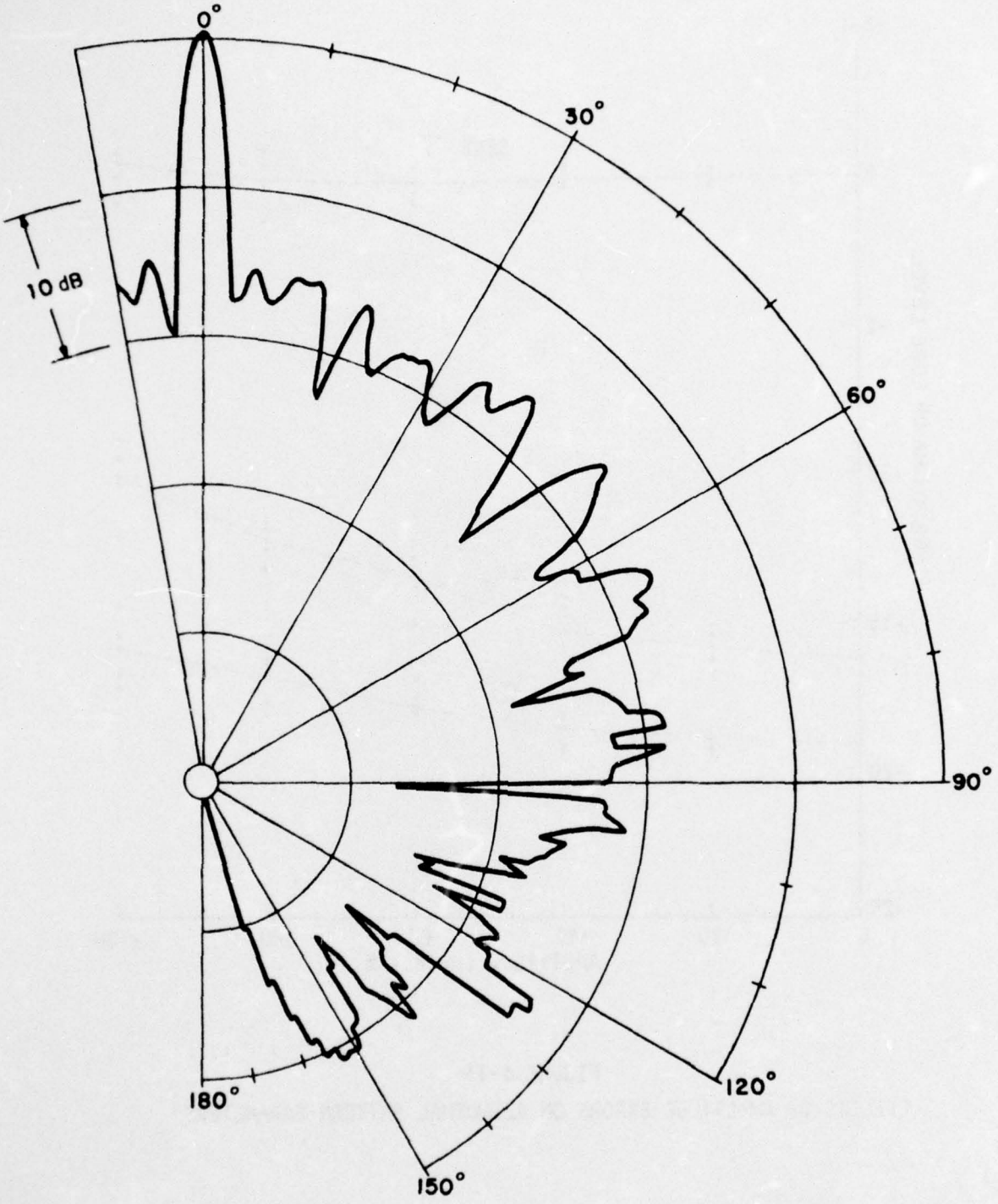

FIGURE 4-13

AZIMUTHAL BEAM PATTERN
POINT ELEMENTS WITH ±40% SHADING ERRORS
R = 12.3 N = 38

AS-74-1703
DAS-0031-3

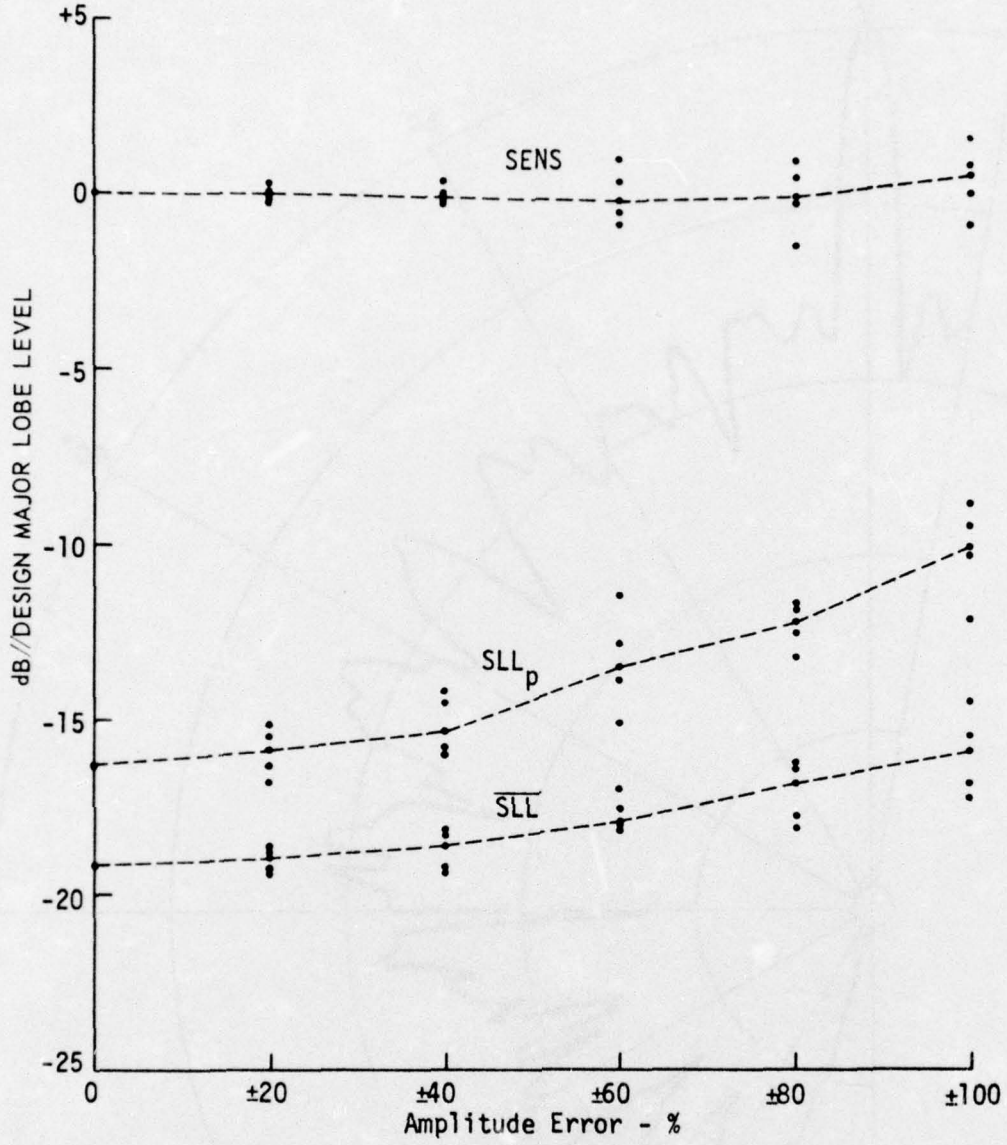

FIGURE 4-14

EFFECTS OF AMPLITUDE ERRORS ON AZIMUTHAL PATTERN PARAMETERS

AS-74-1691
DAS-0031-3

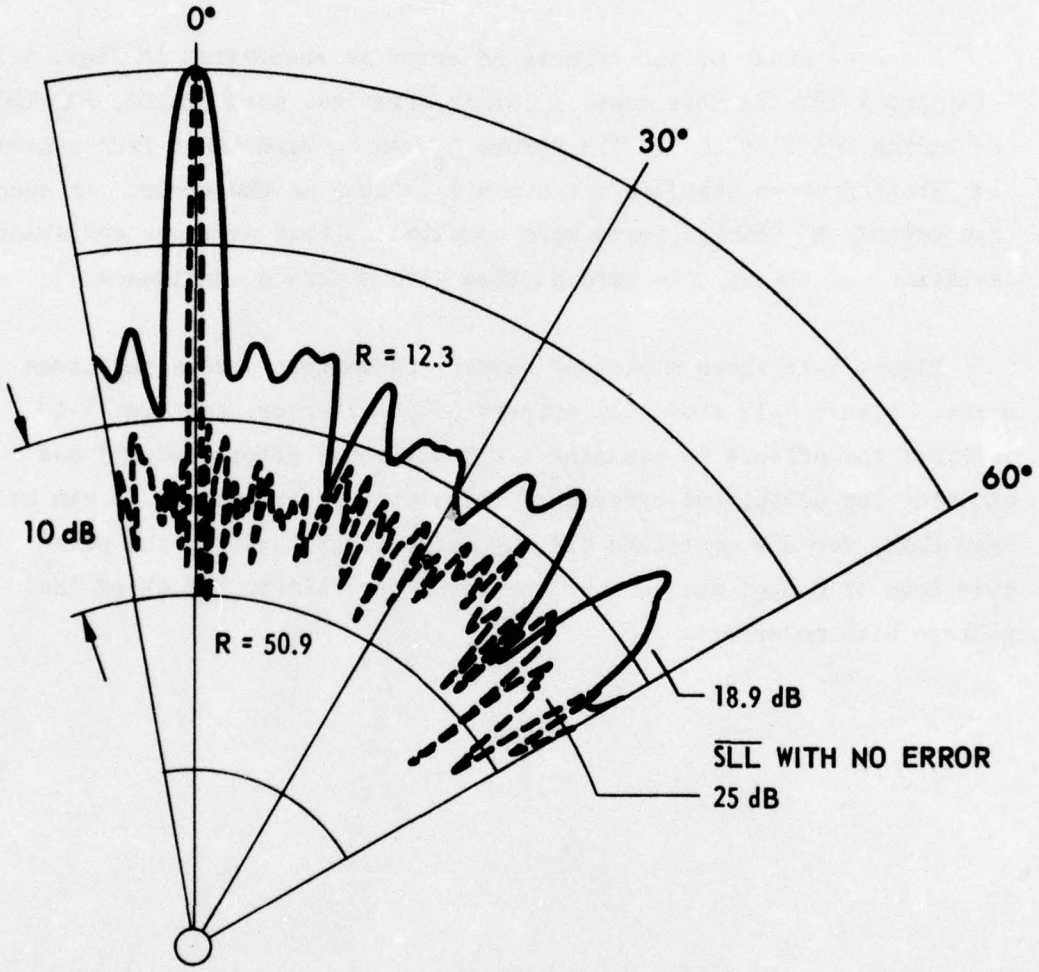

FIGURE 4-15

AZIMUTHAL BEAM PATTERNS FOR TWO DIFFERENT SIZED ARRAYS SHOWING PERCENTAGE SCATTER AROUND PREDICTED AVERAGE SIDE LOBE LEVEL INDEPENDENT OF RADIUS

±40% AMPLITUDE ERROR

ARL - UT
AS-75-379-S
DAS-DR
3 - 19 - 75

variance is nearly constant in the decibel scale. The conclusion that can be drawn from the above argument is that larger arrays with lower side lobe levels do not require the use of a more uniform set of elements.

A second study of the effects of error is summarized in Figs. 4-16, 4-17, and 4-18. In this case, a larger array was used (R=120, $2\alpha_N$=120°, containing 503 elements). The errors δ_n and Δ_n were taken from a normal distribution whose standard deviation is stated as the error. In each case tested, 25 beam patterns were computed so that averages and standard deviations of the effects were plotted with moderate confidence.

Figure 4-16 shows a plot of several parameters versus amplitude error. Figure 4-17 shows the effects of phase error, and Fig. 4-18 combines the effects by assuming a 25% amplitude error (σ=0.25) and plotting the additional effects of increasing phase error. It can be seen that, for 25% amplitude and 10° phase error (σ=10°), the peak side lobe of 80% of the computed patterns fell within 1.5 dB of the pattern with no error.

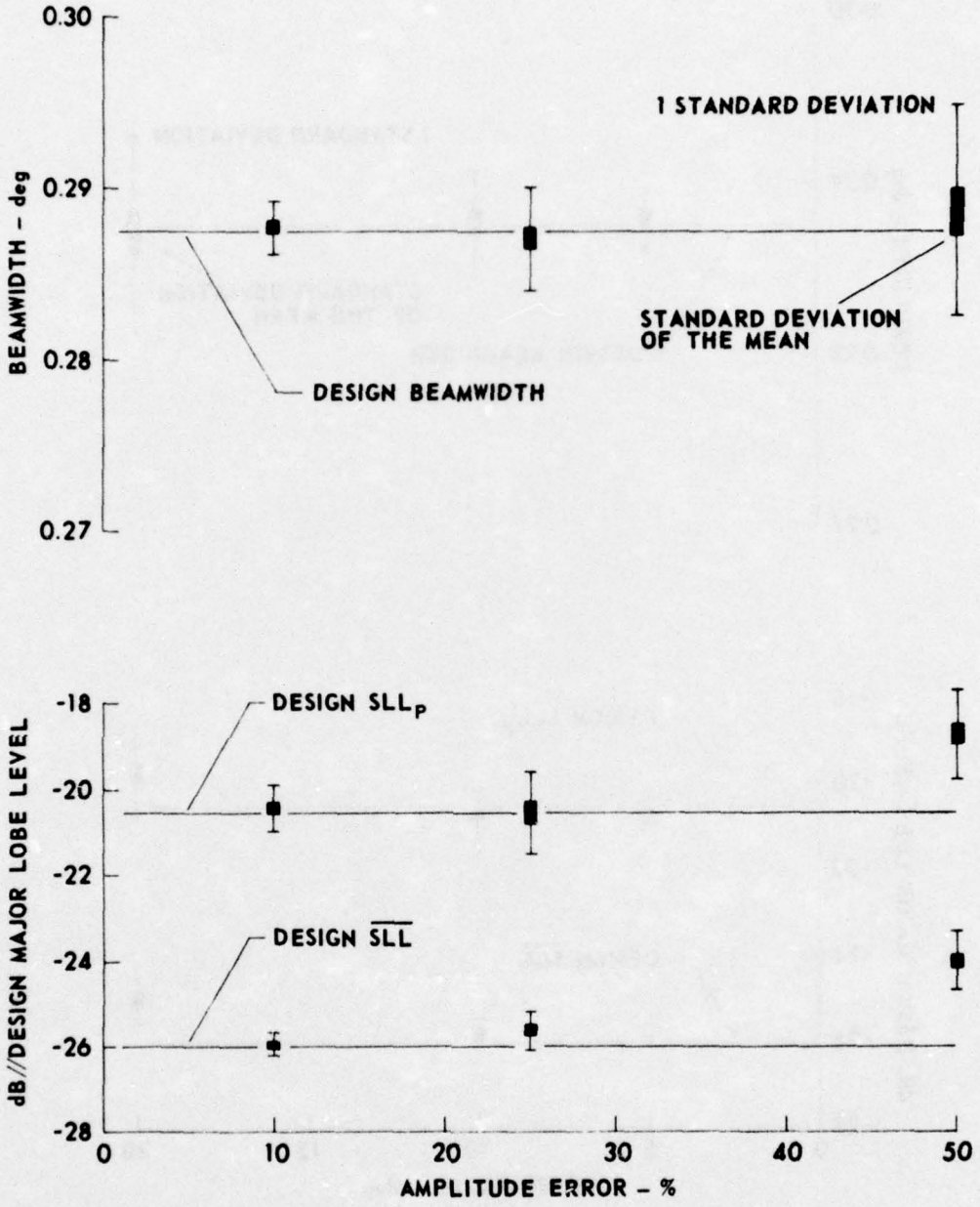

FIGURE 4-16
BEAMWIDTH, SLL$_p$, AND $\overline{SLL}$ VERSUS AMPLITUDE ERROR
RADIUS = 120 λ APERTURE = 120°
TAYLOR: DSLL = 27, $\bar{N}$ = 14

ARL - UT
AS-76-71
DAS - DR
1 - 29 - 76

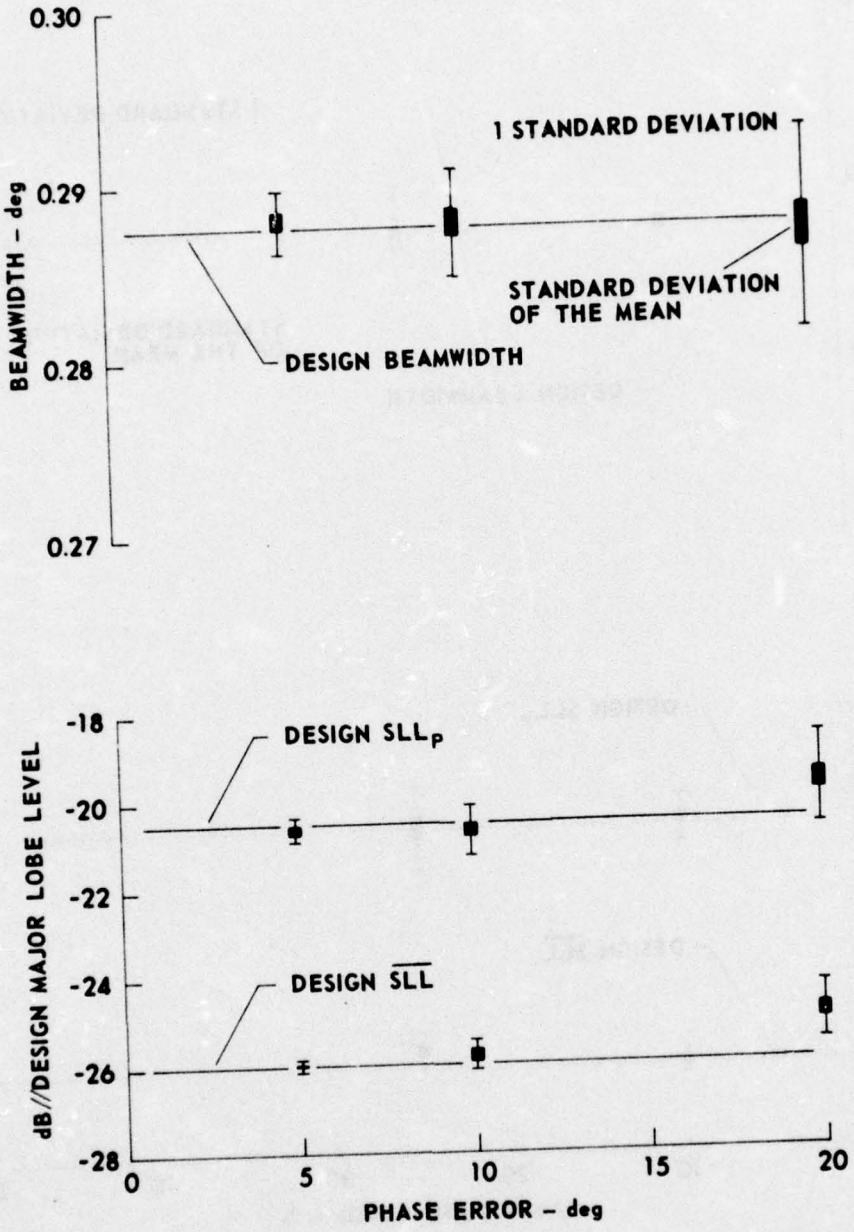

FIGURE 4-17
BEAMWIDTH, SLL$_p$, AND $\overline{SLL}$ VERSUS PHASE ERROR
RADIUS = 120 λ APERTURE = 120°
TAYLOR: DSLL = 27, $\bar{N}$ = 14

ARL - UT
AS-76-72
DAS - DR
1 - 29 - 76

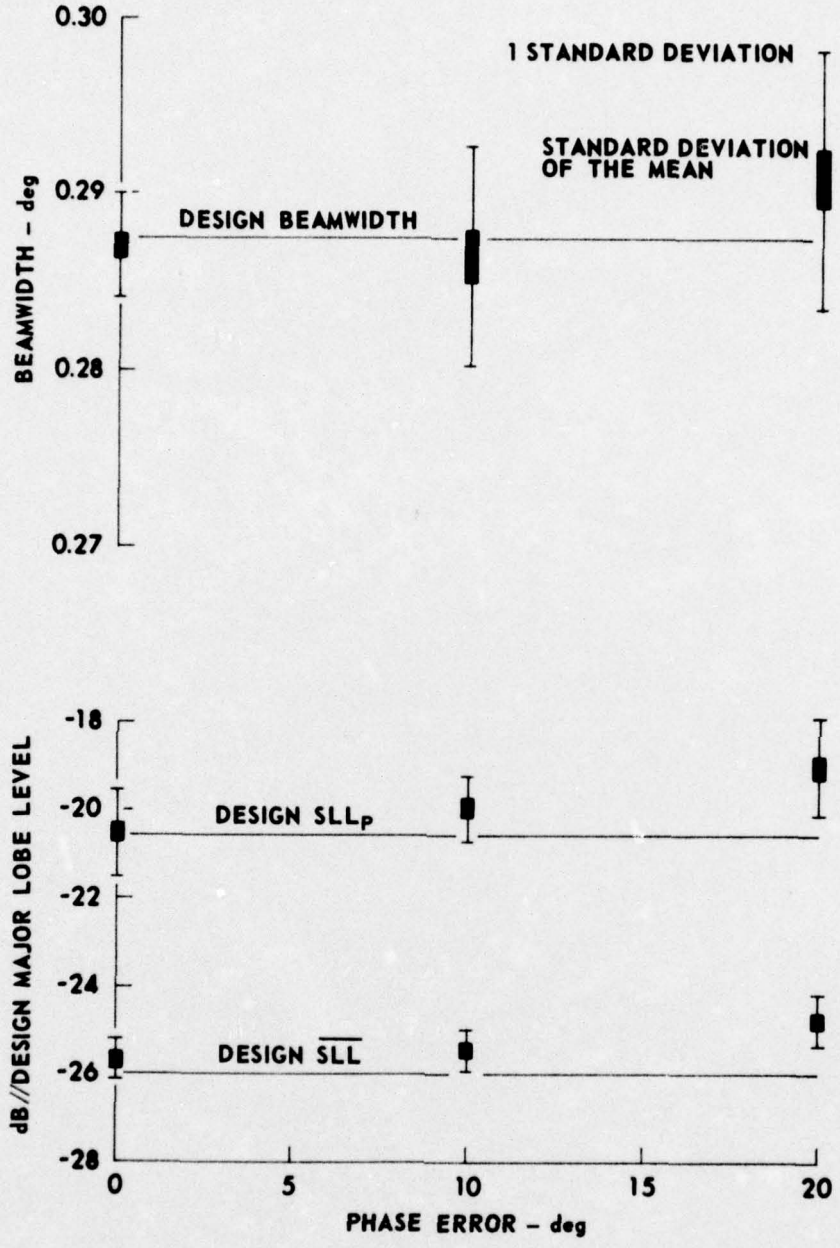

FIGURE 4-18
BEAMWIDTH, SLL_p, AND $\overline{SLL}$ VERSUS PHASE ERROR
WITH 25% AMPLITUDE ERROR

RADIUS = 120 λ APERTURE = 120°
TAYLOR: DSLL = 27, $\overline{N}$ = 14

ARL - UT
AS-76-73
DAS - DR
1 - 29 - 76

V. THE ARRAY FILL TIME PROBLEM AND PROPOSED SOLUTIONS

A. The Fill Time Problem

If an array of sensors used for beamforming subtends some nonzero dimension in the direction of signal propagation, and does not utilize time delay processing, then it will exhibit some array rise time. The effect is caused by the time required for the signal to fully insonify the array. During the rise time, the sensitivity is lower than usual (because not all elements are insonified), and the beamwidth is larger than usual (because only the center section of elements making up a smaller aperture are insonified). This effect is separate and distinct from the effect of signal rise time caused by bandwidth restrictions in the receiver channels.

The solid curve in Fig. 5-1 shows the speed with which the array output level rises as a rectangular pulse insonifies the reference array. The rapid rise and fall of the output level is due mainly to the weight of array elements near the front center which are insonified first and which are first to be uninsonified as the pulse leaves the array. The dashed curve in the figure shows the growth in the aperture W as the pulse comes on the array. The resultant relative beamwidth is related to the reciprocal of the aperture.

Another point of interest in Fig. 5-1 is that the apparent pulse length is very nearly equal to the real pulse length, unelongated by the array. The conclusion is that the range resolution achievable with the simple cylindrical array is, as with other arrays, related to one-half the pulse length.

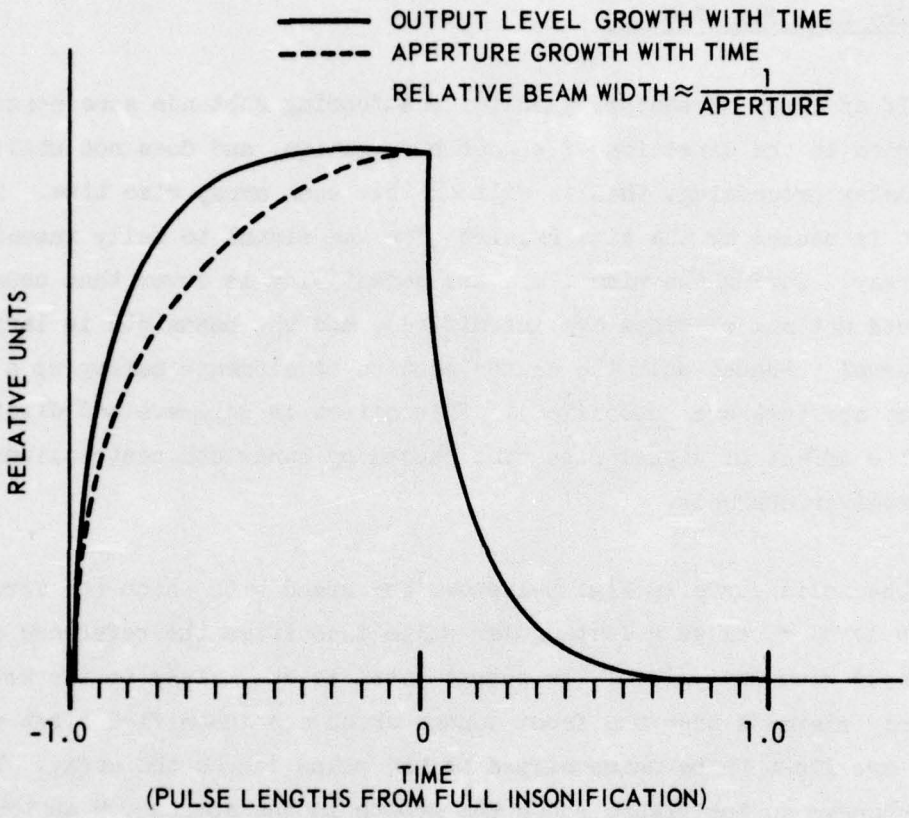

FIGURE 5-1
ARRAY RISE TIME EFFECTS FOR RECTANGULAR CW PULSE OF LENGTH R/f_0 WITH ARRAY RADIUS R AND $2\alpha_N = 180°$

AS-74-1812
DAS-0031-3

If the pulse just covers the array radius (the minimum usable length), the pulse length τ is

$$\tau = \frac{r}{c} = \frac{R}{f} \quad , \tag{5-1}$$

and then the range resolution

$$\Delta x = \frac{c\tau}{2} \tag{5-2}$$

is

$$\Delta x = \frac{c}{2}\frac{R}{f} = \frac{r}{2} \quad . \tag{5-3}$$

Now, the crossrange resolution Δy at a target range ρ yards from a sonar with beamwidth BW degrees is given by

$$\Delta y = \rho BW \frac{\pi}{180} \text{ yards} \quad . \tag{5-4}$$

But, for the correlation beamformer,

$$BW = \frac{K}{2R} \text{ degrees} \quad , \tag{5-5}$$

where K is the aperture constant. This results in the expression

$$\Delta y = \frac{\rho K \pi}{360\ R} \times 3 \text{ feet} \quad , \tag{5-6}$$

for the crossrange resolution. We can now compute the area of a resolution cell at range ρ yd as

$$\text{Area} = \Delta x \Delta y = \frac{cR}{2f} \cdot \frac{\rho K \pi 3}{360\ R} \text{ ft}^2 \quad , \tag{5-7}$$

$$\text{Area} = \frac{\rho}{f} \text{ x(constant)} \quad . \tag{5-8}$$

The point is that the area of a resolution cell is independent of the array size. That is, as one constructs larger arrays to achieve better crossrange resolution, the pulse length must grow to cover the larger array, with the result that the resolution area at some range ρ remains constant.

In summary, if the sonar designer wishes a system with pulse length PL (seconds) and beamwidth BW (degrees) operating at frequency f_o (hertz), and if the product

$$f_o * PL * BW \geq 30 \quad , \tag{5-9}$$

he can use the correlation beamformer with a simple rectangular CW pulse and $2\alpha_N = 180°$. The array diameter will be

$$2r = \frac{2Kc_o}{BWf_o} \text{ feet} \quad . \tag{5-10}$$

If, on the other hand,

$$f_o * PL * BW < 30 \quad , \tag{5-11}$$

then the required pulse length will be too short for the array. This represents the rise time problem for the correlation array, and two solutions are presently recognized as possible. They are (1) reduction of the depth of the array by reducing $2\alpha_N$ or, (2) utilizing a coded pulse transmission and performing a replica correlation on the receiving array. The two methods will be treated separately in the following two sections.

B. The First Solution--Reduced Sector of Elements in the Aperture

One suggested solution to the rise time or range resolution problem is to reduce the sector of active elements on the cylinder. Normally, $2\alpha_N \cong 180°$, which means that a pulse must be long enough to insonify the

radius of the array for on-axis targets. If the sector angle $2\alpha_N$ were reduced, the pulse length required to insonify the array would be reduced. However, a disadvantage of this procedure is the attendant reduction in the effective beamforming aperture W if R is not increased with a reduction in L.

The depth of aperture is given by

$$L = R(1 - \cos \alpha_N) \quad . \tag{5-12}$$

The effective beamforming aperture W is given by

$$W = 2R \sin \alpha_N \quad , \tag{5-13}$$

where α_N is one-half the total angular sector of elements on the array.

Equations (5-12) and (5-13) can be rewritten to show the ratios

$$\frac{L}{R} = 1 - \cos \alpha_N \tag{5-14}$$

and

$$\frac{W}{2R} = \sin \alpha_N \quad , \tag{5-15}$$

and to illustrate how these ratios depend upon α_N.

Now, if one wishes to decrease L in order to shorten the apparent pulse length while preserving the beamwidth, then one must solve both Eqs. (5-12) and (5-13) simultaneously. Solving Eq. (5-13) for R yields

$$R = \frac{W}{2 \sin \alpha_N} \quad . \tag{5-16}$$

Substituting Eq. (5-16) into Eq. (5-12) yields

$$L = \frac{W}{2}\left(\frac{1 - \cos \alpha_N}{\sin \alpha_N}\right) \quad , \tag{5-17}$$

which illustrates the reduction in L achievable by reducing α_N. Figure A-4 in Appendix A is a plot of the angle function expressed in Eq. (5-17). By entering that plot with the required fractional reductions in L below the original R value, the corresponding angle α_N can be obtained. This angle can then be substituted into Eq. (5-16) to find the new value of R.

Small reductions in L below the $2\alpha_N=180°$ value can be accomplished with little increase in R; however, further reductions in L lead finally to alarming increases in R.

This method of resolving the array rise time problem is rather limited and is costly in other areas as well as those discussed above. For example, there is an increase in the number of elements/staves and associated preamplifier channels required when several preformed beams are considered. Appendix A contains a discussion of these areas and other associated factors when the sector of active elements is reduced, for whatever reason.

C. The Second Solution--A Coded Pulse Transmission and Replica Correlation at the Receiving Array

Because the array has depth in the direction of signal propagation, it can be used as a correlator. Correlation is normally implemented with some sort of delay element (delay line, shift register, etc.) and a summer. We recognize that the delay element in our case is the array itself, with the signal propagating past the array at the speed of sound. Since the array has depth L, it can simultaneously sample as many as L cycles of the signal. In the reference array case, $2\alpha_N=180°$, and L=R.

In Fig. 5-2, we imagine the array as being collapsed on the x-axis, occupying the region from the origin (the array center) out to R (in wavelengths). The leading edge of the pulsed signal begins at g distance from the origin at time t. The signal description is $S(\tau)$ in a moving

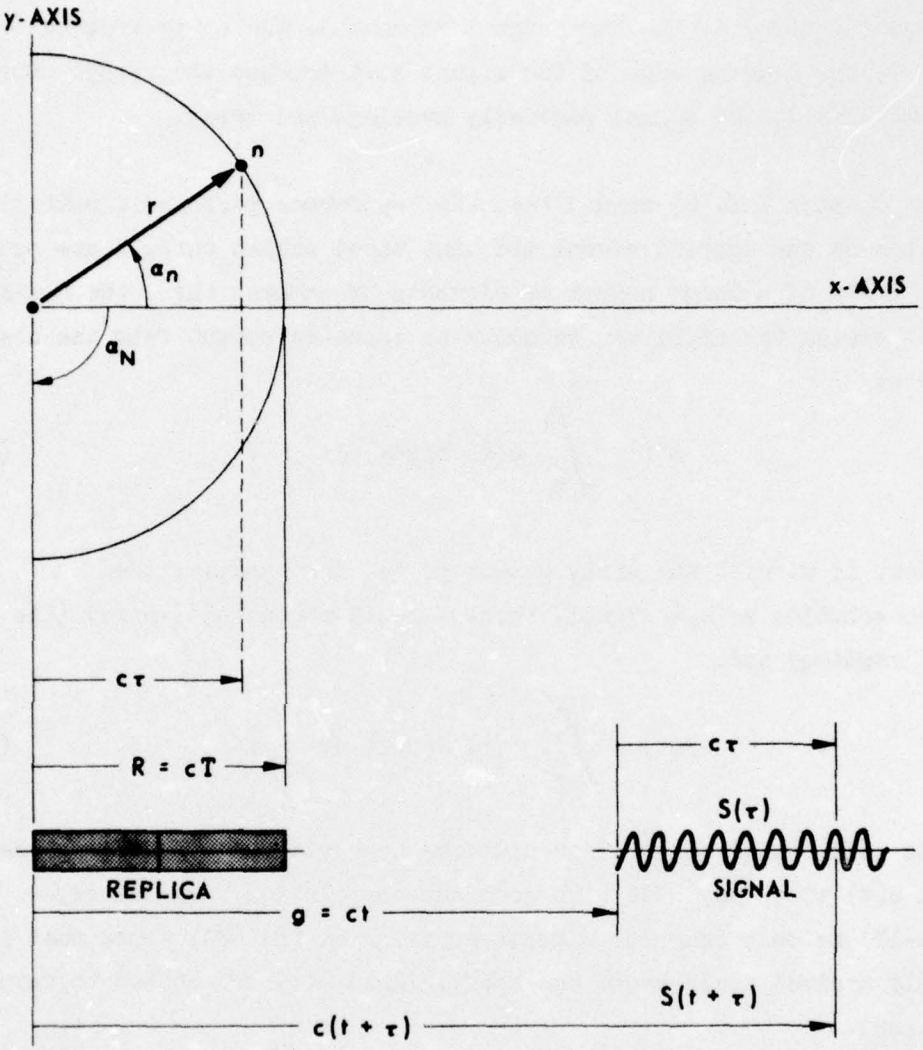

FIGURE 5-2
REPLICA-CORRELATION GEOMETRY

ARL - UT
AS-76-62
DAS - DR
1 - 28 - 76

coordinate system, or $S(t+\tau)$ in the array centered system. Imagine t time running down, so that the signal approaches the array from the right. When t=T, the leading edge of the signal just touches the array. During the time $-T<t<T$, the signal partially overlaps the array.

In Chapter III, we argued that the beamformer performs a multiply operation on the sampled signal and that these scaled outputs are summed. In the limit of a large number of elements or samples then, the moving signal passing the array can be shown to cause an output from the beamformer of

$$E(t) = \int_{o}^{\tau} A(\tau)\ S(t+\tau)\ d\tau \quad . \tag{5-18}$$

Now, if we wish the array output to be, for example, the self-convolution of the signal, then we could choose $A(\tau)=S(\tau)$, (the signal replica) and

$$E(t) = \int_{-\infty}^{\infty} S(\tau)\ S(t+\tau)\ d\tau \quad . \tag{5-19}$$

In this case, pulse compression could be accomplished by choosing the signal $S(\tau)$ to be any code with good autocorrelation. Of course, Eq. (5-18) is only true for signals arriving on the MRA, since that is the only arrival angle where the coefficients $A(\tau)$ are chosen to match the signal.

Now, several complications arise in practice because the angular response of the array must also be considered. It is conjectured that if the coded pulse is fully incident on the array, that is, t=0, and the pulse is phase coded digitally so that the carrier wavelength is constant throughout the pulse, the resultant fully insonified azimuthal beam pattern will not be too different from the long CW signal case. This conjecture allows us to separate the time and angle response of the array during the

design phase, and then to test the conjecture by computer trial. An example will be presented later.

In view of the conjecture, one can first design the azimuthal pattern with a long CW pulse and determine the shading coefficients as described in Chapters III and IV [they are $A(\alpha_n)$]. These coefficients expressed in the time domain are $A(\tau)$ and are seen to be quite different from $S(\tau)$. This, then, is the major problem with choosing a suitably coded pulse; that is, Eq. (5-18) becomes

$$E(t) = \int_0^\tau A'(\tau)\, S(\tau)\, S(t+\tau)\, d\tau \quad , \tag{5-20}$$

where

$$A'(\tau)\, S(\tau) = A(\tau) \quad . \tag{5-21}$$

Equation (5-20) is no longer a simple self-convolution, like Eq. (5-19), but a complicated crosscorrelation with a highly asymmetric window function, $A'(\tau)$. The object then is to find a phase coded pulse $S(\tau)$ such that the $E(t)$ has the appropriate pulsewidth with low time side lobes.

At this point in the study, no organized method of determining $S(\tau)$ has been found. A trial and error approach, modified somewhat by intuition, has led to a code class that shows promise, but is surely not optimum. The following paragraphs outline the code selection procedure, and the results of computer trials are shown in the form of contour maps of $E(\varphi,t)$, showing the composite time and angle response of the array with various signal types. The first section will consider an uncoded, short, CW pulse with rectangular envelope. The major difficulty with rectangular envelopes will be described. The second section will consider a phase coded, triangular envelope, CW pulse, which exhibits the desired pulse compression.

1. The Rectangular Envelope CW Pulse

Consider a signal $S(\tau)$ with rectangular envelope of length $(T/2)+\epsilon$ sec, which is to cover the front 120° of elements on a cylindrical array of radius R. The signal envelope

$$|S(\tau)| = 1 \text{ when } \frac{T}{2} \leq \tau \leq T + \epsilon \quad , \tag{5-22}$$

where ϵ will be explained later, and

$$|S(\tau)| = 0 \text{ otherwise.} \tag{5-23}$$

When the signal is full on the array, t=0 and, aligned to φ_o=0, the signal replica factor $A_1(\alpha)$ can be found as shown in Chapter III. As can be seen from Fig. 5-2, when t=0,

$$r \cos \alpha = c\tau \quad , \tag{5-24}$$

which leads to

$$\tau = T \cos \alpha \tag{5-25}$$

and

$$\alpha = \arccos \frac{\tau}{T} \quad . \tag{5-26}$$

These relations allow the change of coordinates required to change

$$A_1(\alpha) = |S(\alpha)| \cos[2\pi R(1 - \cos \alpha)] \tag{5-27}$$

to

$$A_1(\tau) = |S(\tau)| \cos[2\pi R(1 - \frac{\tau}{T})] \quad . \tag{5-28}$$

Following the development shown in Chapter III.A.2., the sensor density corrector can be found. Equation (3-10) shows the effect of the element density alone. Actually, we should include the envelope of the

signal and A_1 in the sensor density corrector. Thus

$$|A_1(Y)|\ |S(Y)|\ \frac{q}{dY}$$

represents the effective A_1* signal aperture function. Of course, in this case

$$|A_1(\tau)| = |S(\tau)| = 1$$

so that, just as in Chapter III,

$$A_2(\alpha) = \cos \alpha$$

since it causes

$$|A_1(Y)|\ |S(Y)|\ \frac{q}{dY}\ A_2(Y) = \text{constant}.$$

$A_3(Y)$ is the aperture window function and, in the reference array, was chosen to be a "house top," $\sqrt{1-(Y/R)^2}$, which leads to $A_3(\alpha)=\cos \alpha$. In our present case, we let $A_3(Y)$ be a Taylor shading function with a design side lobe level of 27 dB and $\bar{N}=14$. This function is reflected back to the cylinder and sampled to obtain $A_3(\alpha)$. The Taylor function and its reflection to the cylinder are too complicated to present here; however, the method should be clear.

Now, the considered array is R=120 and $2\alpha_N=120°$, with 503 point elements spaced $\lambda/2$ apart, the signal is a cosinusoid with rectangular envelope as described previously, and the coefficients are selected as described above. The resulting azimuthal beam pattern is shown in Fig. 5-3. It will be remembered that the pulse is ϵ sec longer than the depth of active elements. In this case, the pulse was 5 cycles longer than the array depth (60 λ), giving a total pulse time duration of 325 μsec. The stated time in the figure is time from first signal insonification on the array and is one pulse length different from the t time in Fig. 5-2.

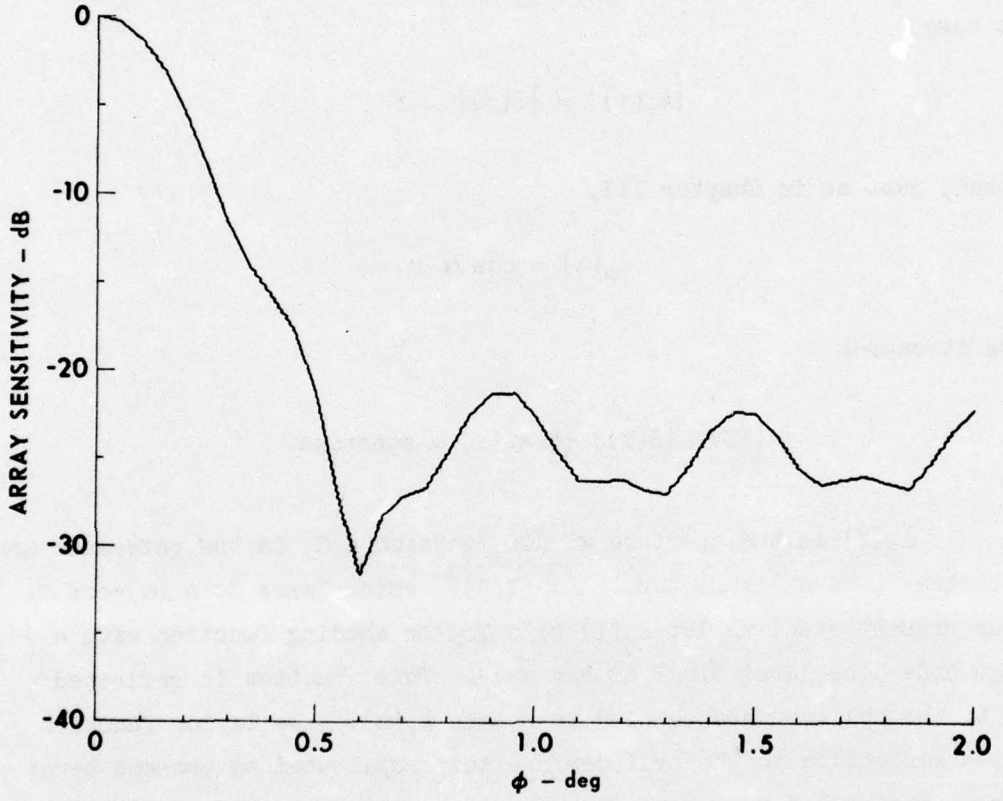

FIGURE 5-3
BEAM PATTERN
TIME: 325.0
SIGNAL - NO PHASE CODE

ARL - UT
AS-76-70
DAS - DR
1 - 28 - 76

Therefore, the time indicated on the plots τ is related to t time by

$$\tau = \frac{T}{2} - t \quad . \tag{5-29}$$

Also, as t time runs down, τ time increases. Of course, full insonification occurs during the time duration ϵ from

$$0 \geqq t \geqq -\epsilon \quad , \tag{5-30}$$

or

$$\frac{T}{2} \geqq \tau \geqq \frac{T}{2} + \epsilon = 325 \ \mu\text{sec} \tag{5-31}$$

for this case.

Figure 5-3 thus represents a fully insonified beam pattern. The 3 dB beamwidth is less than 0.3° (0.2988°), and the minimum side lobe suppression is 21.27 dB.

Figure 5-4 shows the time response of the uncoded pulse case for the signal arriving on the major lobe, or from the φ_o=0 direction. The plot starts at τ=25 μsec, where the signal is already 5 cycles into the array, and at that time the array response is already within 10 dB of the peak response.

Questions such as "What is the beamwidth of the azimuthal pattern when the pulse is partially on the array?" or "What is the time duration of some particular side lobe?" can be answered by combining beam patterns measured at many different τ times into a contour map of the array response as a function of τ time and φ angle. Figure 5-5 is such a contour map. It is instructive to compare Figs. 5-3 and 5-4 with Fig. 5-5, inasmuch as they are simply cuts from the contour map at τ=325 μsec and at φ=0. All response parameters of interest can be read from a plot of the type shown in Fig. 5-5.

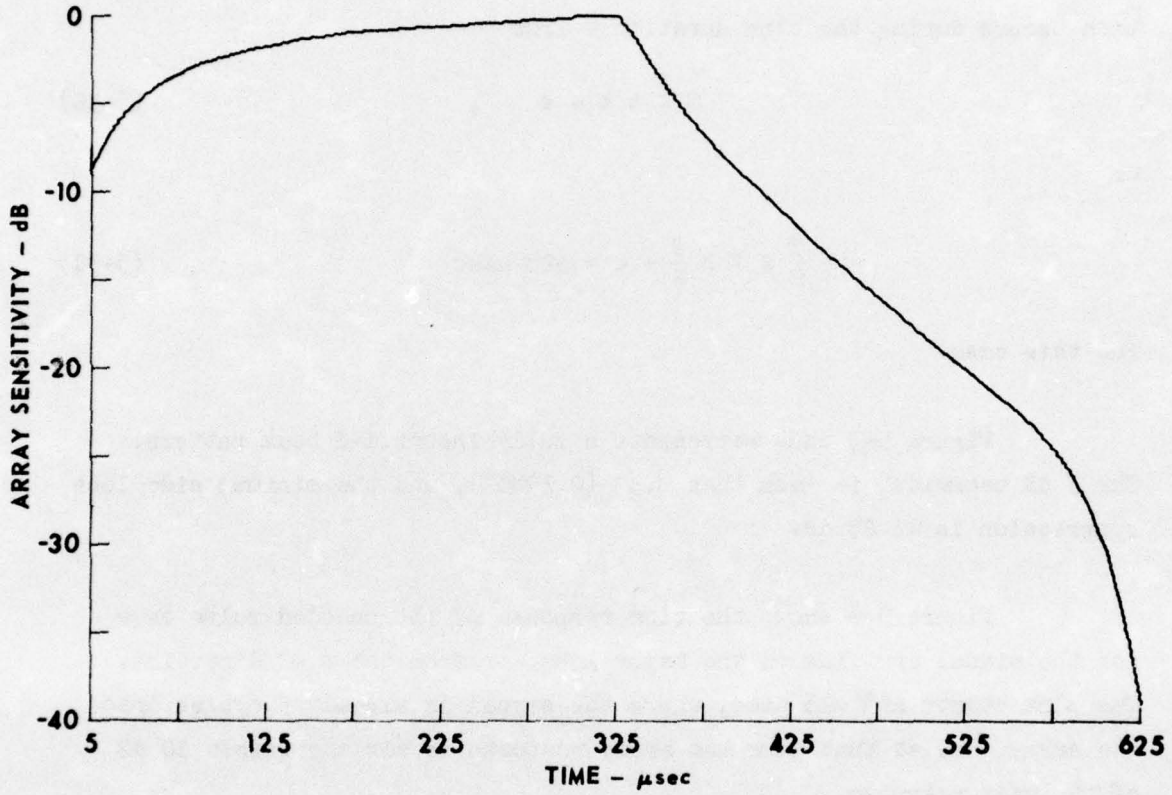

FIGURE 5-4
TIME FUNCTION
$\phi = 0$
SIGNAL – NO PHASE CODE

ARL - UT
AS-76-69
DAS - DR
1 - 28 - 76

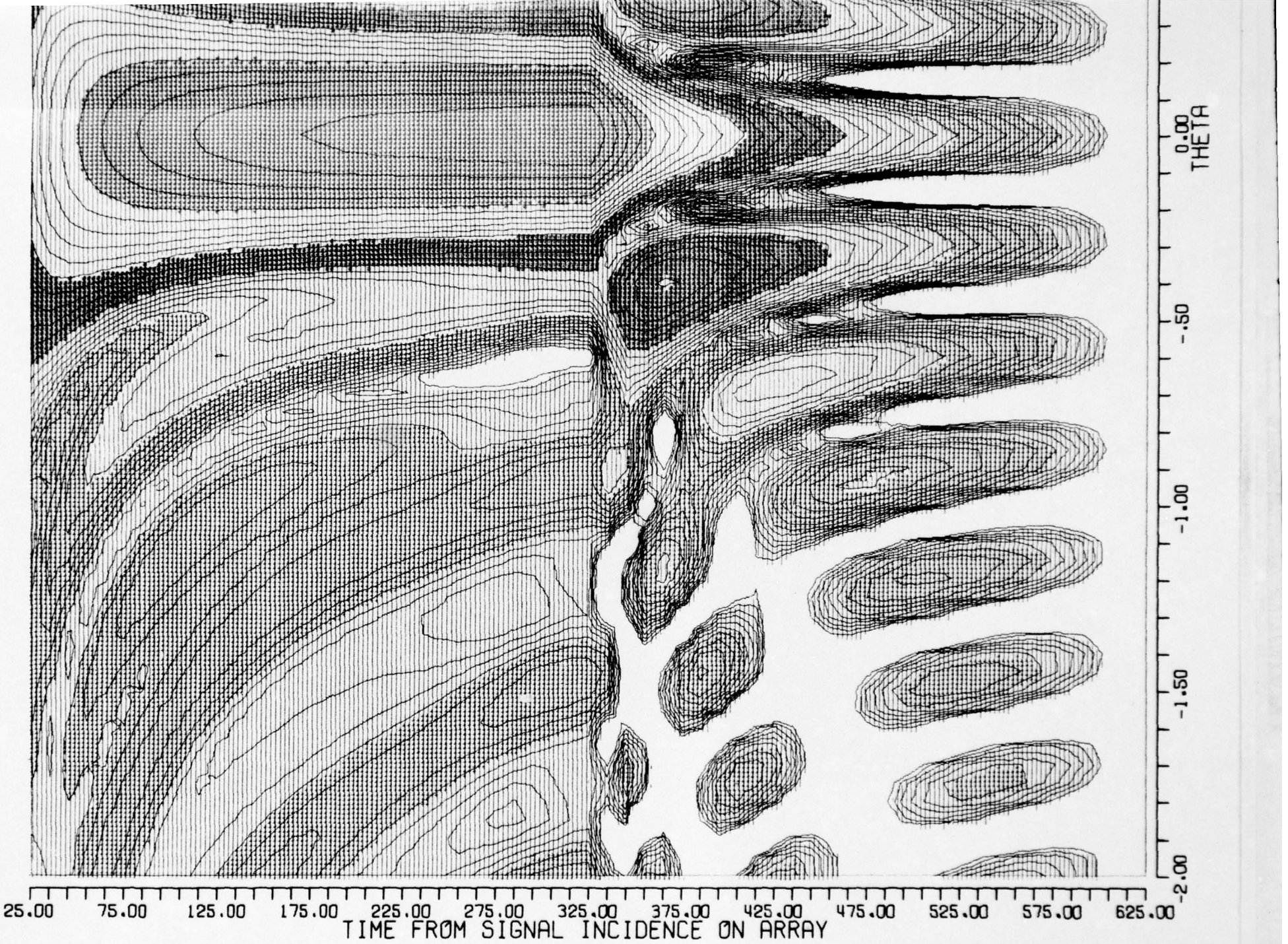
0.00
-.50
-1.00
-1.50
-2.00
THETA
25.00
75.00
125.00
175.00
225.00
275.00
325.00
375.00
425.00
475.00
525.00
575.00
625.00
TIME FROM SIGNAL INCIDENCE ON ARRAY

0 TØ	5.000
5.000 TØ	10.000
10.000 TØ	15.000
15.000 TØ	20.000
20.000 TØ	25.000
25.000 TØ	30.000

ARRAY SENSITIVITY – dB
BLACK LINES EACH 1 dB
COLOR CHANGES EACH 5 dB

FIGURE 5-5
TIME-ANGLE BEAM PATTERN
CONTOUR MAP FOR UNCODED PULSE

ARL - UT
BS-76-75
DAS - DR
2 - 2 - 76

So far in this chapter no attempt has yet been made to use pulse compression. The previous paragraphs serve only to introduce notation and plotting format, and to show the resulting response if no pulse compression is utilized. If a shorter effective pulse length is required at the same beamwidth and, therefore, array size, then pulse compression will be necessary. In spite of the possible existence of many code classes which will achieve useful pulse compression on a cylindrical array, only one has so far been found. It will be described in the following paragraphs.

2. The Triangular Envelope--Phase Coded Pulse

The object of pulse compression is twofold. First, the apparent pulse length out of the beamformer is required to be shorter than the real pulse length in the water. Second, it is required that at all other times (other than the peak) the response be less than some level (the time side lobe level).

When phase coded pulses were first investigated, it was found that the first time side lobe could not be adequately controlled by phase changes. Apparently the reason was that a rectangular pulse (large amplitude at the beginning) and the array with large weights concentrated near the leading edge combined to cause a large output as the pulse entered the array. Of course, we would like the array response to remain low until the pulse covers the array. This early response peak or time side lobe can be controlled by utilizing a triangular envelope signal. The slowly increasing signal strength gives sufficient time for phase changes to be effective in controlling the resulting time side lobes.

Given a triangular envelope for the signal, the next step was to determine the locations of 180° carrier phase shifts that would keep time side lobes within bounds and allow the peak response to remain up for a useful time. This selection was accomplished empirically, essentially a trial and error approach. If only two phase changes are allowed, and the code is represented by 13 equal time increments or bits, then the

best code found is

$$++++--+++++++ \quad , \tag{5-32}$$

which shows that the phase changes occur after the fourth and sixth bits.

If we apply such a coded pulse to the previous case of R=120, $2\alpha_N$=120°, and 503 elements spaced $\lambda/2$ apart at f_o=200 kHz, we find that the active depth of array is R cos α_N = 60. If we let ϵ be the time required for 5 extra cycles, the total pulse length can be broken into 13 equal time segments or bits of 5 cycles each. The duration of each bit (5 cycles) sets the transmitter and receiver bandwidth required to reproduce the signal.

Figure 5-6 shows a time plot (upper) of the unfiltered phase coded pulse of 325 μsec length. Just below is shown the time plot of a filtered version (simulating the composite transmitter and receiver bandwidth of 32 kHz) of the same coded pulse. It is slightly delayed and elongated by the filter. Let $S(\tau')$ represent the unfiltered signal and $S'(\tau')$ represent the filtered waveform. The shading coefficients will now be computed and the results shown.

The signal replica $A_1(\tau)$ can be found by setting

$$A_1(\tau) = S'(\tau') \tag{5-33}$$

where the relationship between τ and τ' is most important and is responsible for the signal placement on the array at the time of maximum response. Let us choose

$$\tau' = \tau - \frac{T}{2} + \epsilon \quad , \tag{5-34}$$

making t=0 for the time of maximum response, as shown in Fig. 5-7. In the case under consideration

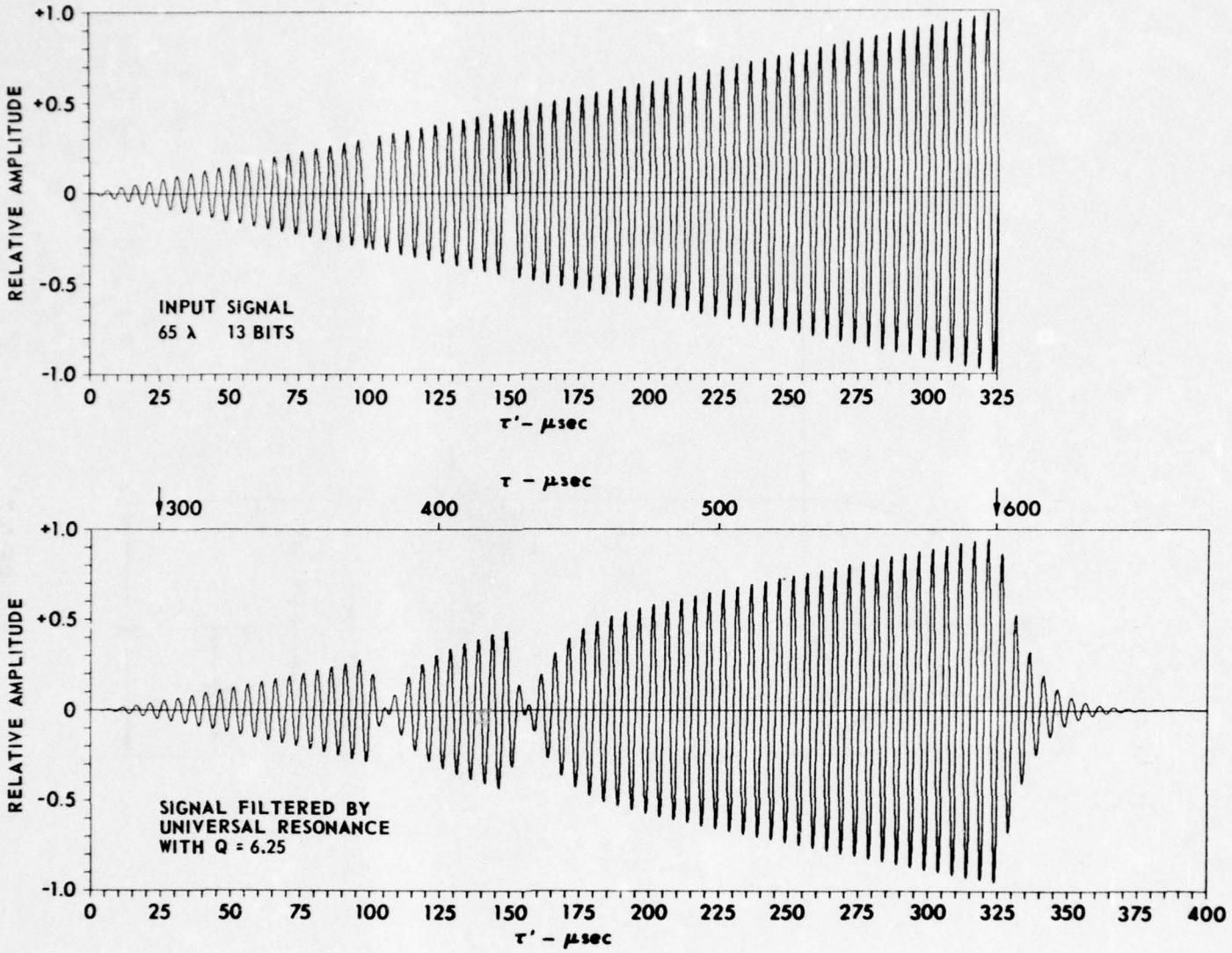

FIGURE 5-6
CODED SIGNAL PULSE WAVEFORM
BEFORE AND AFTER FILTERING

ARL - UT
AS-76-41
DAS - DR
1 - 13 - 76

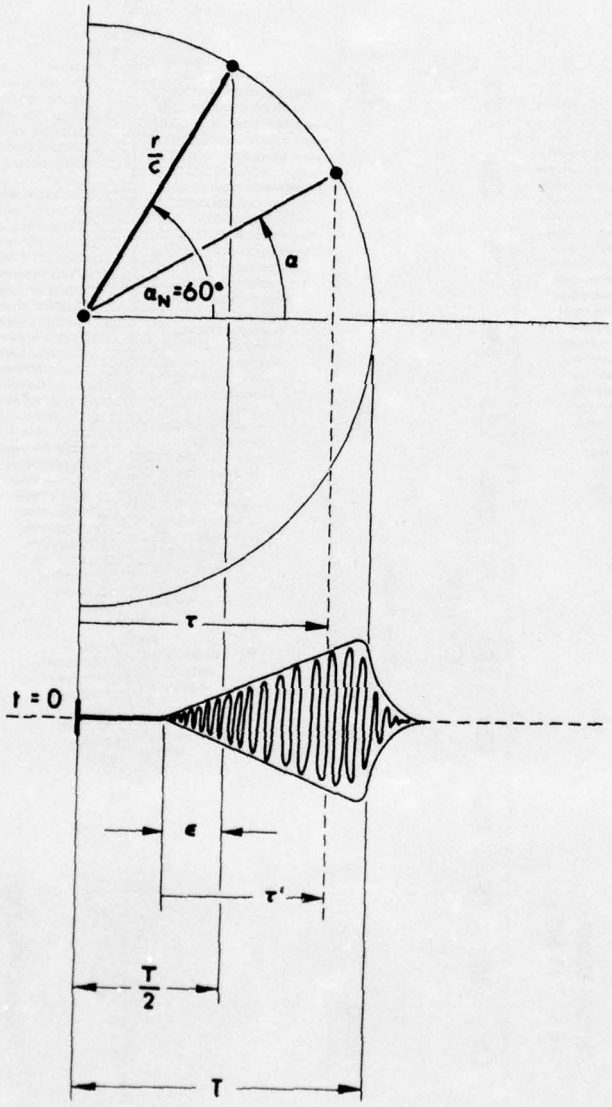

FIGURE 5-7
REPLICA-CORRELATION GEOMETRY
FOR CODED WAVEFORM

ARL - UT
AS-76-63
DAS - DR
1 - 28 - 76

$$\frac{T}{2} = 300 \ \mu\text{sec} \quad , \tag{5-35}$$

and ϵ is the time required for 5 cycles. Therefore,

$$\epsilon = 25 \ \mu\text{sec} \tag{5-36}$$

and

$$\tau' = \tau - 275 \ \mu\text{sec} \quad . \tag{5-37}$$

The upper scale in the lower plot of Fig. 5-6 illustrates the relationship between τ and τ' at t=0, the time of maximum response. Also, the arrows at τ=300 and τ=600 show the portion of the signal incident on the array at t=0.

The array is cylindrical with equally spaced elements, so that the element density along the W line is, as before,

$$\frac{q}{dY} = \frac{q}{d\alpha} \frac{1}{R \cos \alpha} \quad . \tag{5-38}$$

But this time, the signal envelope and A_1 envelope are not constant in time. We should use the detailed envelope of the filtered signal $S'(\tau')$; however, because of its complexity, we will say that the signal has an average envelope like $S(\tau')$, which is

$$|S(\tau')| = \frac{\tau'}{\frac{T}{2} + \epsilon} \quad , \tag{5-39}$$

when

$$0 \leq \tau' \leq \frac{T}{2} + \epsilon \quad . \tag{5-40}$$

By using Eqs. (5-33) and (5-34), Eq. (5-39) becomes

$$|A_1(\tau)| = \frac{2\tau - T + 2\epsilon}{T + 2\epsilon} \quad , \tag{5-41}$$

AD-A033 113 TEXAS UNIV AT AUSTIN APPLIED RESEARCH LABS F/G 17/1
THE CORRELATION BEAMFORMER -- A METHOD OF BEAM CONTROL WITHOUT --ETC(U)
OCT 76 D A SMITH N61339-74-C-0031
UNCLASSIFIED ARL-TR-76-2-REV NL

2 OF 3
AD A033113

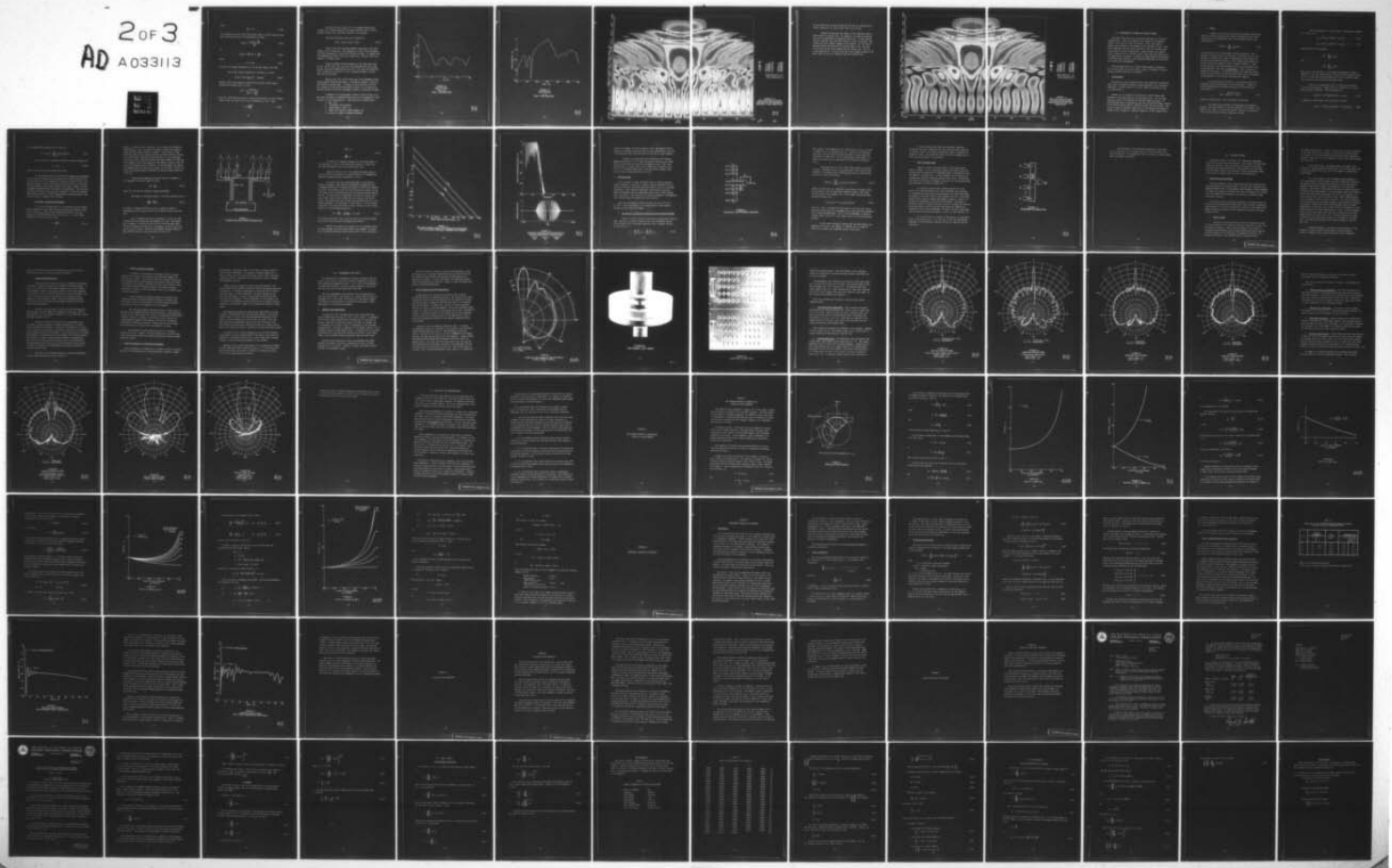

where

$$\frac{T}{2} \leq \tau \leq T \quad . \tag{5-42}$$

If we divide by T in Eq. (5-41) and use the value of T and ϵ except in the first term where $\tau/T=\cos\alpha$ is substituted, we obtain

$$|A_1(\alpha)| = \frac{2\cos\alpha - \frac{11}{12}}{\frac{13}{12}} \quad , \tag{5-43}$$

or

$$|A_1(\alpha)| = \frac{24}{13}\left(\cos\alpha - \frac{11}{24}\right) \quad , \tag{5-44}$$

where

$$0 \leq \alpha \leq 60° \quad . \tag{5-45}$$

Of course, the signal description on τ in the same range is the same.

Now we have enough information to determine A_2 so that

$$|A_1(Y)|\ |S(Y)|\ \frac{q}{dY} A_2(Y) = \text{constant.} \tag{5-46}$$

From Eq. (5-44), ignoring the constant factor, and Eq. (5-38), again ignoring the constant factor, we have

$$A_2(\alpha) = \frac{Q\cos\alpha}{\left(\cos\alpha - \frac{11}{24}\right)^2} \quad , \tag{5-47}$$

where Eq. (5-46) has been couched in terms of α and where Q is the constant in Eq. (5-46), but which we will use to normalize A_2 at $\alpha=0$. Thus,

$$Q = \left(\frac{13}{24}\right)^2 \quad . \tag{5-48}$$

Now $A_3(\alpha)$ will be chosen, as in the example without pulse coding, to be a Taylor function with design side lobe level of 27 dB and $\bar{N}=14$ on the W line, and then reflected to the cylinder.

The total coefficients can now be computed by

$$A(\alpha) = A_1(\alpha) * A_2(\alpha) * A_3(\alpha) \quad . \tag{5-49}$$

Figure 5-8 is the resulting azimuthal beam pattern with pulse coding at t=0 or T=325 μsec. The beamwidth is 0.3235° with the largest side lobe suppressed to a level 21.87 dB below the peak. It appears that the beamwidth grew about 8% over the uncoded case. The side lobe level, however, is slightly lower.

Figure 5-9 shows the time response for the coded pulse case at φ=0. The two early time side lobes are suppressed more than 15 dB, and the -6 dB pulse length measures 120 μsec. The large back time side lobe is caused by the choice of t time of maximum response, of which more will be said later.

Finally, Fig. 5-10 is the contour map of the beamformer output plotted against both time and angle. It should be compared to Fig. 5-5, which shows the uncoded case. It should be noted that Fig. 5-10 does not represent the best pattern achievable; however, it is a pattern of some use and has the distinct advantage of having an explainable lineage.

A summary of the choices made in order to arrive at Fig. 5-10 may convey the number of parameters that need to be investigated in order to arrive at some optimum pattern. These choices are, among others:

1. $2\alpha_N = 120°$,
2. "triangular" wave envelope,
3. signal length = $(T/2) + \epsilon$,
4. number and location of phase changes, and
5. position of signal at maximum responses.

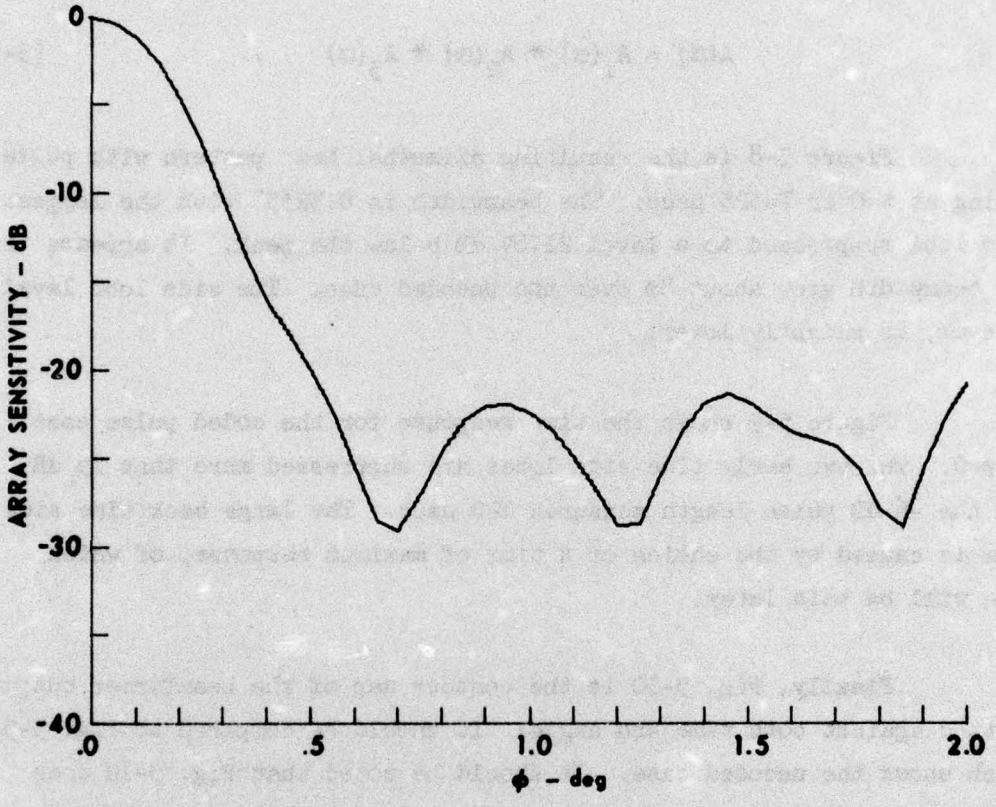

FIGURE 5-8
BEAM PATTERN
TIME: 325.0
SIGNAL – WITH PHASE CODE

ARL - UT
AS-76-68
DAS - DR
1 - 28 - 76

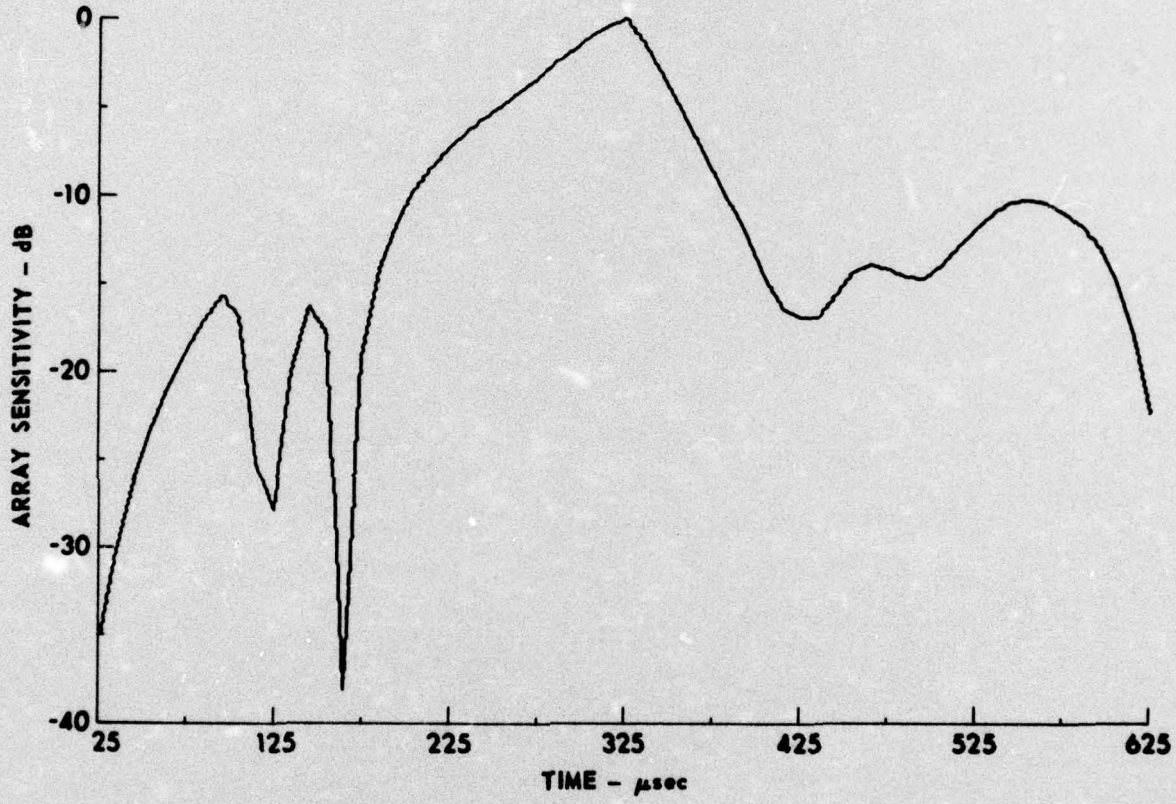

FIGURE 5-9
TIME FUNCTION
$\phi = 0$
SIGNAL - WITH PHASE CODE

ARL - UT
AS-76-67
DAS - DR
1 - 28 - 76

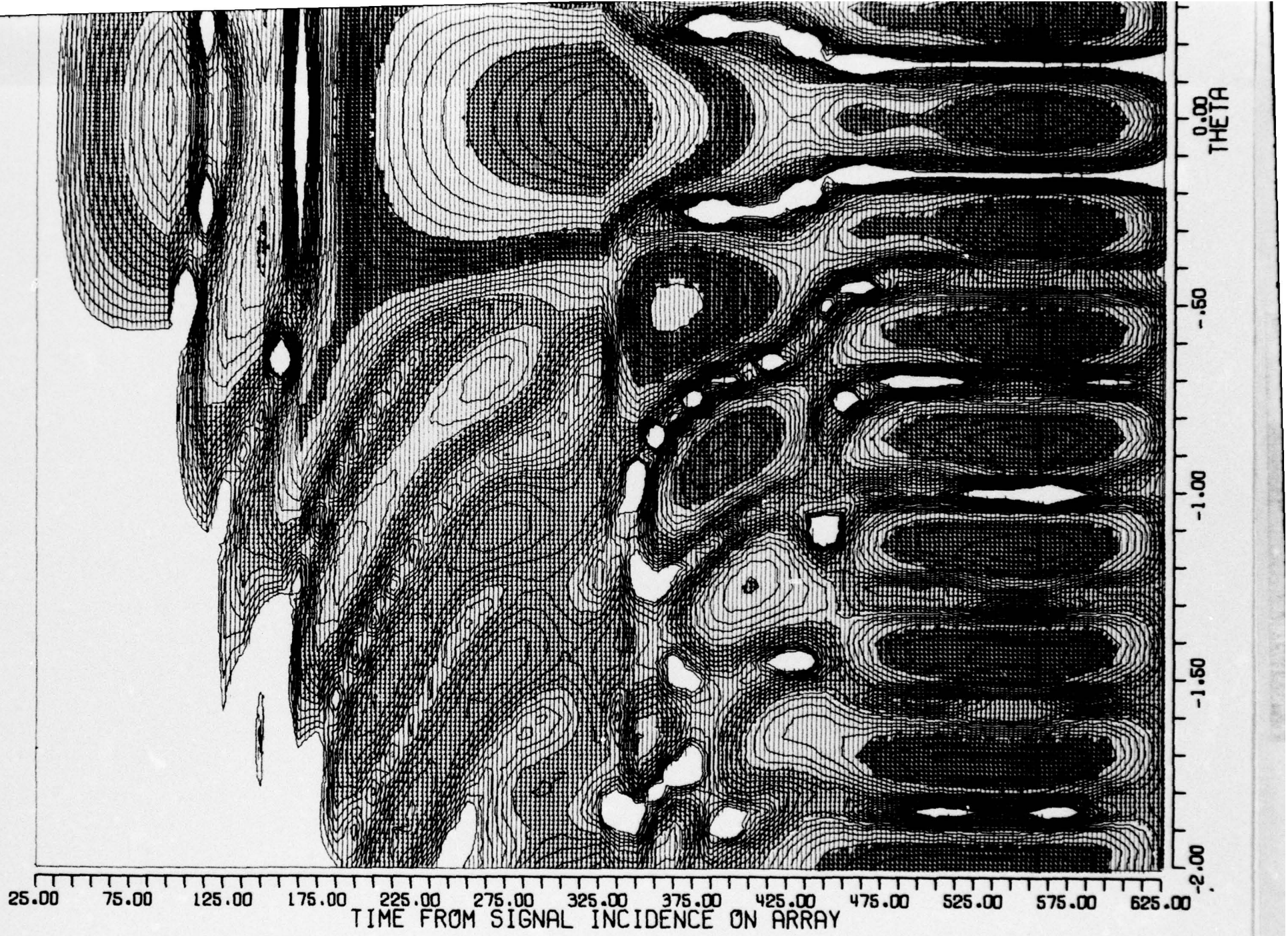
0.00
-.50
-1.00
-1.50
-2.00
THETA
25.00
75.00
125.00
175.00
225.00
275.00
325.00
375.00
425.00
475.00
525.00
575.00
625.00
TIME FROM SIGNAL INCIDENCE ON ARRAY

0 TØ	5.000
5.000 TØ	10.000
10.000 TØ	15.000
15.000 TØ	20.000
20.000 TØ	25.000
25.000 TØ	30.000

ARRAY SENSITIVITY$_m$ – dB
BLACK LINES EACH 1 dB
COLOR CHANGES EACH 5 dB

FIGURE 5-10
TIME-ANGLE BEAM PATTERN CONTOUR MAP FOR TRIANGULAR ENVELOPE, PHASE CODED PULSE

ARL - UT
BS-76-76
DAS - DR
2 - 2 - 76

One can easily see the many combinations that must be studied and the effects understood if a "good" pulse code is to be found.

Figure 5-10 displays some large (-11 dB) "grating" lobes at times between 500 and 600 μsec. An example of the pattern tailoring that can be accomplished is presented in Fig. 5-11. In that pattern, the late "grating" lobes have been reduced to about -19 dB peak. The coefficients were slightly changed in two respects: (1) the time of maximum response was selected to be earlier than in Fig. 5-10, and (2) the value of $A_2(\alpha)$ was changed from that shown in Eq. (5-47) to a value $A_2(\alpha)=\sec \alpha$. It can be seen that little change occurred in the major lobe, but the late "grating" lobes were reduced 8 dB.

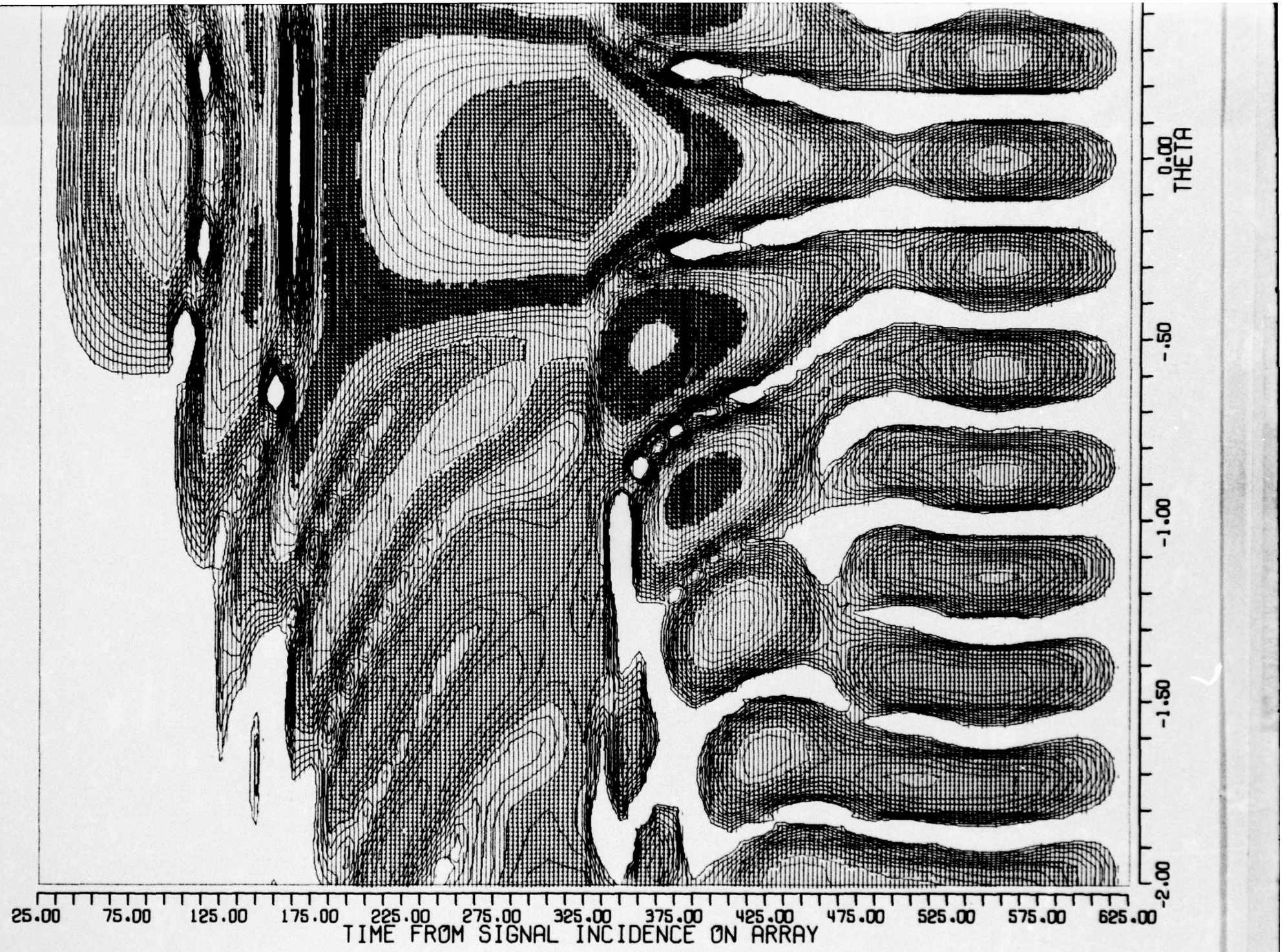
0.00
-.50
-1.00
-1.50
-2.00
THETA
25.00
75.00
125.00
175.00
225.00
275.00
325.00
375.00
425.00
475.00
525.00
575.00
625.00
TIME FROM SIGNAL INCIDENCE ON ARRAY

0 TØ	5.000
5.000 TØ	10.000
10.000 TØ	15.000
15.000 TØ	20.000
20.000 TØ	25.000
25.000 TØ	30.000

ARRAY SENSITIVITY – dB
BLACK LINES EACH 1 dB
COLOR CHANGES EACH 5 dB

FIGURE 5-11
TIME-ANGLE BEAM PATTERN CONTOUR MAP FOR MODIFIED TRIANGULAR ENVELOPE, PHASE CODED PULSE

ARL-UT
BS-76-74
DAS-DR
2-2-76

2

VI. IMPLEMENTATION--SCANNED AND PREFORMED BEAMS

The major advantage of the correlation beamformer is its ease of implementation. Delay line beamformers are limited by the maximum length of the delay line that can be used. Hence, they cannot in general take advantage of the diameter of the cylindrical array. Phase shift beamformers have not taken advantage of the total possible aperture because of the rise time problem. Phase shifters also require time to operate; that is, several cycles of the signal are required for an analog shifter to operate. Compared to either scanned beam operation or preformed beam operation, the correlation beamformer can scan faster and is more easily implemented.

The following sections will discuss beam scanning, its purpose, how it can be done, and at what speed. Finally, two methods of implementing preformed beams will be presented.

A. Scanned Beams

The ability to scan a single beam at a rate which has no theoretical upper bound is perhaps the greatest single advantage of the correlation beamformer. The scan rate is, of course, limited by the state of the art in electronics.

Another use for scanning or the ability to rapidly change some parameter of the formed beam is in time varying focus. For very high resolution arrays, the apertures and farfield ranges are large. If the operating range is substantially less than the farfield range, focusing at the expected target range (a function of time) will be required. The ability to rapidly change the application of the shading coefficients to element output voltages is a necessary condition to time varying focus.

1. Method

A repeat of Eq. (3-1), which shows the essential beamforming operation with the output carrier intact, indicates the factor which leads to ease of implementation and to the unlimited speed of scan. The equation is:

$$E^*(\varphi,t) = \sum_{n=-N}^{N} A_n e_n^*(\varphi,t) \quad , \tag{6-1}$$

and is written so as to form a beam in the φ_o=0 direction. The * indicates a complex wave, or in real life, a real wave which is time varying. Note that at any time t' infinitesimally short samples of e_n* may be simultaneously acquired. These samples may be multiplied by the values A_n and summed to derive a sample of $E^*(\varphi,t')$. With several samples of E*, the beamformer output (including carrier) may be reconstructed. Note that, in principle, no time is required to sample the beam output. In practice, however, the sample has finite width, and the multiply and sum operations require time as determined by the bandwidth of the circuits performing the operation.

Of more importance in terms of time consuming operations is the method by which the envelope of E* is determined. Perhaps the fastest method involves quadrature sampling of E* and retrieving the envelope via

$$|E^*| = \sqrt{(E_1^*)^2 + (E_2^*)^2} \tag{6-2}$$

where the samples marked 1 and 2 are taken in quadrature.

Two methods are available for determining the quadrature samples. The first method is to acquire sample E_1* at any time t' and wait T/4 sec, where T is the carrier period. Then E_2* is acquired at t'+T/4 in the same way the first sample was acquired.

The second method is to use two sets of coefficients differing by ψ. Thus, let

$$ {}_1A_n = \cos^2 \alpha_n \cos[2\pi R(1 - \cos \alpha_n)] \quad , \qquad (6\text{-}3) $$

$$ {}_2A_n = \cos^2 \alpha_n \cos[2\pi R(1 - \cos \alpha_n) - \psi] \quad , \qquad (6\text{-}4) $$

and then perform the operations

$$ E_1^* = \sum_{n=-N}^{N} {}_1A_n e_n^* \quad , $$

and

$$ E_2^* = \sum_{n=-N}^{N} {}_2A_n e_n^* \quad , $$

where e_n^* is only one sample of the element instantaneous voltages taken at t', but ψ has been selected to shift the array acoustic center by $\lambda/4$. In this way, the final objective, that is, a sample of $|E^*|$, can be acquired at the single infinitesimal time t'.

Now, we will rewrite Eq. (6-1) in a form more descriptive of the scanning operation. Equation (6-1) is written so as to form a beam in the φ_o=0 direction. The coefficients are

$$ A_n(\varphi_o{=}0) = \cos^2(\alpha_n)\cos[2\pi R(1 - \cos \alpha_n)] \quad . \qquad (6\text{-}7) $$

In general, to form a beam in the φ_o direction, we have

$$ A_n(\varphi_o) = \cos^2(\alpha_n - \varphi_o)\cos\left(2\pi R[1 - \cos(\alpha_n - \varphi_o)]\right) \quad , \qquad (6\text{-}8) $$

and the beamforming equation may be written as

$$E^*(\varphi-\varphi_o,t) = \sum_{n=-N}^{N} A_n(\varphi_o)\, e_n^*(\varphi,t) \quad . \tag{6-9}$$

Now, in order to scan E* as a function of time, we simply let

$$\varphi_o = \omega_s t \quad , \tag{6-10}$$

where ω_s is the scan rate in radians per second.

It can be seen in Eq. (6-9) that the e* samples are independent of $\alpha-\varphi$, and that scanning can be accomplished by simply changing the A_n. The fact that the A_n is described by a continuous function of $\alpha-\varphi_o$, and that the function is even, allows the continuous function A to be swept past the elements, continuously forming a swept beam. Figure 6-1 shows a suggested implementation of one-half of the beamformer. The other half contains coefficients of the ${}_2A_n$ type including ψ, so that by combining their outputs using Eq. (6-2), an instantaneous sweeping estimate of the returned energy of targets can be obtained.

2. Scan Speed - Bandwidth Requirements

If an active scanning sonar is to be designed with BW (degree) angular beamwidth and $\Delta\rho$ range resolution, covering the azimuthal plane out to a range ρ_{max}, then one must sample 360/BW beams in the time required for the transmitted pulse to travel $\Delta\rho$ yd. Or, since range resolution is usually given in τ μsec,

$$\tau = \frac{2\Delta\rho}{c_1} \quad , \tag{6-11}$$

where c_1 is speed of sound in yd/μsec. So, one must scan through all 360/BW beams in τ μsec, in order to be ready to repeat the operation during the next range increment of length τ. Since sonars of high resolution (BW<0.5°) may contain more than 720 beams and have a resolution on the order of hundreds of microseconds, it is most important to be able to form a beam and estimate the target energy in a time very short compared to the time required for the speed of sound to carry one cycle of the carrier across an element. To our knowledge, the correlation beamformer is the only process capable of this speed. We will now develop the required speed or bandwidth for the multipliers shown by X in Fig. 6-1.

A correlation beamformer with total sector of elements of 180° ($2\alpha_N$=180°) can form a beam with width

$$BW = \frac{K}{2R} \quad , \tag{6-12}$$

where K is the aperture constant in degree-wavelengths.

The number of such beams needed to cover the azimuthal plane is

$$\frac{360}{BW} = \frac{720\ R}{K} \quad . \tag{6-13}$$

The number of elements required to cover a cylinder of radius R wavelengths spaced $\lambda/2$ apart is $4\pi R$, $2\pi R$ of which are used in any one beam.

Now, if 720R/K beams are to be scanned in τ μsec, then the coefficients must be swept past $4\pi R$ elements in τ μsec. The highest rate of change of coefficient value occurs at the array edge, where the rate of change is one cycle per two elements, as can be seen from the way $A_1(\alpha)$ is chosen. Therefore, the highest frequency present at the coefficient input to the multipliers is found to be

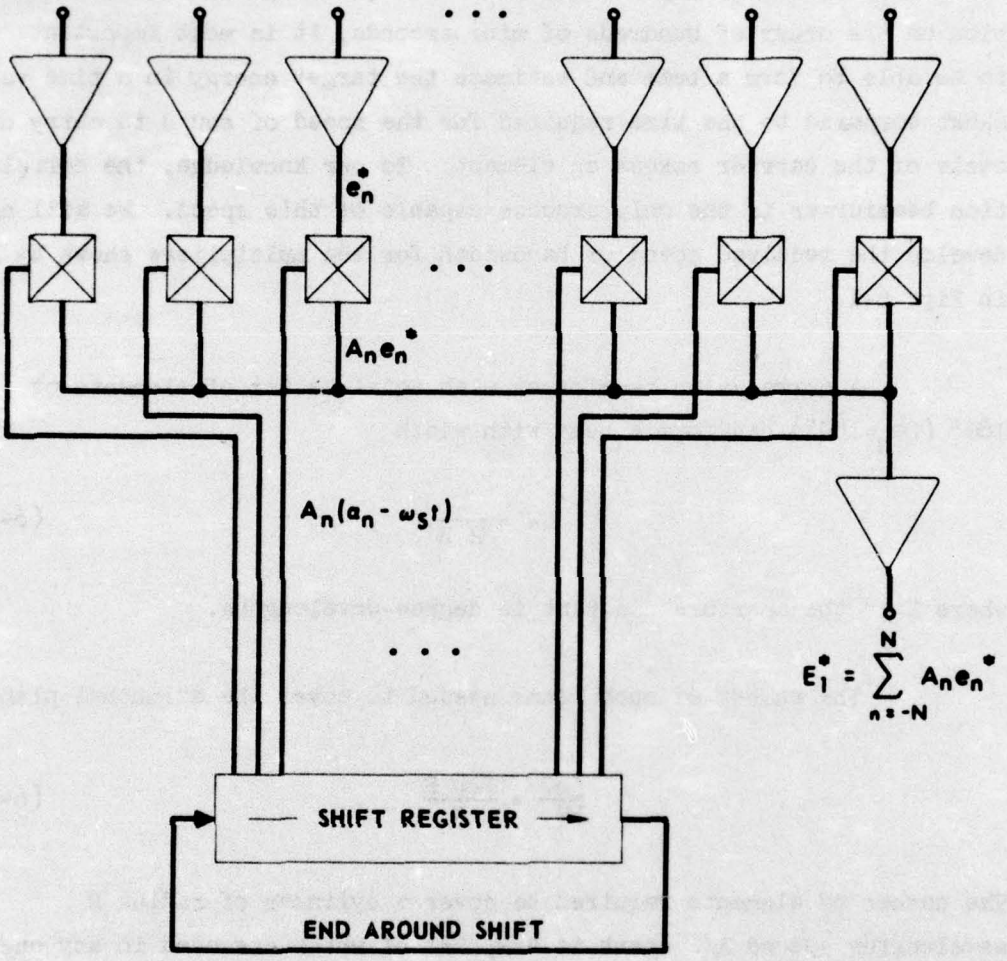

FIGURE 6-1
SCANNED BEAM MULTIPLIER IMPLEMENTATION

ARL - UT
AS-76-64
DAS - DR
1 - 28 - 76

$$\frac{2\pi R}{\tau} \text{ Hz}$$

or (6-14)

$$\frac{\pi K}{\tau BW} \text{ Hz} \quad .$$

Of course, the frequency presented to the element input of the multiplier is just f_o, the transmitted frequency, a great deal less than the megacycle rate at the coefficient input.

Figure 6-2 shows a plot of the maximum frequency required for the multiplier and adder in a scanned beam sonar of beamwidth BW degrees and range resolution equivalent of τ μsec.

In order to test the simple development of the required frequency response, a fast Fourier transform was performed on a set of shading coefficients, including the effects of finite size elements. The results are plotted in Fig. 6-3, and show the time function at the coefficient input to the multiplier and its frequency spectrum through the FFT. The time scale is normalized to one scan per second, and a small radius array is used to show the cyclic nature of the coefficients. The results show that for each scan per second at R=12.5, the maximum frequency at the multiplier is about 100 Hz. For one scanner revolution in 100 μsec, and scaling up the R from 12.5 to 300 (a beamwidth of 0.1°) the maximum frequency is

$$100 \cdot \frac{300}{12.5} \cdot \frac{1 \text{ sec}}{100 \text{ μsec}} = 24.0 \text{ MHz} \qquad (6\text{-}15)$$

at the 40 dB down point. The 10 dB down point in the spectrum agrees very closely with the simple development given earlier.

Several FFT's were run for various R's and different sectors of active elements, with and without finite size elements. In every case, the maximum frequency scales directly with R. Also, the case of

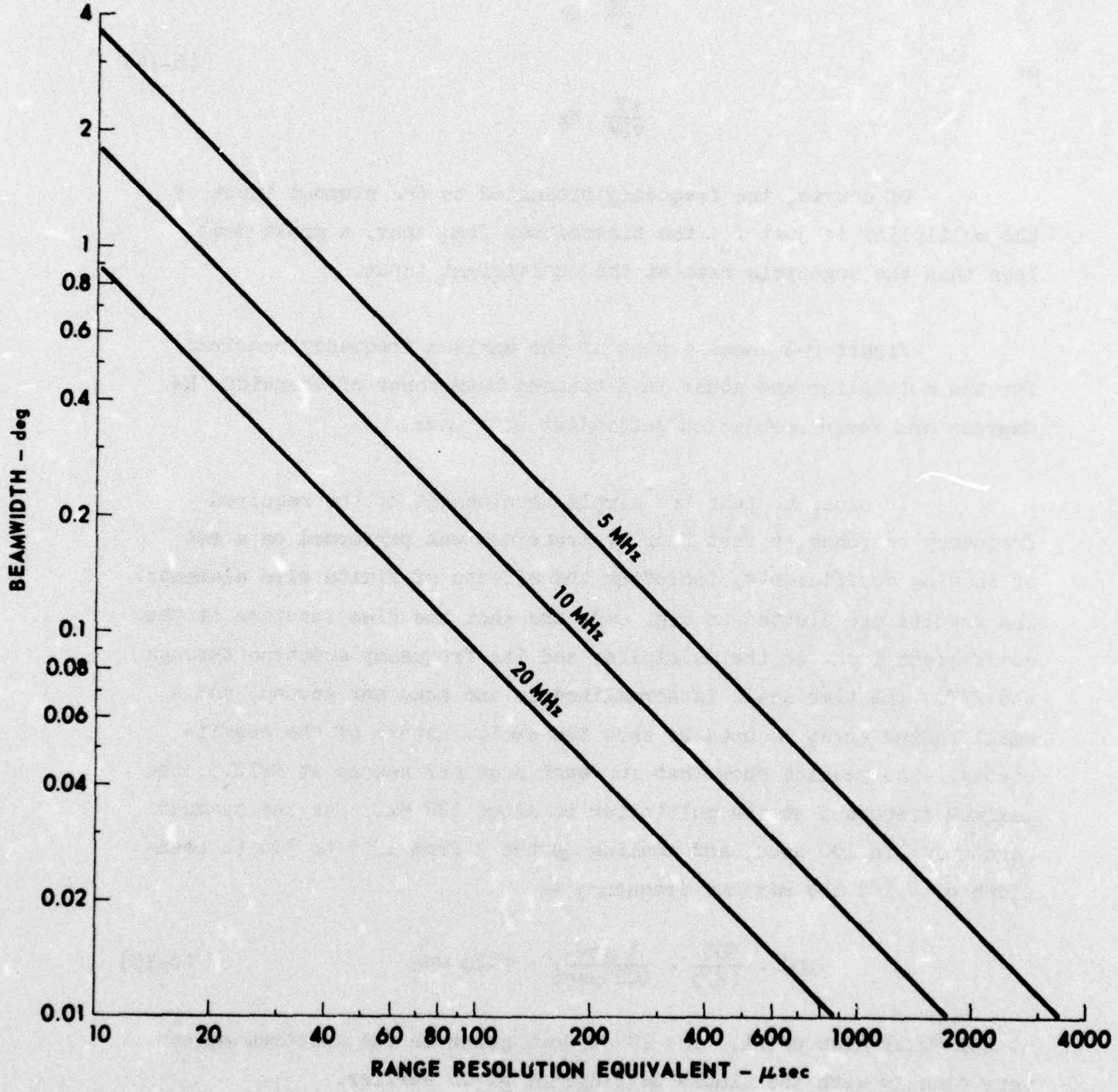

FIGURE 6-2
RELATION BETWEEN SONAR SYSTEM RESOLUTION PARAMETERS AND THE MAXIMUM FREQUENCY REQUIRED FOR SCANNER

ARL - UT
AS-76-52
DAS - DR
1 - 20 - 76

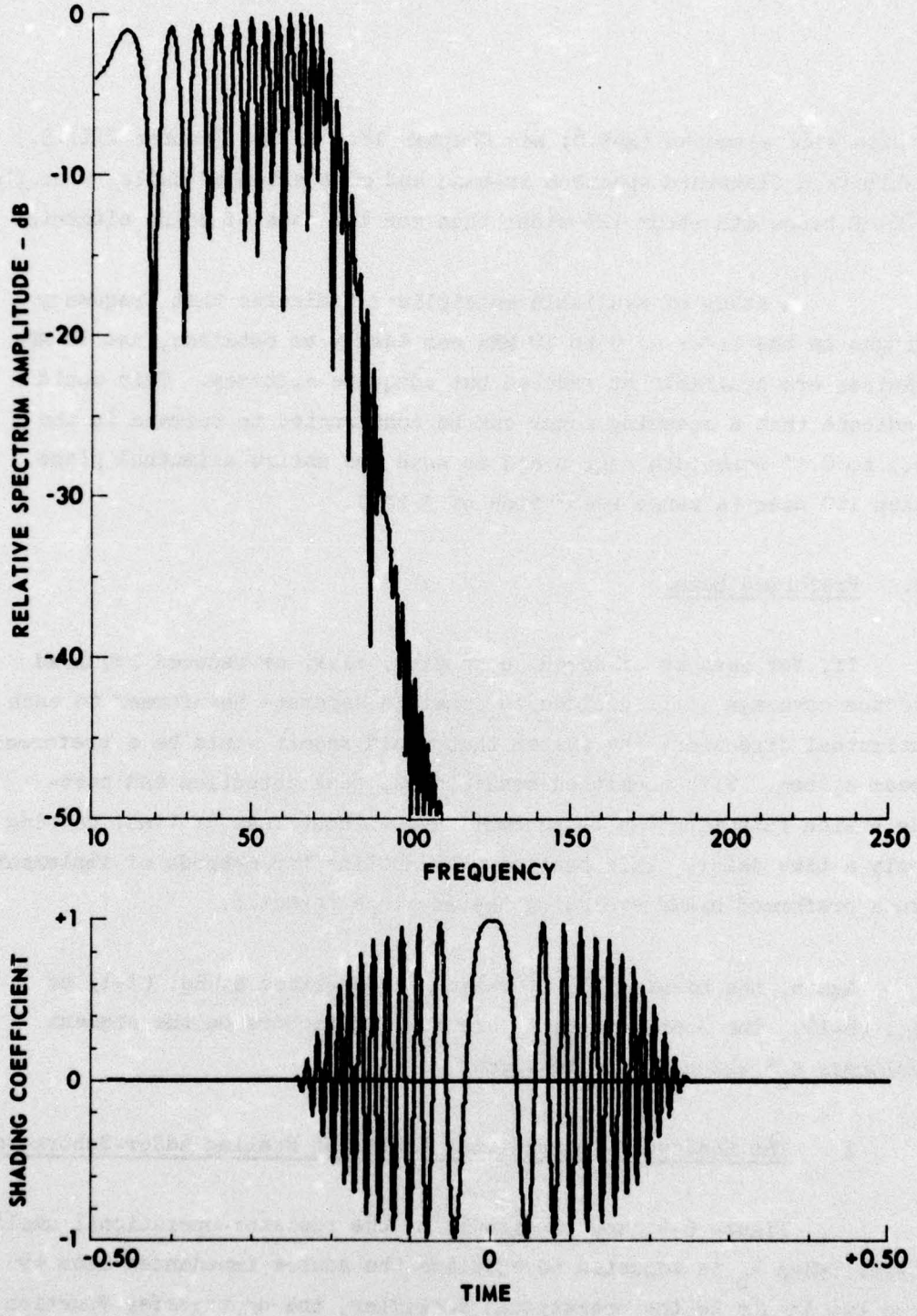

FIGURE 6-3
FREQUENCY SPECTRUM AND TIME FUNCTION OF SHADING COEFFICIENTS IN SCANNED BEAM

ARL - UT
AS-76-65
DAS - DR
1 - 27 - 76

RADIUS	2 ALPHA N	ELEMENT
12.5	180	YES

finite size elements (x=3.8; see Chapter IV.A.1. and Chapter VIII.B.) exhibits a flattened spectrum in-band and more extended tails, with the -20 dB bandwidth about 12% wider than for the case of point elements.

A study of available multipliers indicates that frequency ranges on the order of 5 to 10 MHz can easily be obtained, and 20 MHz devices are available at reduced but adequate accuracy. This would indicate that a scanning sonar can be constructed to operate in the 0.3 to 0.1° beamwidth region and to scan the entire azimuthal plane each 100 μsec (a range resolution of 3 in.).

B. Preformed Beams

If, for reasons of speed, economics, risk, or reduced required sector coverage it is decided to commit a separate beamformer to each azimuthal direction, the system that would result would be a preformed beam system. With committed beamformers, peak detection and post-detection filtering can be accomplished without loss of time, costing only a time delay. This section will outline two methods of implementing such preformed beams excluding the envelope detector.

Again, the beamforming operation is described by Eq. (3-1) or Eq. (6-1). The coefficients A_n are scaling factors on the element voltages e_n* which are to be summed.

1. The Resistor - Operational Amplifier Scaling Adder-Subtractor

Figure 6-4 shows a circuit of the resistor-operational amplifier type. When R_b is adjusted to equalize the source impedances seen by the two inputs to the operational amplifier, the dc transfer function for the circuit is

$$e_o = \sum_{i=1}^{M} \frac{R_F}{R_{+i}} e_{+i} - \sum_{i=1}^{N} \frac{R_F}{R_{-i}} e_{-i} \quad , \qquad (6\text{-}16)$$

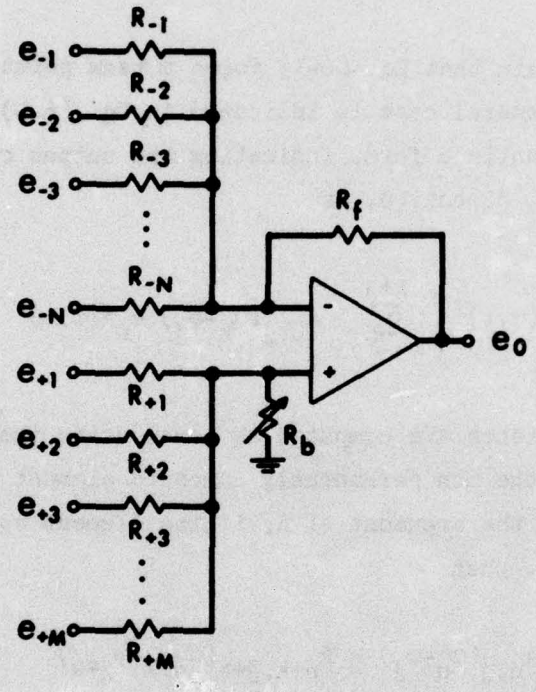

FIGURE 6-4
SCALING SUM AND DIFFERENCE AMPLIFIER

ARL - UT
AS-76-53
DAS - DR
1 - 27 - 76

where $R_F/R_{\pm i}$ is the magnitude of the scaling factor for $e_{\pm i}$; the term is added for e_{+i}, and subtracted for e_{-i}. Equation (6-1) indicates that terms with $A_n>0$ should be added and terms with $A_n<0$ should be subtracted from the total. This is accomplished if the terms to be added correspond to e_{+i} and the terms to be subtracted correspond to e_{-i}.

Note again that Eq. (6-1) forms a beam pointing in the $\varphi_o=0$ direction. The general case is indicated in Eq. (6-9), which can be rewritten in a quantized form, indicating the output of the jth beam pointing in the φ_j direction, as

$$E_j^*(\varphi,t) = \sum_{n=-N+j}^{N+j} A_{n,j}(\alpha_n-\varphi_j)\, e_n^*(\varphi,t) \quad , \tag{6-17}$$

where the coefficients are computed as usual using the argument $\alpha_n-\varphi_j$, and α_n points to the nth permanently numbered element in the array. As can be seen by the argument of A, if the element spacing and beam spacing are equal, then

$$A_{n,j}(\alpha_n-\varphi_j) = A_{n+k,j+k}(\alpha_{n+k}-\varphi_{j+k}) \tag{6-18}$$

for any k. Also, one should note the limits on the sum in Eq. (6-17). These two effects result in the symmetry which simplifies the implementation of many preformed beams. That is, every beamformer is identical to every other, except for a unit change in the n for the contributing elements.

If the element spacing is smaller than the beam spacing, some symmetry still exists. For example, if $2\Delta\varphi=3\Delta\alpha$, then two types of beams can be formed, and alternately placed on the array.

A resistor-operational amplifier beamformer containing 97 resistors has been constructed and used in the TDA tests described in the next chapter. The resistor-operational adder is therefore considered low risk. The system does require the use of preamplifiers to drive the many resistors on each element.

2. The Transformer Adder

Figure 6-5 shows an obvious method of scaling and adding several voltages. If all transformer primaries have equal turns, the scaling can be accomplished in a quantized manner by choosing the sense and number of secondary turns. If the secondaries are in series, the voltages add, yielding a quantized version of Eq. (6-9). The quantization occurs on the A(n) as discussed in Chapter IV.G. and proved during the experimental validation, Chapter VIII.

For several preformed beams, several secondaries can be wound on the same transformer core. Some experiments were conducted to investigate possible problems associated with the transformer adder. For example, it was shown that an array element can drive a transformer primary without greatly changing the element's response. Another test involved six transformers, each with 20 secondaries. Secondary to secondary feedover, secondary resonance, and null voltages were measured. No serious defects could be found and the secondaries combined the transformer outputs just as expected. Of course, the more transformers used and the more separate secondaries on each, the more feedover, etc.

It was not possible to analyze a large matrix of transformers, except in the simplest way. It is felt that a full size experimental beamformer of the transformer type must be built in order to test the feasibility.

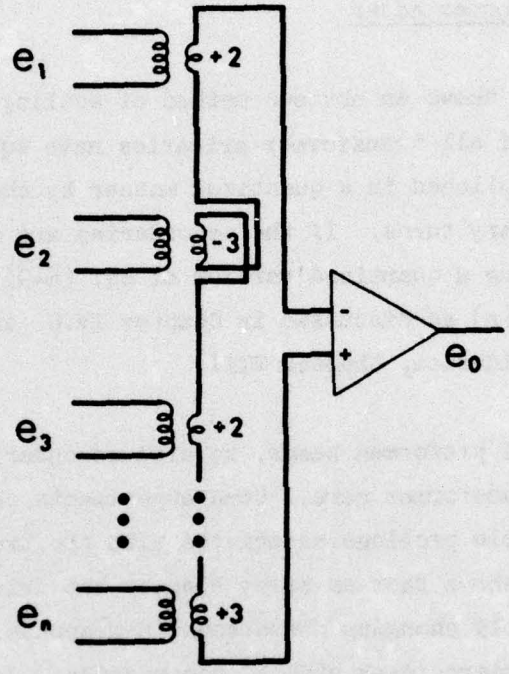

FIGURE 6-5
TRANSFORMER IMPLEMENTATION

ARL - UT
AS-76-51
DAS - DR
1 - 20 - 76

The advantage of the transformer beamformer is that there are no active devices in the beamformer; the first active device is the beam amplifier. No preamplifiers mean less noise, much more dynamic range, and higher reliability.

VII. ANCILLARY STUDIES

During the course of the study of the correlation beamformer, several ancillary studies were indicated. This chapter describes these studies in two parts. The first deals with the practical problems associated with array construction. The second part will describe a short but useful study of the technique of linear programming, potentially useful in finding codes for use in pulse compression.

A. Array Construction Problems

By far the majority of work reported here has been concerned with beamforming theory and computer models. In every case, except the error analysis (Chapter IV.G.), it was assumed that transducer elements generate a voltage that faithfully reproduces the acoustic pressure on the element face. The elements were assumed to be placed in a cylindrical array with perfect accuracy.

In order to test the correlation beamformer, it became necessary to construct the Two-Degree Array (TDA), and, to test the pulse compression codes (Chapter V), it will be necessary to construct a much larger array. Several practical problems had to be addressed in order to build high accuracy arrays.

1. Element Design

Previously constructed arrays at ARL have consisted of staves of several elements in the elevation direction (Z direction in Fig. 4-2). The purpose was twofold. First, when the dimension of any side of a rectangular parallelopiped ceramic element becomes much larger than the resonance dimension, the possibility of sympathetic vibration in an unwanted mode exists. Such unwanted modes can adversely affect

the element beam patterns. Second, low side lobes are usually required in the array elevation beam pattern, and the stave elevation pattern was thought to be the main contributor; therefore bizonal shading was applied to each stave of several elements to control the stave elevation side lobe level.

Our discovery that a cylindrical array with depth in the direction of signal propagation behaved much as an end-fire array, with an elevation pattern of its own, led to the attempt to simplify the stave design.

If a single element stave (rectangular parallelopiped) is cut to be resonant in the thickness mode (the intermediate dimension), the radiating face has width (small dimension) in the array circumferential direction and length (long dimension) in the elevation direction. The width is controlled by the required element spacing on the array and the stave length is an open parameter which can be used to control the stave elevation response. In fact, if the length is cut to be resonant near $f_o/3$, the stave face will "flap", superimposing a sort of shading on the face velocity function. The relative amplitude of the long mode can be controlled somewhat by mismatching the frequency relationship. Figure 8-9 in the following chapter shows an element beam pattern from the TDA. This pattern would be unacceptable for line arrays because of the large second lobes at -14 dB. For the cylindrical array, however, the large second lobe will be moderated by the array pattern (see solid curve in Fig. 3-7). The first lobe will be nearly unaffected by the array pattern because of its nearness to the major lobe. The composite experimental TDA elevation pattern is shown in Fig. 8-10.

By taking advantage of the array elevation pattern, it was possible to construct the TDA (next chapter) with 180 elements. Another 2° beamwidth array constructed earlier at this laboratory

required 180 9-element staves (1620 elements total), but it was no better than the TDA in elevation pattern performance.

2. Element Selection Criteria

During any array construction project, elements are designed, the design is tested and approved, and element construction begins. In spite of all precautions, manufactured elements are not very uniform in performance. Some sort of element selection criteria are required to choose that subset of elements which will be used in the array. The classic criteria have been a tight grouping of frequency at which minimum air loaded impedance occurs. The allowed frequency spread, and in fact, the very choice of that parameter, appeared to be more arbitrary than scientific.

Actually, one would hope to control the final amplitude and phase response of each element after mounting in the array. There is some question that "air resonance frequency" is a good indicator of that amplitude and phase control.

During our construction of the TDA (an experimental array described in the next chapter), elaborate measurements of the manufactured elements were obtained. Selection of the elements to be used in the array was accomplished by an objective comparison of air impedance versus frequency plots for each element. After construction of the array, measurements of the amplitude and phase response of the mounted elements were acquired. A study of the correlation between the measurements made in air before mounting and measurements made in the array after mounting indicated that additional in-air measurements (over and above "resonance" frequency) would substantially increase the uniformity of elements after mounting.

The details of the element selection criteria and the method by which they were obtained is given in Ref. 9.

3. Array Construction Technique

An additional contributor to the phase scatter of mounted elements in an array is the inaccuracy with which the elements are placed on the cylinder. The normal construction technique begins with the cylinder; glue and backing material are applied, then the elements are applied to the backing. Cylinder inaccuracy, glue thickness variation, backing material thickness variation, and element thickness variation all combine to cause the element faces to be scattered around the proper positions.

A new construction technique designed to eliminate these construction errors has been developed and tested on a small scale. The results indicate that the method can increase element placement accuracy by a factor of ten compared to the old methods.

The construction method involves the use of a mold, which is machined to hold element faces in the proper position. Backing material is glued to the element backs and, finally, the cylindrical baffle and/or electronic housing is inserted. Hard epoxy is used to connect the element-backing assembly to the housing. The mold is then removed, permitting the elements to be wired. Through the use of soft epoxy and a modification to the mold, the face material is poured.

The new method is more expensive than the old technique because of the mold. However, the extra expense can be justified when large, high frequency arrays are constructed requiring the best element placement accuracy.

B. Linear Programming - An Optimization Technique

Linear programming is a mathematical technique by which an objective function can be optimized while constraining other functions to remain

within bounds. The method appears to be useful in several aspects of the correlation beamformer. For example, the method appears to be able to choose or solve for the best signal code for use in the pulse compression problem. Much more work is required in order to achieve that capability, however.

Another problem or question involves the effectiveness of the heuristically derived shading coefficient selection algorithms described in Chapter III. Can other coefficients be found which lead to better side lobe levels, or better beamwidth? How nearly optimum are the selection algorithms? In order to answer these questions and learn more about the technique of linear programming, it was decided to try to linearize the beamformer problem and exercise the supplied software available on the CDC 6600 computer at The University of Texas at Austin campus.

The beamformer problem was linearized and beam pattern runs were compared to beam patterns from the algorithmic approach. The results indicate that, for R=12.3, the algorithm approach discussed in this report is nearly optimum; the side lobe level is within 1 dB of the best value and the beamwidth is within about 20% of the best value. The optimum coefficients were listed and plotted but no sense could be made of the computer selection. Certainly no scaling rules were evident.

It appears that if linear programming is used to select shading coefficients, it must be accomplished for the specific size under consideration. The problem cannot be run for very large arrays, however, because of time and storage requirements of the software.

Appendix B gives a brief description of the optimization technique and shows the beam patterns achieved at R=12.3. It is felt that more work on this subject would lead to a method of choosing pulse codes for use in the range resolution problem.

VIII. EXPERIMENTAL VERIFICATION

Two separate sets of experiments have been conducted during the period of this study to verify the predictive capability of the computer implemented mathematical model. In all cases, the measurements confirmed the predictions, not only in basic character, but also in the detail structure of the beam pattern side lobes.

The first measurements were conducted on an existing array of very small radius ($R \approx 4$). The purpose was a "quick-look" test and was performed early in the study. The second tests were better planned and utilized an array especially constructed for the tests. These experiments will be described separately.

A. AN/SQS-23 Array Experiments

In early April 1974, the STEP barge at ARL's Lake Travis Test Station (LTTS) became available for use on this contract. An AN/SQS-23 sonar array had been suspended under the barge and was available for testing. The array is physically large (8 ft diam, 5 ft height, and 5 ton weight), but its size is small in wavelengths at the operating frequency ($R \approx 4$). The array is comprised of 432 elements (spaced $\approx 0.5\ \lambda$), arranged in staves of nine elements each. A contiguous set of 25 staves (the front half of the array) was selected and routed to a test beamformer of the "variable resistor-operational amplifier adder" type.

Because of the large physical size, the experiment was rather limited, and because of the small normalized size ($R \approx 4$), the beam patterns do not look "good". However, in every case tested, the predictions and measurements agreed.

The test included a rough error sensitivity measurement, proved the feasibility of steering a beam between staves, measured both sum and difference beam patterns, and measured sum beam patterns as a function of frequency. In every case tested, the comparison between theory and experiment was very good. Figure 8-1 shows an example plot of one of the measured patterns.

B. The Two-Degree Array (TDA) Experiments

During October 1974, tests were conducted on the specially constructed TDA and its beamformer test bed. The system had been under construction since early in the contract, and its purpose was to make available an array of adequate normalized size ($R \approx 14.5$) for detailed tests of the method. Of course, its size and its channel bandwidth were both too small to make measurements of the pulse compression ideas; however, all other tests were to be performed with the TDA. Reference 10 contains a complete description of the system and the tests performed. In this section, the system and tests will be summarized in order to again show the predictive ability of the computer implemented mathematical model.

Figure 8-2 shows the completed transducer array. It contains 180 hydrophones spaced on 2° centers on the cylinder so that the array outside diameter measures 17.33 in. The hydrophone elements are 1.650 in. by 0.624 in. by 0.265 in. blocks of CHANNELITE 5500® ceramic material, resonant near 100 kHz in the 0.624 dimension. Single element beam patterns were measured and the analytic description given in Chapter IV.A.1., Eq. (4-5), with $\chi=3.8$ was found to give the best fit. Each element output is separately conveyed to the beamformer test bed, the front panel of which is shown in Fig. 8-3. The test bed panel is composed of 95, 10-turn potentiometers, whose purpose is to separately

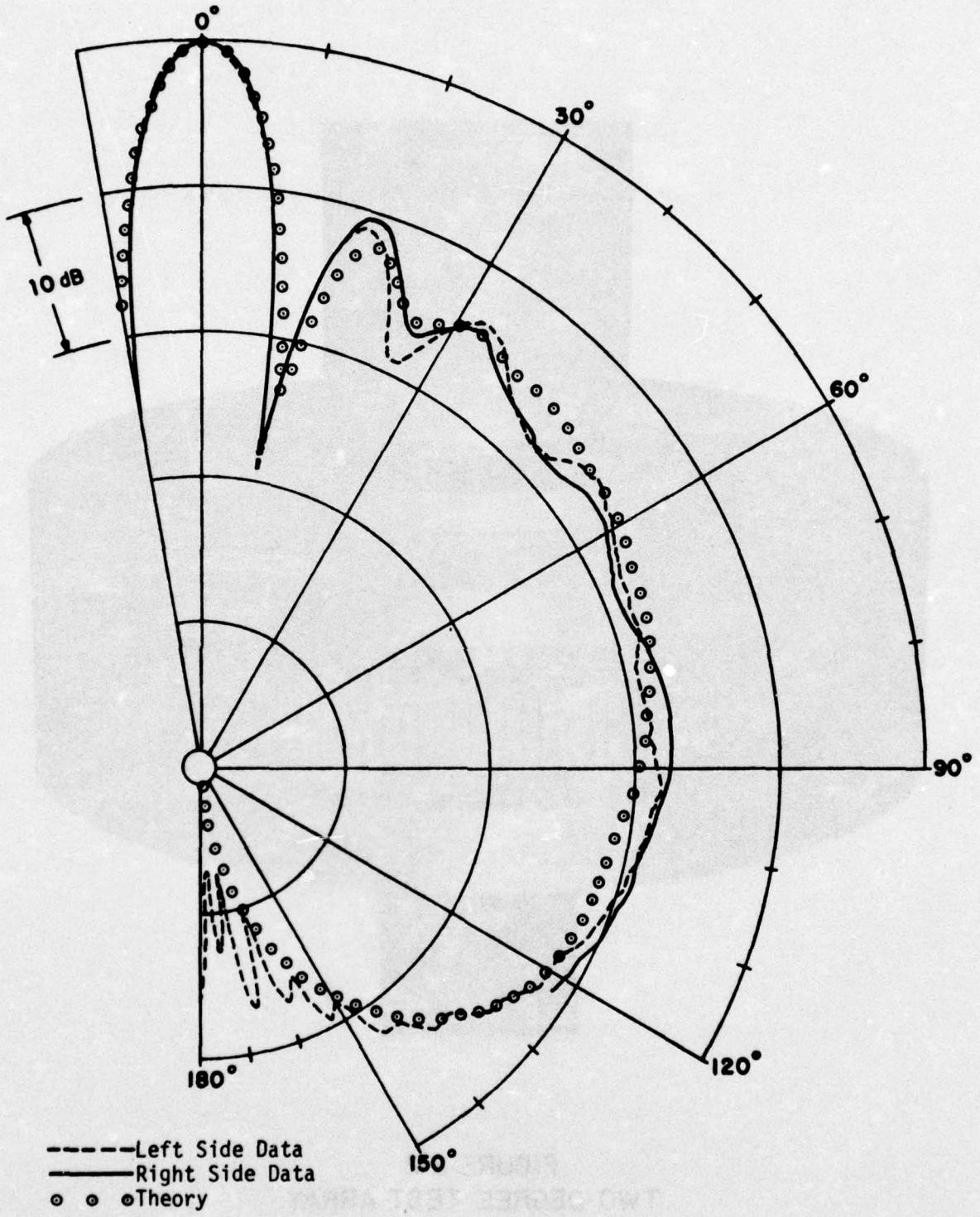

FIGURE 8-1

THEORETICAL AND EXPERIMENTAL BEAM PATTERNS OF
AN/SQS-23 ARRAY AT 4800 Hz

AS-74-1781
DAS-0031-3

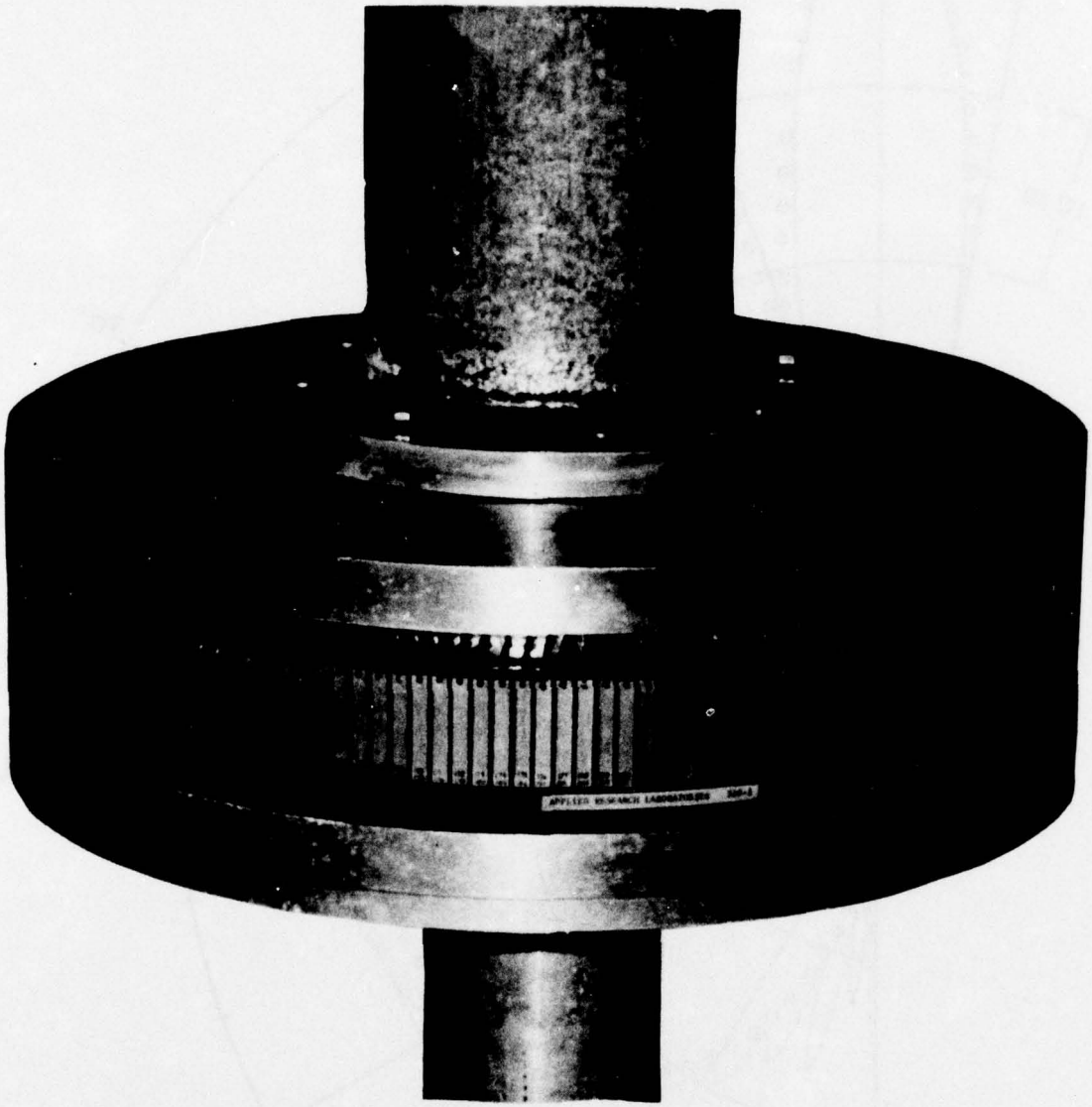

FIGURE 8-2
TWO-DEGREE TEST ARRAY

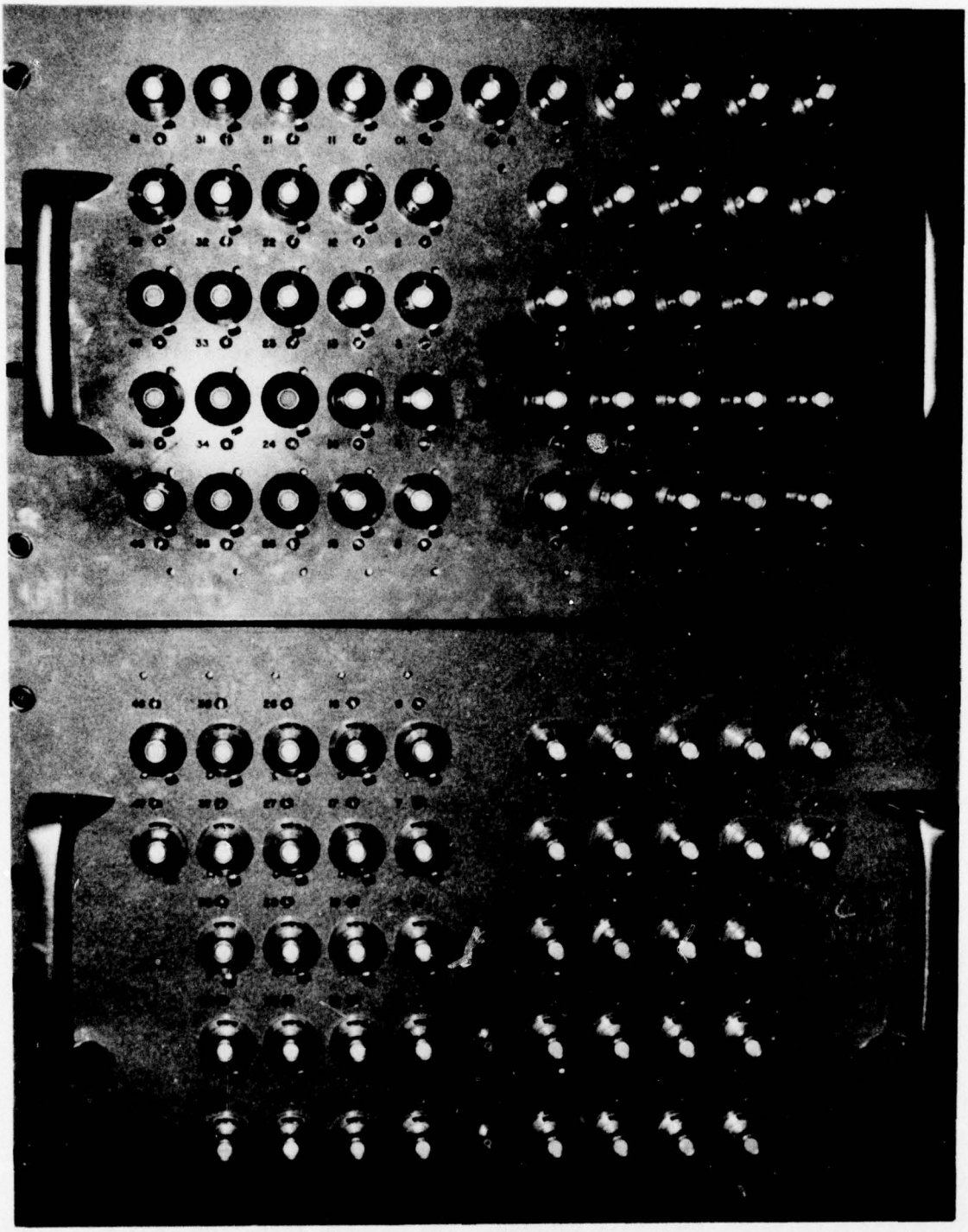

FIGURE 8-3
BEAMFORMER TESTBED PANEL

control the shading weight of the array elements before combining. In this way, experiments requiring different shading coefficients can be easily performed.

The experiments were conducted in the ARL sonar model tank, which is 15 ft wide, 60 ft long, and 12 ft deep. The farfield range for the TDA, estimated from D^2/λ, is about 42 ft. The maximum usable test range, however, was 26 ft. Thus, the majority of tests were conducted at 0.62 D^2/λ, and in general the array was focused for that range. No true farfield beam patterns were acquired.

The tests performed with the TDA are listed and the results summarized below.

1. Error Sensitivity Experiments. Exact shading coefficients were computed and linearly quantized into several levels, ranging from +1 to -1 in value. Figure 8-4 shows the exact coefficient case, and Fig. 8-5 shows the effect of quantizing the exact coefficients into five levels (+1, +0.5, 0, -0.5, -1). Both cases are compared to the computer model for that case. The 5-level case represents the most coarse quantification that appears useful.

Other interesting patterns were obtained in this category. Examples include a pattern for all coefficients uniform (A_n=1) and the case of 2-level quantized coefficients A_n=±1 (see Ref. 10).

2. Focusing Experiments. All experiments were performed at some focused range. The minimum focused range used was 12 ft. This range represents 0.29 D^2/λ and is only 8.3 array diameters. Figure 8-6 is a plot of the pattern for a 12 ft target with the 12 ft focused array. The pattern is still very well behaved. The pattern resulting from a 12 ft target when the array is not focused (or farfield focused) is shown in Fig. 8-7. As expected, without focusing the sensitivity is

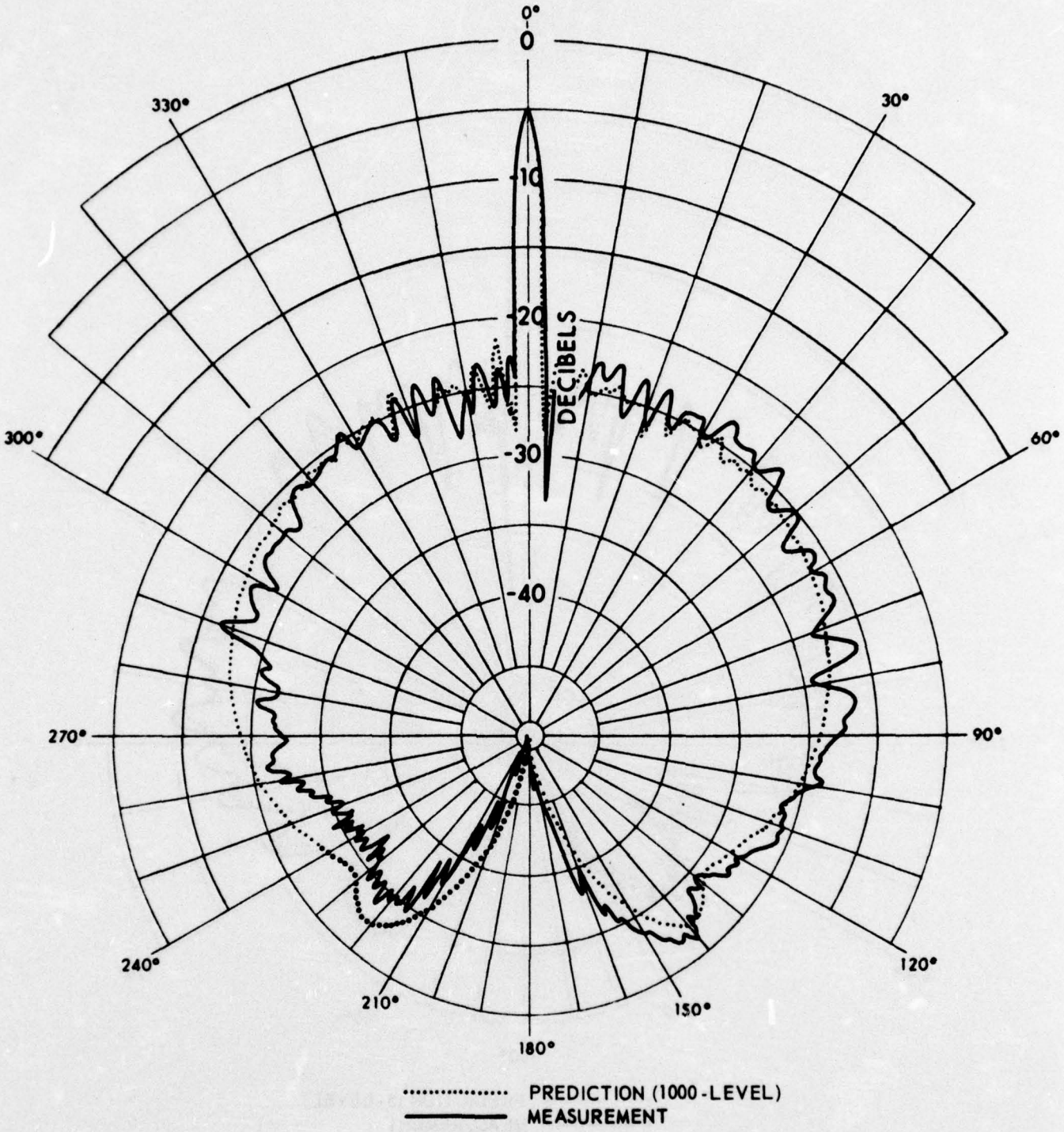

FIGURE 8-4
AZIMUTHAL BEAM PATTERN
EXACT (1000-LEVEL) SHADING COEFFICIENTS
TARGET RANGE: 26 ft
FOCUS RANGE: 26 ft

ARL - UT
AS-74-1238
BOM - DR
11 - 15 - 74

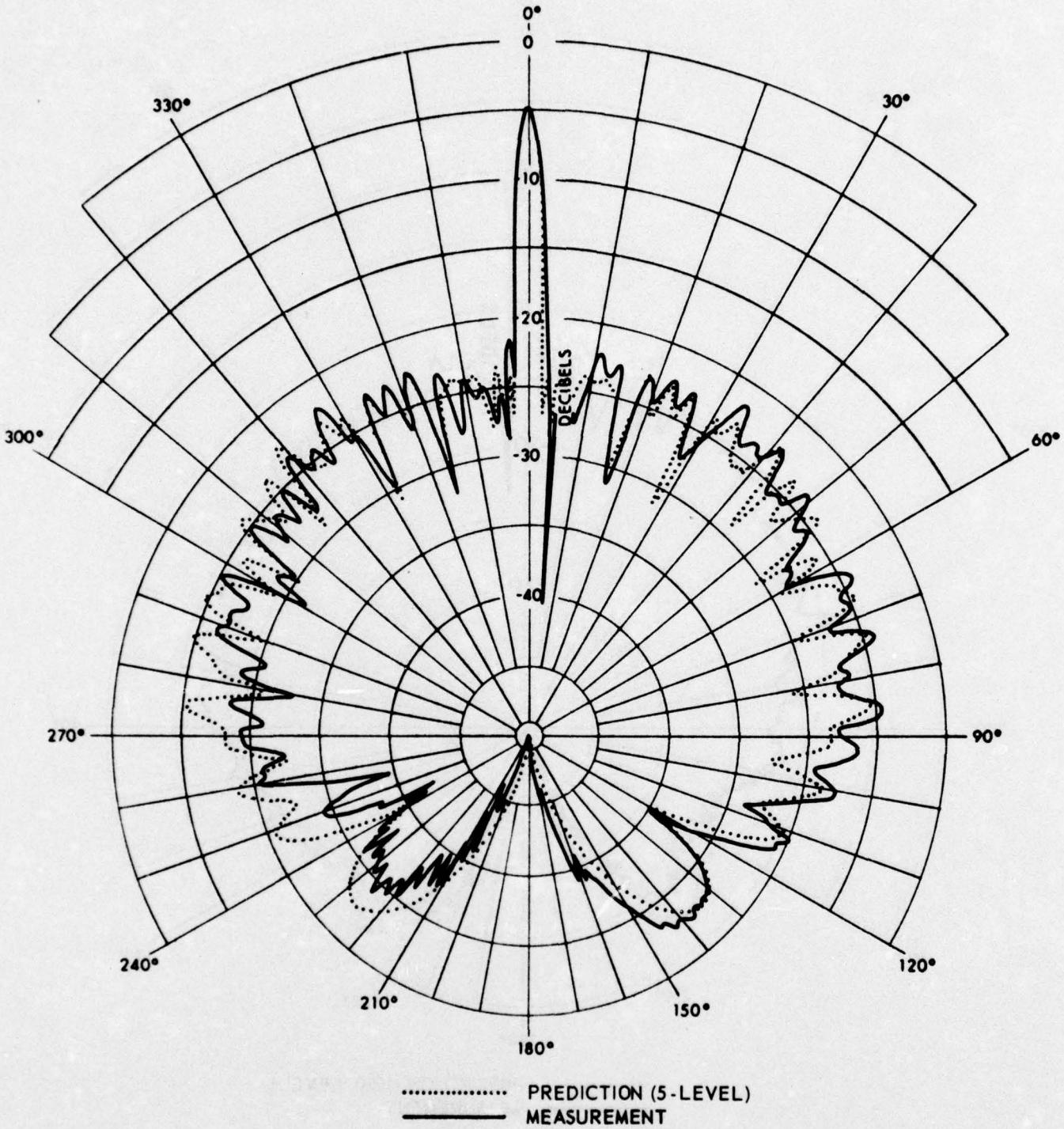

FIGURE 8-5
AZIMUTHAL BEAM PATTERN
5-LEVEL SHADING COEFFICIENTS
TARGET RANGE: 26 ft
FOCUS RANGE: 26 ft

ARL - UT
AS-74-1243
BOM - DR
11 - 15 - 74

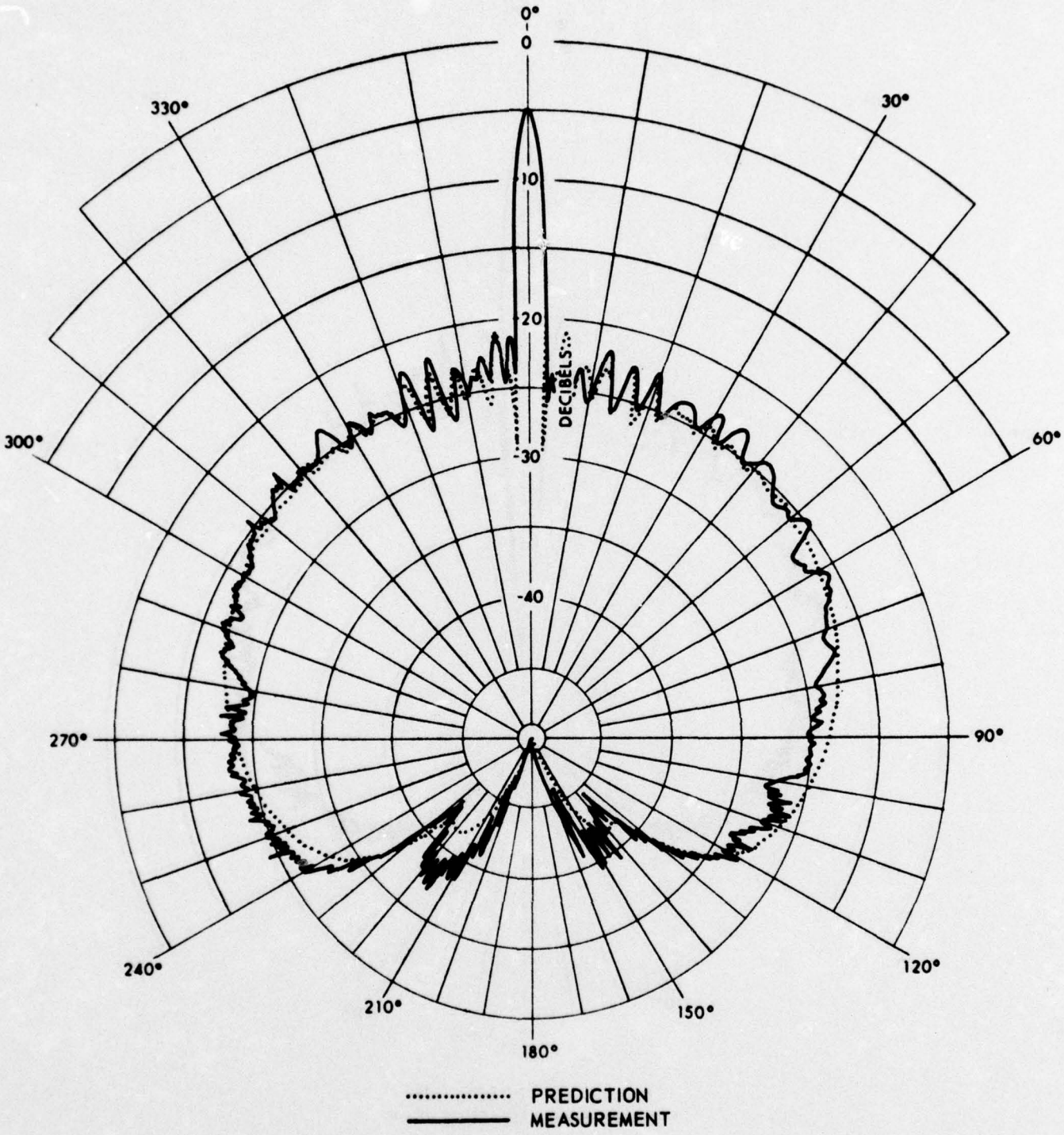

FIGURE 8-6
AZIMUTHAL BEAM PATTERN
TARGET RANGE: 12 ft
FOCUS RANGE: 12 ft

ARL - UT
AS-74-1250
BOM - DR
11 - 15 - 74

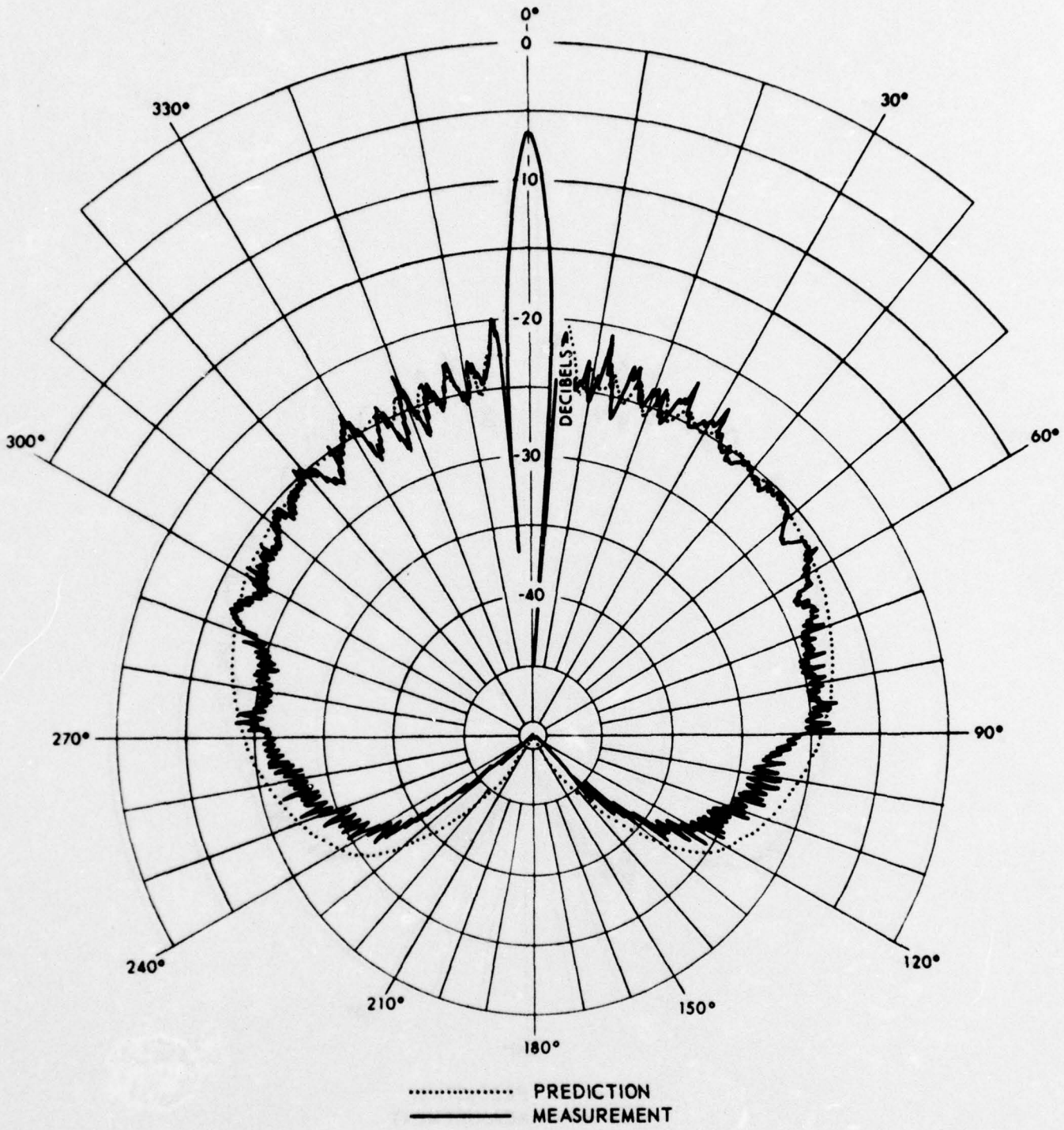

FIGURE 8-7
AZIMUTHAL BEAM PATTERN
TARGET RANGE: 12 ft
FOCUS RANGE: 10,000 ft

ARL - UT
AS-74-1249
BOM - DR
11 - 15 - 74

down, the side lobes higher, and the major lobe shape is bulbous. This pattern should be compared to Fig. 8-6.

Many other patterns were acquired to determine such parameters as depth-of-field.

3. Frequency Response Experiments. The array was matched for a particular frequency, then several patterns were acquired at different operating frequencies. The purpose was to determine the useful bandwidth, and if the computer predictions were valid for this case. Figure 8-8 is presented to show that the computer prediction is good, even outside the useful bandwidth of the correlating processor.

4. Reduced Sector Experiments. The sector of active elements was reduced to 80° and then to 40°. The behavior was as expected, with computer prediction and measurements closely correlated.

5. Split-Beam Experiments. Several patterns were obtained which represent "half-beam" and "split-beam" patterns. The patterns presented herein represent the sum of two "half-beams". The "split-beam" represents the difference of two "half-beams". No computer predictions were made, but the behavior was as one would intuitively expect.

6. Elevation Beam Patterns. Single element elevation beam patterns, of which Fig. 8-9 is an example, and the array elevation pattern through the azimuthal major lobe shown in Fig. 8-10, were obtained and compared with the theory developed in Chapter IV.A.2. As can be seen, the rather unsightly element patterns are not detrimental to the array elevation pattern; the latter displays side lobes more than 25 dB below the major lobe.

In summary, two separate experiments were performed which show that the method is a viable beamforming technique. The experiments

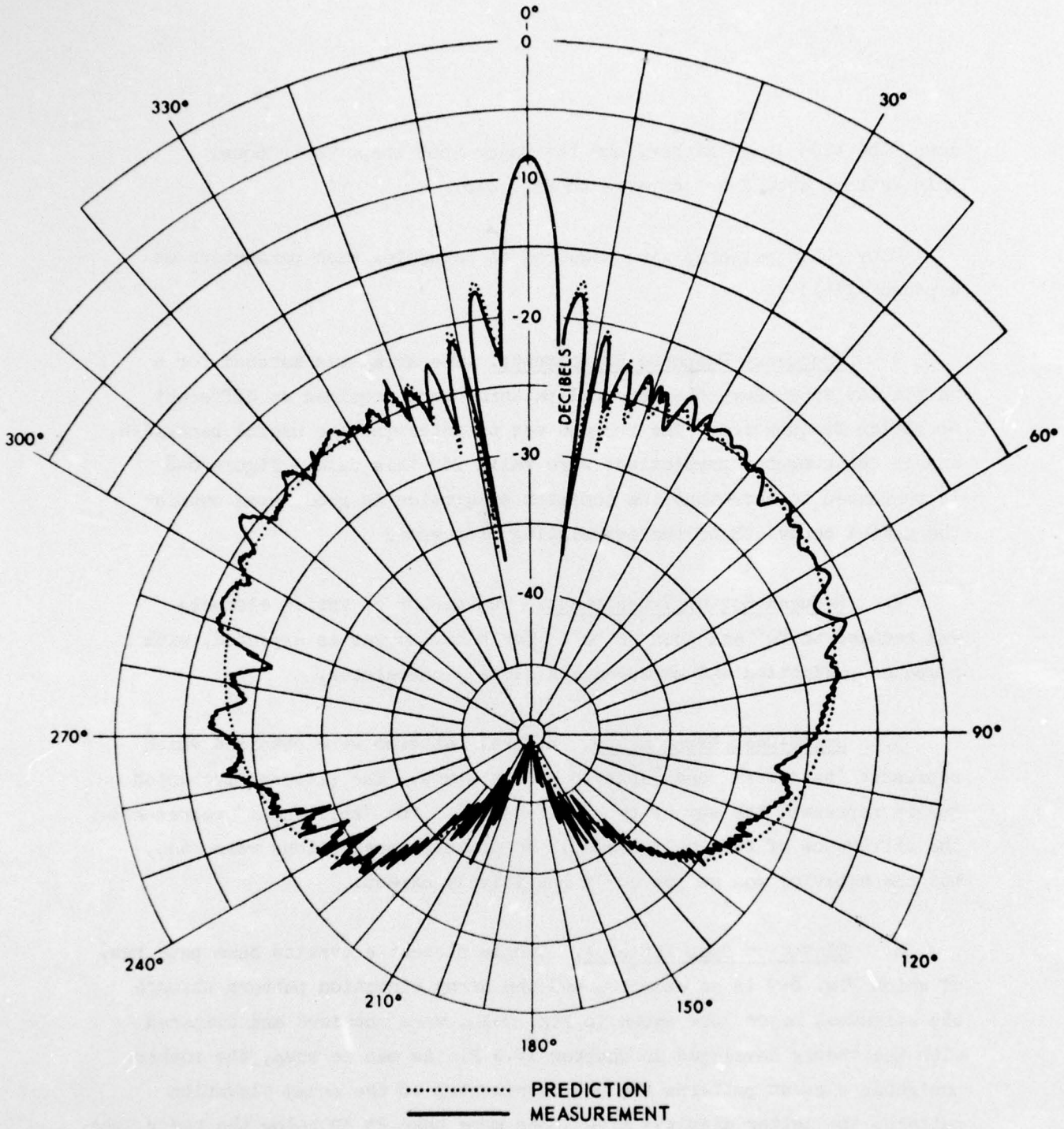

FIGURE 8-8
AZIMUTHAL BEAM PATTERN

PATTERN MEASURED AT 100 kHz
COEFFICIENTS COMPUTED FOR 92 kHz
TARGET RANGE: 25.5 ft
FOCUS RANGE: 25.5 ft

ARL - UT
AS-74-1255
BOM - DR
11 - 15 - 74

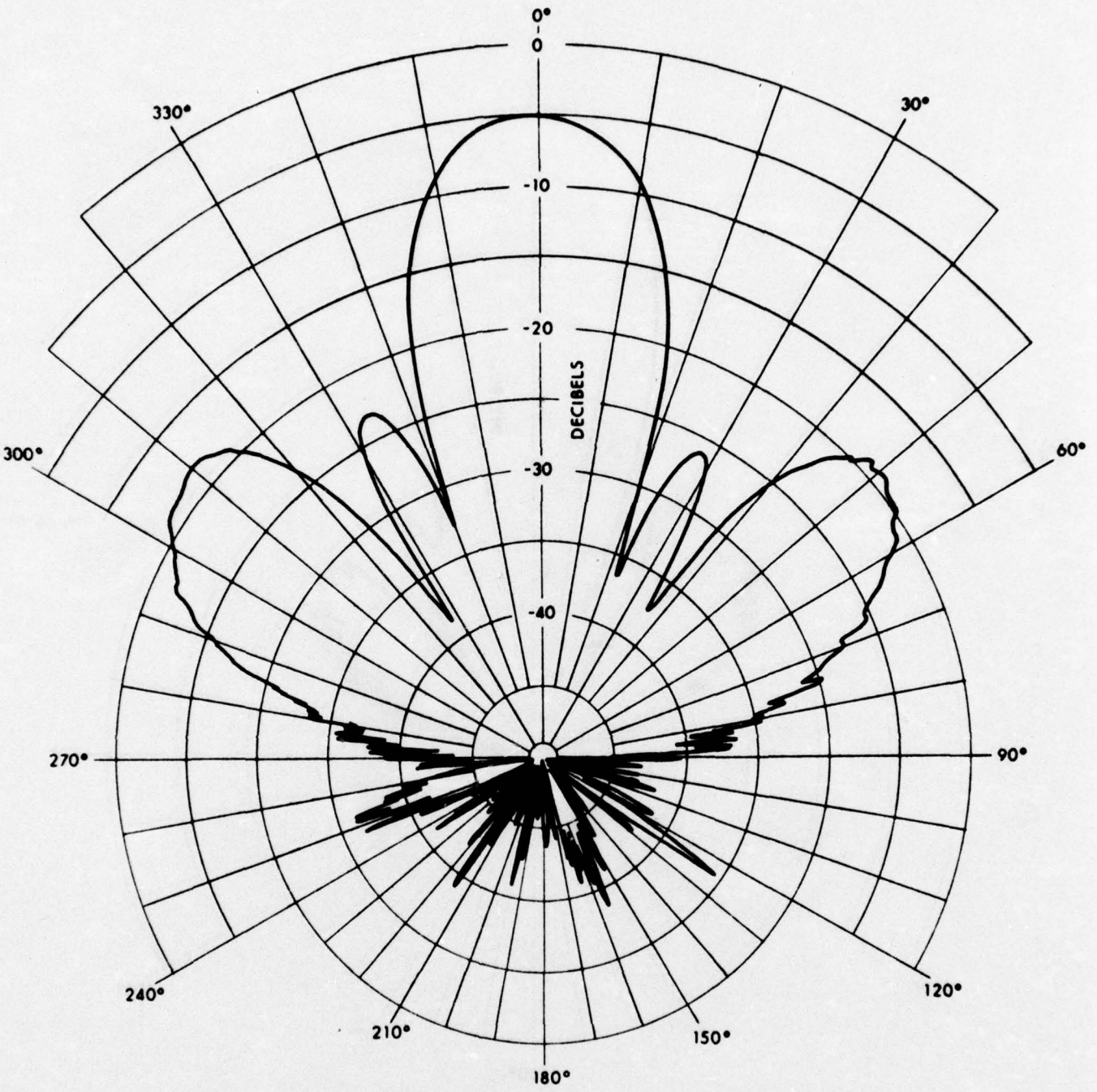

FIGURE 8-9
VERTICAL BEAM PATTERN
TYPICAL ARRAY ELEMENT

ARL - UT
AS-74-1264
BOM - DR
11 - 15 - 74

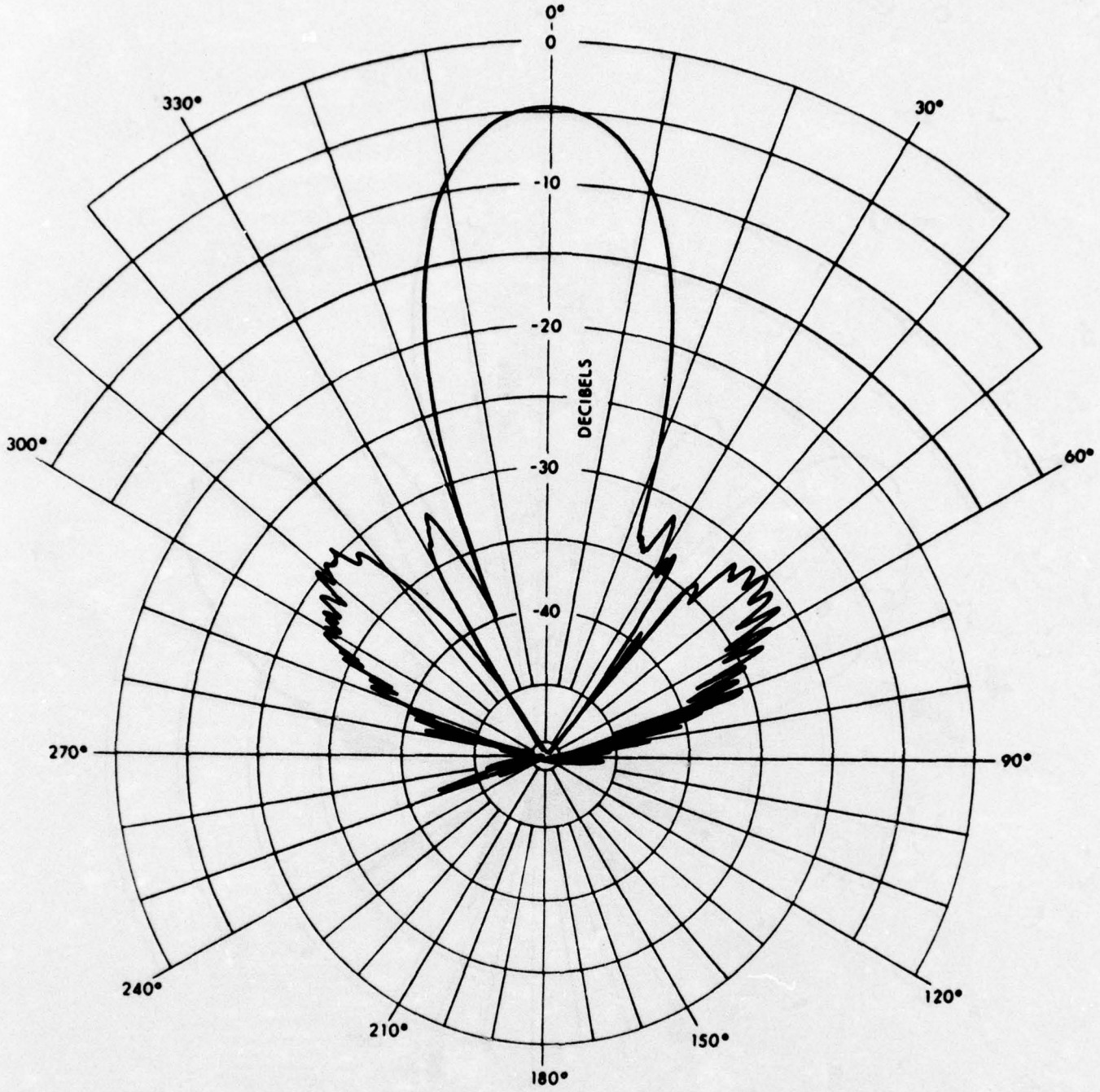

FIGURE 8-10
VERTICAL BEAM PATTERN

COMPOSITE ARRAY
TARGET RANGE: 26 ft
FOCUS RANGE: 26 ft

ARL - UT
AS-74-1265
BOM - DR
11 - 15 - 74

further show that the computer implemented mathematical model is able to predict the true results, not only in basic character, but also in the detail structure of the side lobe region.

IX. CONCLUSIONS AND RECOMMENDATIONS

It has been shown that beam formation can be accomplished with elements or staves on the surface of a cylindrical baffle without the use of delay lines or phase shift networks. The shading coefficients can be real (vice complex) numbers. The ease of implementation is the greatest advantage accruing from the use of the method.

This report has summarized the results of a study of the correlation beamformer. Coefficient selection algorithms have been developed which, when used, result in a specific useful array performance. The method may involve the use of a coded transmission so that replica correlation can take place on the array during reception. In fact, the method takes advantage of the cylindrical shape of the array in all respects rather than, as was done before this study, attempting to make the array appear as a plane.

Another advantage of this approach is that smaller cylindrical arrays can be made to deliver equal performance. For example, the TDA was configured to deliver equal or better performance in a smaller size than the cylindrical transducer (CT) for an experimental sonar. The CT was 26 in. in diameter and the TDA was 17 in. in diameter. The CT used 1620 elements and the TDA used 180. Both arrays operated at the same frequency and delivered equal beamwidths with the same side lobe performance. Appendix C contains other examples of cost and size comparisons.

The method is relatively easy to implement, even in the preformed beam configuration. Further, Chapter VI describes the capability of scanning a single beam at a rate sufficient to cover the azimuthal plane and discern targets as little as 3 in. apart. Such scanning ability cannot be claimed for time delay or phase shift beamformers. Scanning a single beam further reduces the hardware required to construct high resolution sonar soundheads.

Several aspects of beamforming discussed in this report are equally applicable to other methods of beamforming. For example, the bandwidth and the elevation beam patterns of a phase shift beamformer should behave with array depth as described herein.

It is recommended that the following steps be taken to further prove the method and to show conclusively the performance and the advantages that will accrue by the use of the correlation beamformer.

1. Only one code class for pulse compression has so far been found. Although it does accomplish the objective of pulse compression, it exhibits several undesirable characteristics which should be eliminated. It is recommended that a test of the presently available pulse code be accomplished with suitable hardware. The test should include angle and time response measurements of the array and tests of the ability of the code to operate in bottom reverberation.

2. It is recommended that an additional study of pulse codes be instituted to develop a method for tailoring the array time response to system design goals.

3. It is recommended that a full-scale beam scanner be designed and constructed to verify the hardware savings that can be achieved with the correlation beamformer. Such a scanner could be tested with the array hardware developed in Item 1.

4. It is recommended that suitable hardware be developed and tested which can insonify large angular sectors with the pulse code transmission at suitable source levels.

5. It is recommended that an analytical study of optimization techniques (Chapter VII and Appendix B) be instituted. The technique of linear programming has already demonstrated its capabilities in several beamformer applications. It is expected to be especially useful in pulse code selection.

APPENDIX A

THE ASSORTED EFFECTS OF REDUCING THE SECTOR OF ACTIVE ELEMENTS

APPENDIX A

THE ASSORTED EFFECTS OF REDUCING THE SECTOR OF ACTIVE ELEMENTS

The reference array considered in Chapter III of this report contains active elements on one-half of the cylinder ($2\alpha_N \approx 180°$). The array depth, in the direction of signal propagation, is therefore R (the array radius in wavelengths). This array depth has been shown to influence or control the elevation beam patterns, the frequency response of the beamformer, and the array rise time.

For whatever reason, if the sector of active elements is reduced, there is an attendant reduction in the array depth, the array width (the aperture), the number of contributing elements, and the maximum dimension of the array. If some parameter, such as beamwidth, is to remain unaffected as the sector reduction takes place, the problem becomes more complicated.

This appendix will present design equations and plots of their functional dependence which will be useful in studying or designing a reduced sector array.

A single beam requires an aperture W on a cylinder of radius R, which results in an array depth L. The aperture is composed of a sector of active elements covering an angle on the cylinder of $2\alpha_N$. The design may include several preformed beams covering a region in space measured by the angle S. These statements are illustrated in Fig. A-1. As can be seen from Fig. A-1,

$$W = 2R \sin \alpha_N \qquad \text{(A-1)}$$

and

$$L = R(1 - \cos \alpha_N) \quad . \qquad \text{(A-2)}$$

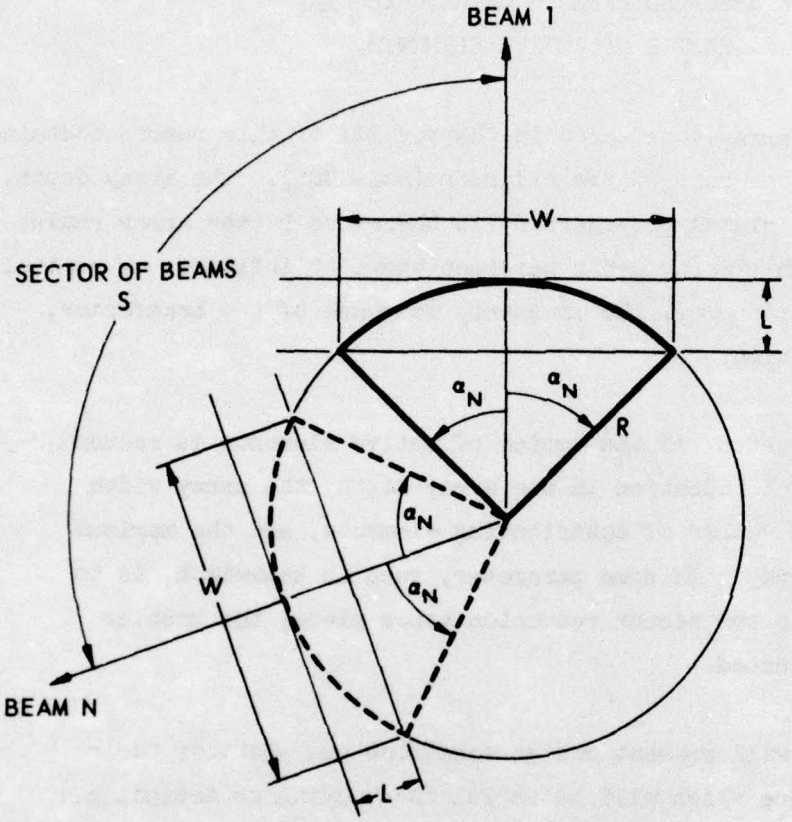

TOTAL SECTOR OF ACTIVE ELEMENTS IS ($S + 2\alpha_N$)

FIGURE A-1
REDUCED SECTOR GEOMETRY

ARL - UT
AS-76-17
DAS - DR
1 - 6 - 76

If one desires a beamwidth of BW (degrees), then an aperture width of W=K/BW wavelengths is required, and R must grow to keep pace with any decrease in sin α_N. That is,

$$R = \frac{R_o}{\sin \alpha_N} = R_o F_1 \quad , \tag{A-3}$$

where

$$R_o = \frac{W}{2} = \frac{K}{2\ BW(deg)} \quad , \tag{A-4}$$

and

$$F_1 = \frac{1}{\sin \alpha_N} \quad , \tag{A-5}$$

a function which is shown graphically in Fig. A-2.

If one wishes an array depth of L wavelengths, and the array radius is R, then either

$$L = R(1 - \cos \alpha_N) \tag{A-6}$$

or

$$R = \frac{L}{(1 - \cos \alpha_N)} \quad . \tag{A-7}$$

Both of these functions are plotted in Fig. A-3.

One can compute the area of the resolution cell of an array with reduced sector by noting that

$$\Delta y = \rho BW(rad) = \frac{K\rho}{W} \frac{\pi}{180} \quad , \tag{A-8}$$

and

$$\Delta X = \frac{L\lambda}{2} = \frac{R\lambda}{2} (1 - \cos \alpha_N) \quad , \tag{A-9}$$

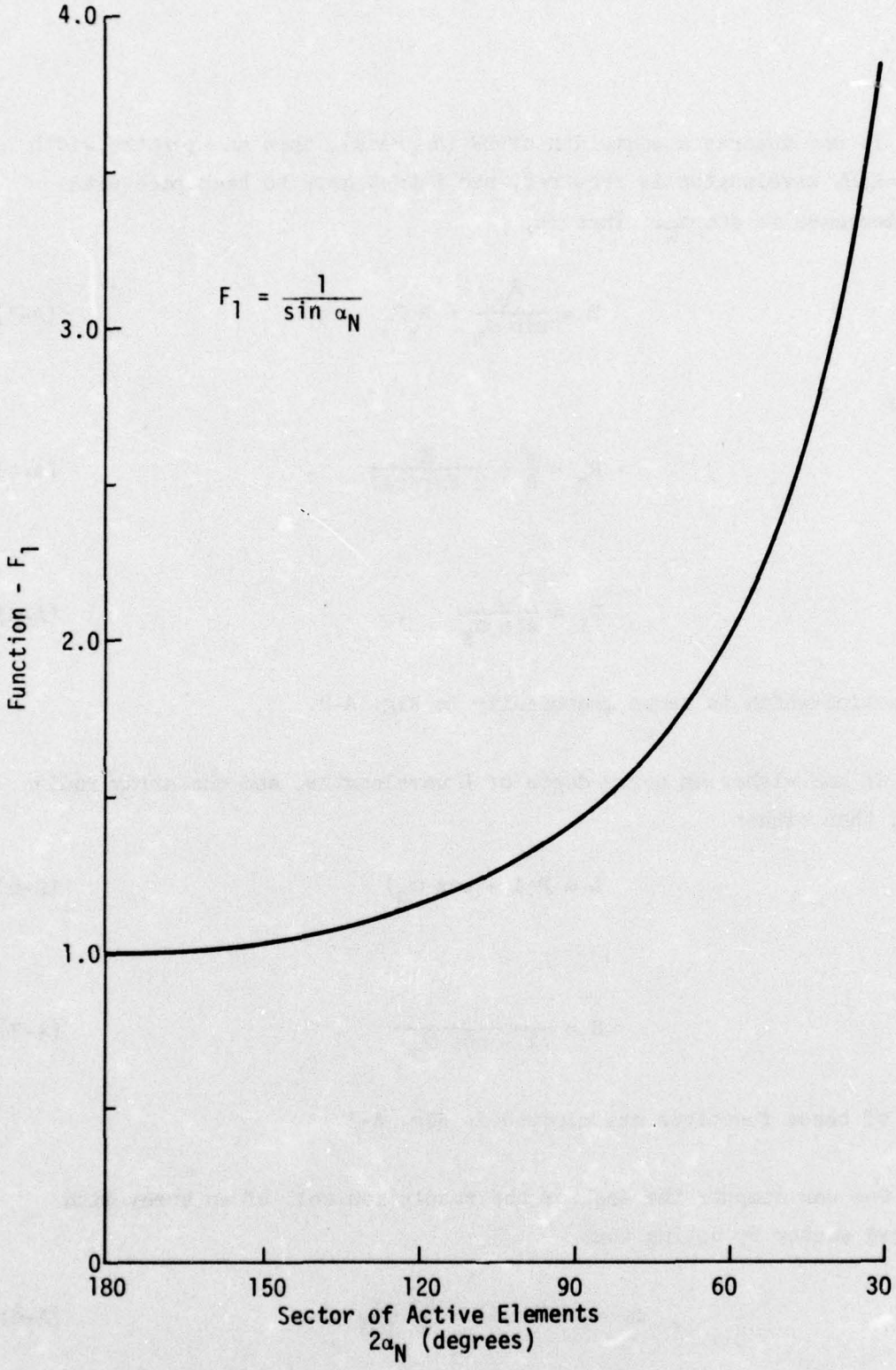

FIGURE A-2
PLOT OF F_1 VERSUS $2\alpha_N$

AS-74-1808
DAS-0031-3

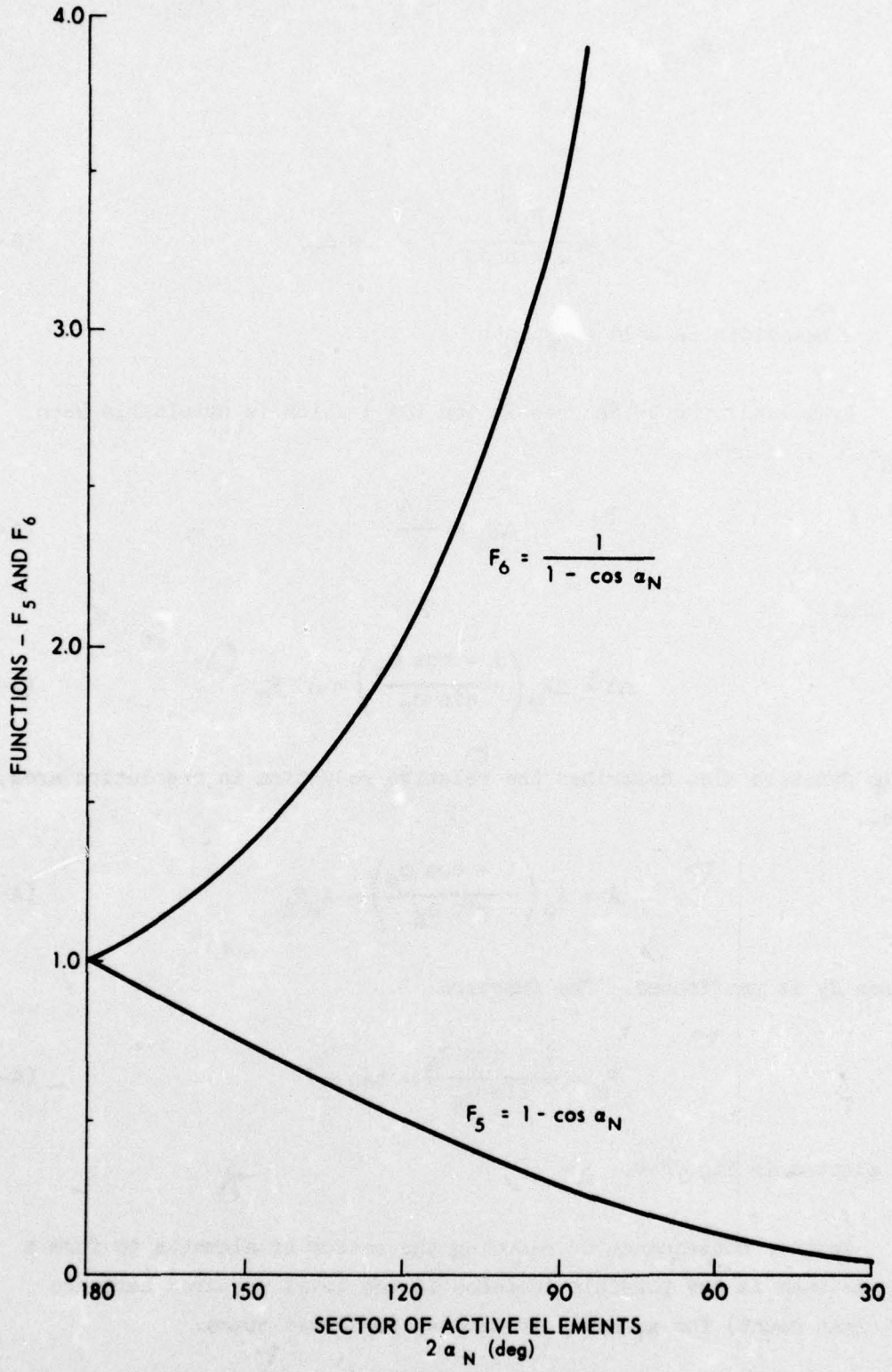

FIGURE A-3
PLOT OF F_5 AND F_6 VERSUS $2\alpha_N$

ARL - UT
AS-76-19
DAS - DR
1 - 6 - 76

or

$$\Delta X = \frac{R_o \lambda}{2 \sin \alpha_N} (1 - \cos \alpha_N) \tag{A-10}$$

if the beamwidth is held constant.

By normalizing to the resolution (ΔX_o) which is obtainable when $2\alpha_N = 180°$, we have

$$\Delta X_o = \frac{R_o \lambda}{2} \quad , \tag{A-11}$$

so that

$$\Delta X = \Delta X_o \left(\frac{1 - \cos \alpha_N}{\sin \alpha_N} \right) = \Delta X_o F_2 \tag{A-12}$$

This function also describes the relative reduction in resolution area, i.e.,

$$A = A_o \left(\frac{1 - \cos \alpha_N}{\sin \alpha_N} \right) = A_o F_2 \tag{A-13}$$

since Δy is unaffected. The function

$$F_2 = \frac{1 - \cos \alpha_N}{\sin \alpha_N} = \tan \frac{\alpha_N}{2} \tag{A-14}$$

is plotted in Fig. A-4.

Another consequence of reducing the sector of elements to form a single beam is the possible increase in the total required hardware (element count) for an array of several preformed beams.

If the angular sector width of active elements for one beam is $2\alpha_N$ radians, and if the sector width covered by additional preformed beams is S radians, then the angle subtended by elements on the cylinder is

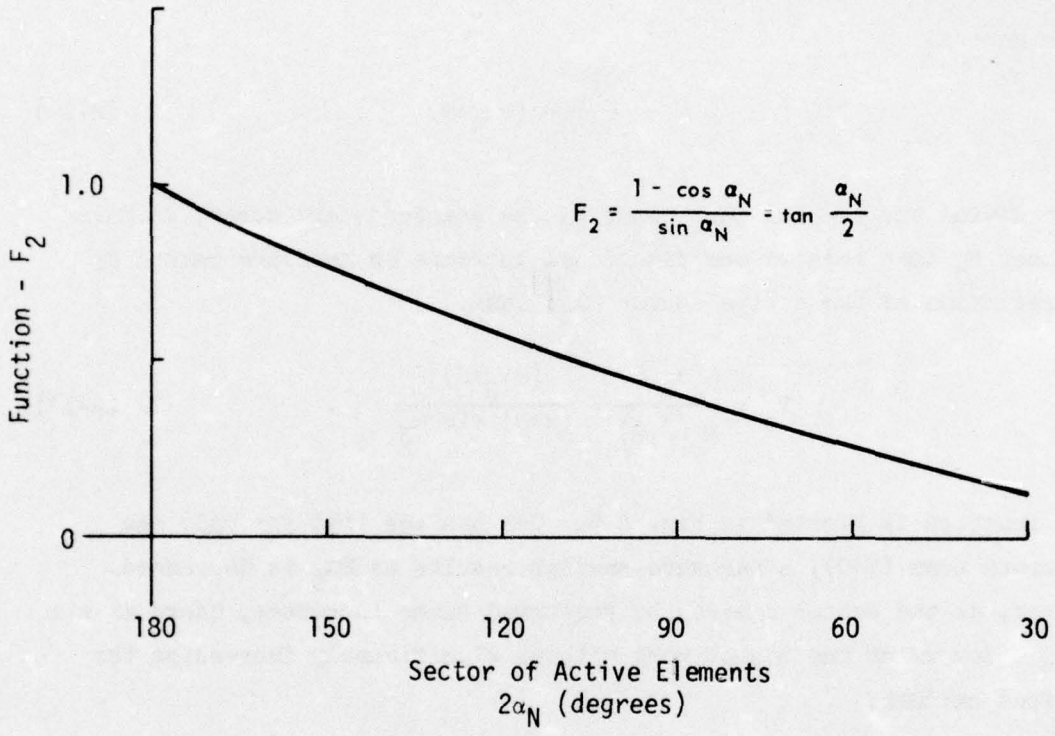

FIGURE A-4
PLOT OF F_2 VERSUS $2\alpha_N$

AS-74-1809
DAS-0031-3

$2\alpha_N+S$ radians. The required length of arc on the cylinder is $R(2\alpha_N+S)$; there are two elements per wavelength, so the number of elements, preamplifiers, and filters each is

$$M = 2R(2\alpha_N+S) \quad , \tag{A-15}$$

or in general

$$M = \frac{2R_o}{\sin \alpha_N} (2\alpha_N+S) \quad . \tag{A-16}$$

If we divide the general part count by the standard part count, we have a number F_3 that relates the fractional increase in hardware caused by the reduction of the active sector $2\alpha_N$; thus,

$$F_3 = \frac{M(\alpha_N,S)}{M_o\left(\frac{\pi}{2},S\right)} = \frac{(2\alpha_N+S)}{(\pi+S)\sin \alpha_N} \quad . \tag{A-17}$$

This function is plotted in Fig. A-5. One can see that for only one preformed beam (S=0), a hardware savings results as $2\alpha_N$ is decreased. However, as the sector covered by preformed beams increases, there exists an α_N below which one cannot work without significantly increasing the required hardware.

An additional function F_4 relates the largest dimension LD of the array to changes in $2\alpha_N$. The sector of active elements is $2\alpha_N+S$. The chord of this arc is

$$\begin{aligned} LD &= 2R \sin\left(\alpha_N + \frac{S}{2}\right) \quad \text{for} \quad \alpha_N + \frac{S}{2} \leq \frac{\pi}{2} \quad ; \\ LD &= 2R \qquad\qquad\qquad\qquad \text{otherwise.} \end{aligned} \tag{A-18}$$

Again, to preserve BW, replace R by $R_o/\sin \alpha_N$, so that

$$LD = \frac{2R_o}{\sin \alpha_N} \sin\left(\alpha_N + \frac{S}{2}\right) \quad . \tag{A-19}$$

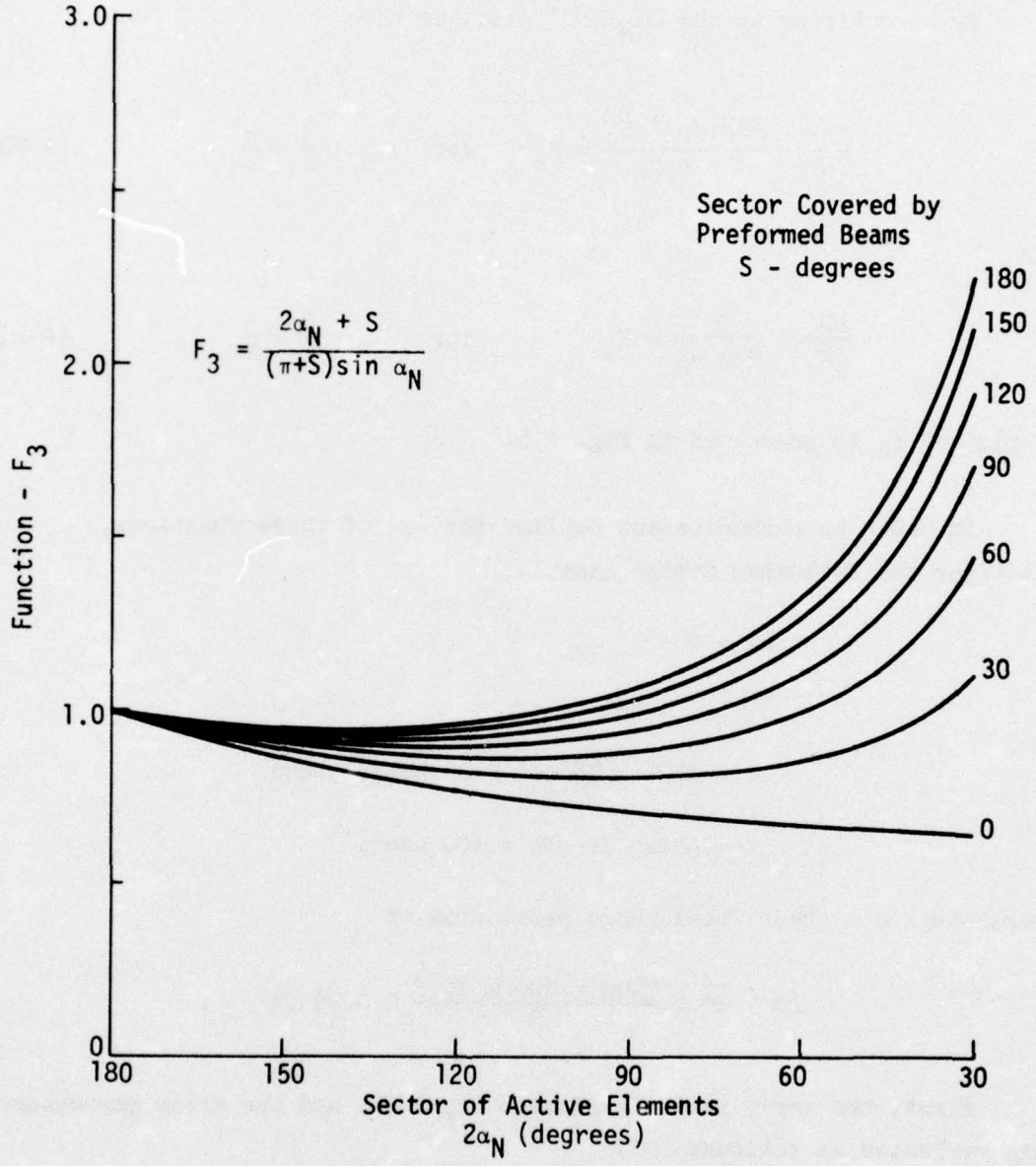

FIGURE A-5

PLOT OF F_3 VERSUS $2\alpha_N$ AND S

AS-74-1807
DAS-0031-3

By normalizing to the $2\alpha_N=180°$ case, we have

$$\frac{LD}{2R_o} = \frac{\sin\left(\alpha_N + \frac{S}{2}\right)}{\sin \alpha_N} = F_4 \quad \text{for} \quad \alpha_N + \frac{S}{2} \leq \frac{\pi}{2} \quad , \tag{A-20}$$

or

$$\frac{LD}{2R_o} = \frac{1}{\sin \alpha_N} = F_4 \quad \text{for} \quad \alpha_N + \frac{S}{2} > \frac{\pi}{2} \quad . \tag{A-21}$$

A plot of F_4 is presented in Fig. A-6.

In order to summarize and outline the use of these functions, consider the following design example:

$$BW = 0.3° \quad ,$$

$$f_o = 300 \text{ kHz} \quad ,$$

$$S = 120° = \frac{2\pi}{3} \text{ rad (400 beams), and}$$

$$\tau = \text{pulse length} = 100 \ \mu\text{sec},$$

resulting in a theoretical range resolution of

$$\Delta X = \frac{c\tau}{2} = \frac{5000 \times 100 \times 10^{-6}}{2} = 0.25 \text{ ft} \quad .$$

First, the array is designed with $2\alpha_N=180°$, and the array parameters are evaluated as follows:

(1) $$\lambda_o = \frac{c}{f_o} = \frac{5000}{300{,}000} = 0.01667 \text{ ft} \quad ,$$

(2) $$R_o = \frac{29.5}{BW} = \frac{29.5}{0.3} = 98.33 \quad ,$$

or

$$R_o\lambda = 98.33 \times 0.01667 = 1.64 \text{ ft} \quad ,$$

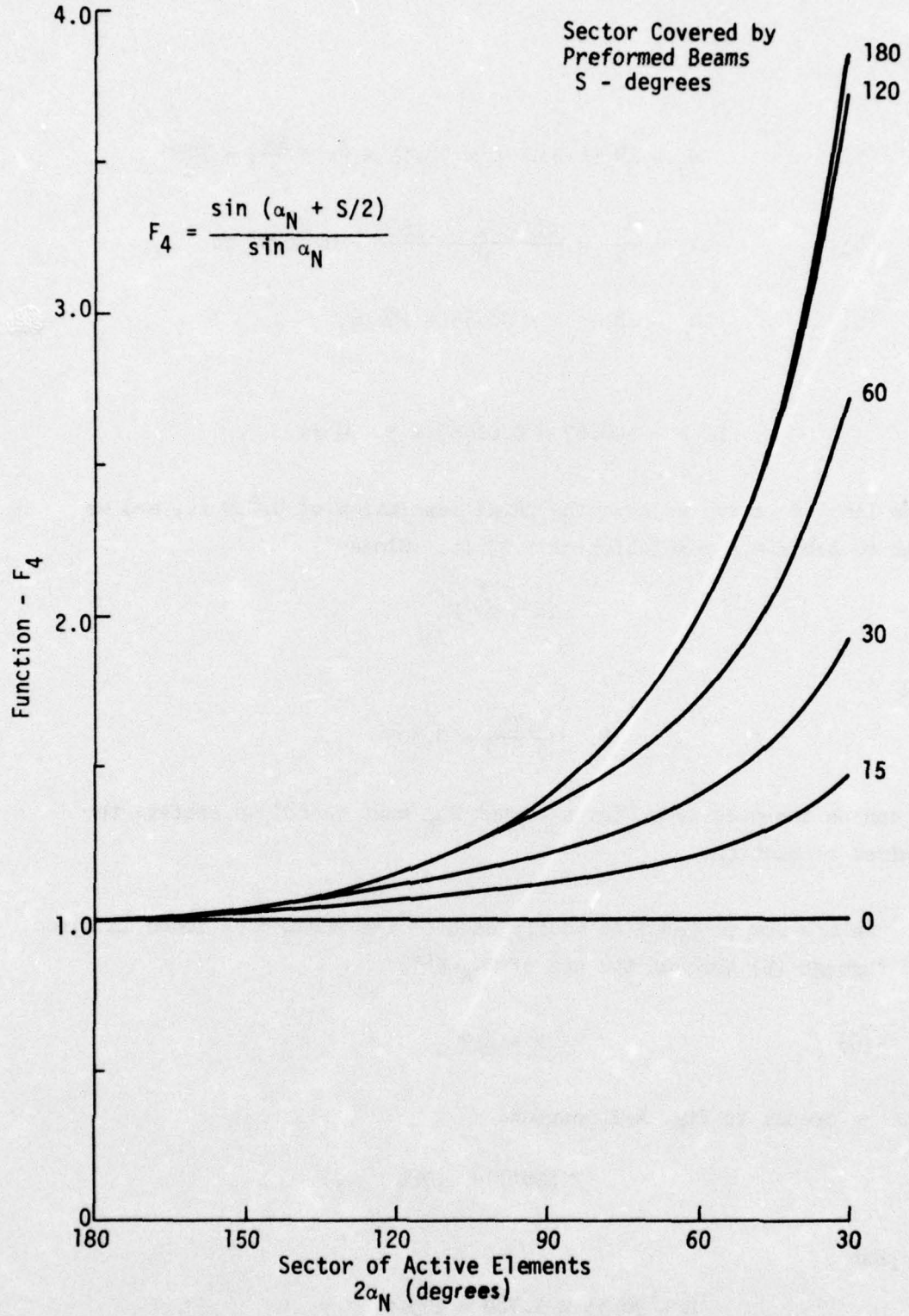

FIGURE A-6

PLOT OF F_4 VERSUS $2\alpha_N$ AND S

AS-74-1806
DAS-0031-3

(3) $$M_o = 2R_o(\pi+S) = 2 \times 98.33 \times \left(\pi + \frac{2\pi}{3}\right) = 1030 \quad ,$$

(4) $$\Delta X_o = \frac{R_o \lambda}{2} = \frac{98.33 \times 0.01667}{2} = 0.81958 \text{ ft} \quad ,$$

(5) $$LD_o = 2R_o = 2 \times 98.33 = 196.67 \quad ,$$

or

$$LD_o\lambda = 196.67 \times 0.01667 = 3.278 \text{ ft} \quad .$$

From line (4) above we have the range resolution of 0.819 ft, and we wish to achieve a resolution of 0.25 ft. Since

$$\Delta X = \Delta X_o F_2$$

and

$$F_2 = \frac{0.25}{0.819} = 0.305 \quad ,$$

it can be computed from Fig. A-4 that $2\alpha_N$ must be 68° to achieve the desired resolution.

We are now prepared to modify each of the parameters found in lines (2) through (5) through the use of $2\alpha_N$=68°:

(6) $$R = R_o F_1 \quad .$$

With reference to Fig. A-2, compute

$$F_1(68°) = 1.788 \quad ,$$

so that

$$R = 98.33 \times 1.788 = 175.8 \quad ,$$

or

$$R\lambda = 175.8 \times 0.01667 = 2.93 \text{ ft} \quad .$$

(7) $$M = M_o F_3 \quad .$$

With reference to Fig. A-5, compute

$$F_3(2\alpha_N, S) = F_3(68°, 120°) = 1.12 \quad ,$$

so that

$$M = 1030 \times 1.12 = 1155 \quad .$$

(8) $$LD = 2R_o F_4 \quad .$$

With reference to Fig. A-6, compute

$$F_4(68°, 120°) = 1.788 \quad ,$$

so that

$$LD = 2 \times 98.33 \times 1.788 = 351.68 \quad ,$$

or

$$LD\lambda = 351.68 \times 0.01667 = 5.86 \text{ ft} \quad .$$

Thus, the adding-only array for these parameters will have the following design features:

maximum dimension	= 5.86 ft ,
number staves (preamplifiers, etc.)	= 1155 ,
range resolution (equivalent to τ=100 μsec)	= 0.25 ft , and
radius of curvature of array	= 2.93 ft .

It should be noted that, even though reducing the sector $2\alpha_N$ will solve some range resolution problems, the best solution is to find a suitable pulse shape that will give the range resolution by pulse compression. When compression is accomplished, this array can be built in a 3.3 ft package, compared to the 5.9 ft indicated above.

APPENDIX B

BEAMFORMER OPTIMIZATION TECHNIQUES

APPENDIX B

BEAMFORMER OPTIMIZATION TECHNIQUES

A. Introduction

At the present time there exists no direct analytic techniques for the selection of shading coefficients to form beams with elements placed in a nonplanar arrangement. Design techniques in use today are either approximations to the planar case, some algorithmic method as described in this report, or else some iterative technique. The technique of "phasing-to-a-plane" is an example of approximating a plane array. Trial and error is an example of an iterative technique. A somewhat more sophisticated iterative technique is linear programming, which is the principal subject of this appendix.

Linear programming has been applied to the problem of determining the real coefficients for a circular array of given element number and spacing. The coefficients were determined by this method to obtain as closely as possible a desired array beam pattern.

The results of this linear programming investigation have been encouraging from several aspects. First of all, the validity of the design technique discussed in other sections of this report has been confirmed. For example, those design procedures are seen to produce beam patterns within 1 dB in peak side lobe response and within about 20% of the minimum beamwidth attainable with the linear programming optimum design. Second, however, this investigation has shown that there are some worthwhile gains to be made by the application of optimization techniques to beamformer design. Besides the narrower beamwidth and improved side lobe control, there are indications that the response of the array to a pulse signal can be tailored, within limits, to meet other system design goals.

The study reported here was brief and centered on only one optimization technique, linear programming. There are other optimization methods which are perhaps more suited to the problem at hand. Linear programming is not, strictly speaking, applicable to the beamformer optimization problem. Therefore we have approximated the true problem by another problem which is directly solved with the linear program. Some other practical optimization technique may be more directly applicable to the beamformer optimization problem. This should be the subject of a further investigation.

The following sections detail the linear programming approach to beamformer optimization.

B. Linear Programming

The linear programming problem that we will solve can be stated in the following form: find the $\{A_i\}$, i=0,1,2,...,N, subject to the constraints

$$\sum_{i=0}^{N} A_i \, c_{ji} \leq b_j \quad , \quad j = 1, 2, \ldots, M \qquad M \geq N + 1 \tag{B-1}$$

such that

$$\sum_{i=0}^{N} A_i \, d_i \tag{B-2}$$

is maximized. We do not require the $A_i \geq 0$ as usually stated in the more general linear programming problem.

One characteristic of linear programs is that, if a solution exists, it can be found in a finite number of iterations. There are also procedures for determining if a solution exists, or if the solution is unbounded.

The primary reason for using linear programming to optimize the beamformer is that there are many computer programs available to solve the problem. This limits the beamformer optimization problem, so far as we are concerned, to setting up the problem in the form previously stated and then using the appropriate routine to find the array coefficients. In the next section we discuss the approximation of the true beamformer problem by one that fits the desired form.

C. The Optimization Problem

The output of the circular array to a signal incident from direction φ can be expressed as the convolution of the array impulse response and the input signal:

$$h(t,\varphi) = \sum_{n=-N}^{N} A_n I(\alpha_n-\varphi) s\left[t + \frac{r}{c}\cos(\alpha_n-\varphi)\right] \quad , \qquad \text{(B-3)}$$

where

A_n = coefficients of the 2N+1 elements,
$I(\alpha_n-\varphi)$ = individual element beam pattern,
$s(t)$ = signal,
c = sound speed, and

α_n, φ, and r are as defined by Fig. 3-1. The time reference for both $s(t)$ and $h(t,\varphi)$ are taken to be the center of the array. Here $h(t,\varphi)$ is the response of the array to the signal $s(t)$ incident on the array in the φ direction, and so $h(t,\varphi)$ actually represents a directivity function or beam pattern for the array.

If the A_n are constrained to be symmetric so that $A_n=A_{-n}$, n=1, 2,...,N, and the individual element beam patterns are also symmetric about their facing directions, then the resulting beam patterns will be symmetric about $\varphi=0$ and we have

$$h(t,\varphi) = A_o I(\varphi) s(t + \frac{r}{c}\cos\varphi)$$

$$+ \sum_{n=1}^{N} A_n \left\{ I(\alpha_n - \varphi) s[t + \frac{r}{c}\cos(\alpha_n - \varphi)] \right. \tag{B-4}$$

$$\left. + I(\alpha_n + \varphi) s[t + \frac{r}{c}\cos(\alpha_n + \varphi)] \right\} \quad .$$

Since the time of arrival of the signal is ordinarily unknown, a more useful characterization of the array beam pattern is the envelope of $h(t,\varphi)$, which we designate by $H(t,\varphi)$.

$$H(t,\varphi) = \left[h^2(t,\varphi) + h'^2(t,\varphi) \right]^{1/2} \quad , \tag{B-5}$$

where the positive square root is taken so $H(t,\varphi)$ is nonnegative and $h'(t,\varphi)$ is the Hilbert transform of $h(t,\varphi)$ with respect to the time variable t. It is easy to show that

$$h'(t,\varphi) = A_o I(\varphi) s'(t + \frac{r}{c}\cos\varphi)$$

$$+ \sum_{n=1}^{N} A_n \left\{ I(\alpha_n - \varphi) s'[t + \frac{r}{c}\cos(\alpha_n - \varphi)] \right. \tag{B-6}$$

$$\left. + I(\alpha_n + \varphi) s'[t + \frac{r}{c}\cos(\alpha_n + \varphi)] \right\} \quad ,$$

where $s'(t)$ represents the Hilbert transform of $s(t)$. We note that both $h(t,\varphi)$ and $h'(t,\varphi)$ are linear functions of the $\{A_n\}$, but $H(t,\varphi)$ is not.

Now, in order to form a beam pattern with peak side lobe level SLL at time $t=t_o$, we require

$$H(t_o,\varphi) = 1, \quad \varphi = 0 \quad , \tag{B-7}$$

$$H(t_o,\varphi) \leq \text{SLL}, \quad \varphi_b \leq \varphi < 100^\circ \quad , \tag{B-8}$$

where φ_b is the angle at which the main lobe response first reaches the peak side lobe level. Thus $2\varphi_b$ is the total width of the main lobe at the side lobe level. The response at $\varphi=0$, the direction of the main lobe, is required to be unity.

Another approach to the requirement stated by Eq. (B-8) is to quantize the angle φ in the range $(\varphi_b, 180°)$. If the quantization interval on φ is small enough, then Eq. (B-8) will effectively be met. Then the side lobe constraints become

$$H(t_o,\varphi_j) \leq \text{SLL} \qquad j = 1, 2, \ldots, M \tag{B-9}$$

and the main lobe response can be assured by maximizing

$$H(t_o,\varphi), \qquad \varphi = 0 \tag{B-10}$$

Equations (B-9) and (B-10) then are similar to Eqs. (B-1) and (B-2) except that Eqs. (B-9) and (B-10) are not linear functions of the $\{A_n\}$. However, the constraints expressed by Eq. (B-9) will be met if all the following linear constraints are met simultaneously:

$$\left.\begin{aligned} h(t_o,\varphi_j) &\leq 0.707\ \text{SLL} \\ -h(t_o,\varphi_j) &\leq 0.707\ \text{SLL} \\ h'(t_o,\varphi_j) &\leq 0.707\ \text{SLL} \\ -h'(t_o,\varphi_j) &\leq 0.707\ \text{SLL} \end{aligned}\right\} \quad j = 1, 2, \ldots, M \tag{B-11}$$

This set of Eq. (B-11) overly constrains the beam pattern, since Eq. (B-11) is a sufficient but not necessary condition for Eq. (B-9). By a similar line of reasoning, Eq. (B-10) can be replaced by maximizing

$$h(t,\varphi) \qquad \varphi = 0 \tag{B-12}$$

We have thus linearized the problem by substituting the set of $4M$ constraints Eq. (B-11) for the M constraints Eq. (B-9), and by changing

the objective function Eq. (B-10) to Eq. (B-12). Equations (B-11) and (B-12) are in the form specified for Eqs. (B-1) and (B-2); therefore the linear programming routine may be applied to the solution of Eqs. (B-11) and (B-12).

In the next section some of the results of the linear programming approach to the problem using Eqs. (B-11) and (B-12) are presented.

D. Linear Programming Results and Conclusions

The linear programming technique discussed in the previous section was applied to the design of a 77-element array of elements spaced on half-wavelength centers around a semicircle of radius 12.3 wavelengths. The objective of the design was to obtain a main lobe beamwidth as narrow as possible while maintaining uniformly low side lobes.

Several slightly different parameter values were chosen for test. The parameter values used and the most important design values resulting therefrom are given in Table B-1. The parameter φ_b controls the main lobe width since the first side lobe constraint is placed at that angle. The remaining side lobe constraints were placed at 1° intervals from 3° to 90°. The parameter t_o is used to control the phasing of the signal to which the array is "matched" by the optimization process. In all these designs the signal was a sine wave with constant amplitude. The value t_o=-0.05 corresponds to the situation where a peak of the sine wave signal is coincident with the front of the array. For t_o=0.0, the signal peak was 18° behind (toward the array center) the front of the array. The latter phasing gives slightly better results, but no effort was made to determine the optimum phasing.

For reference, the beam pattern obtained by choosing the element gains according to the rules outlined in this report is given in Fig. B-1, and the design values are also given in Table B-1. The coefficients chosen were for the reference array.

TABLE B-1

COMPARISON OF BEAM PATTERN PARAMETERS BETWEEN ALGORITHMIC APPROACH AND LINEAR PROGRAMMING TRIALS

TEST	DESIGN PARAMETERS		PEAK SIDE LOBE (dB)	BEAMWIDTH (deg)	
	φ_b	t_o		-3 dB	At Peak Side Lobe Level
0*	—	—	-16.2	2.5	5.3
1	2.7	-0.05	-17.0	2.2	4.5
2	2.0	-0.05	-15.1	2.0	3.9
3	2.7	0	-16.7	2.2	4.5
4	2.2	0	-16.4	2.1	4.3

*Test 0 is the reference array case.

(Test 0 and 1 are shown in Figures B-1 and B-2, respectively.)

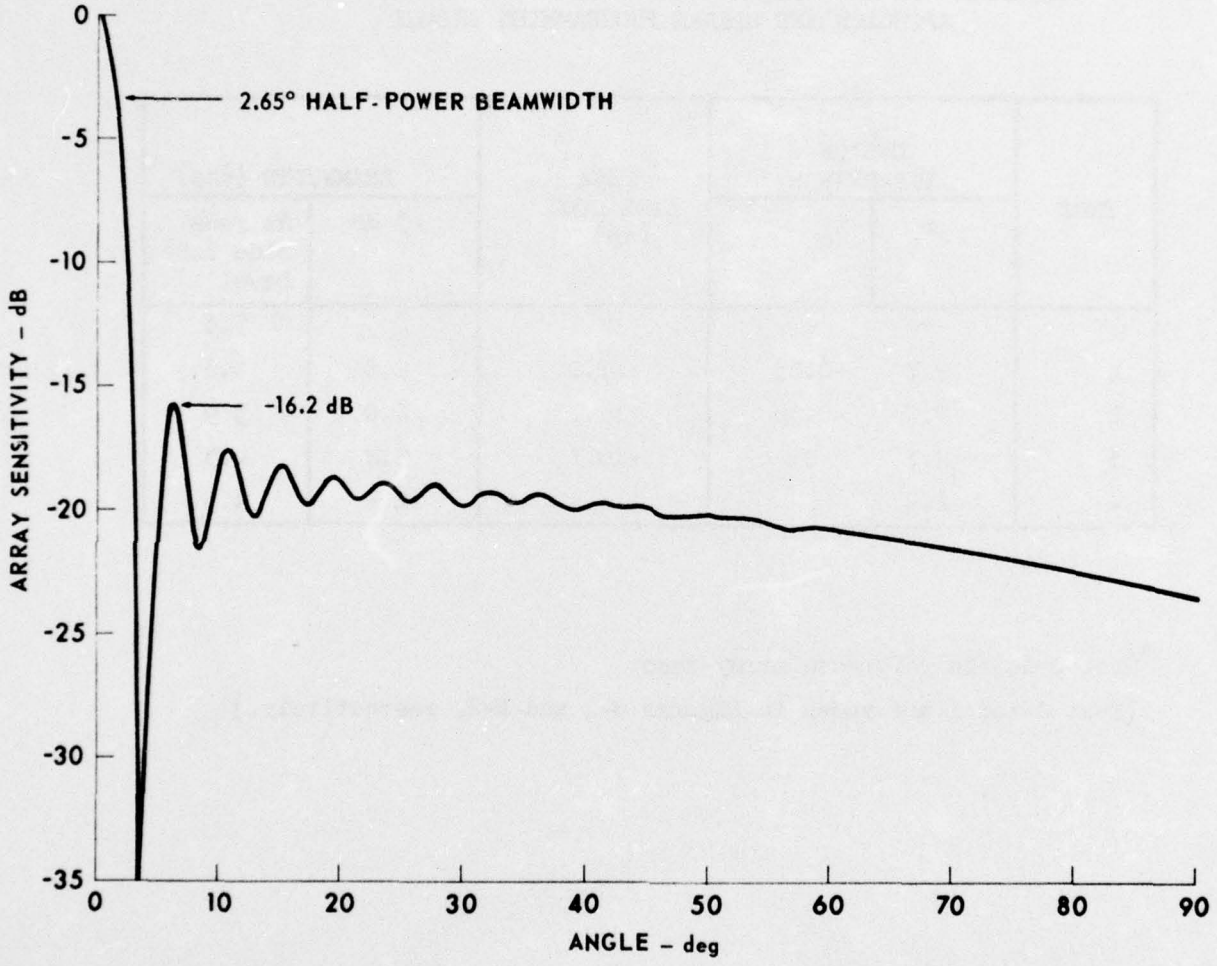

FIGURE B-1
AZIMUTHAL BEAM PATTERN
USING REFERENCE ARRAY COEFFICIENTS

ARL - UT
AS-76-56
DAS - DR
1 - 27 - 76

In all of the designs shown in Table B-1, the individual element patterns were assumed to be $[(1+\cos\beta)/2]^{3.8}$, where the angle β for each element is measured with respect to the direction that element is facing. Better beam patterns not included in this report were obtained assuming unity gain, semicircular, individual element patterns.

In the design values measured and listed in Table B-1, it is apparent that the linear program designs are somewhat better than the design of Fig. B-1. Main lobe widths approximately 14% narrower at both the 3 dB and the peak side lobe level points have been obtained without giving up peak side lobe level, thereby improving the directivity index by almost 1 dB. Perhaps more important, the troublesome first side lobe in Fig. B-1 has been effectively suppressed.

It should be pointed out that the beam patterns achieved in the four examples in the table are almost certainly not optimal because the side lobes are of varying height. Figure B-2 shows an example pattern from the linear program. A better design would reduce the largest side lobes at the expense of raising the smaller side lobes to yield an optimal Chebyshev pattern in which all the side lobes are the same height. Such a design can be approached with the repeated application of the techniques discussed here but no successful optimum designs were accomplished during this short study.

There are other important beamformer parameters, bandwidth and sensitivity, for instance, which have not been directly investigated in this brief study. It does not appear that linear program designs will prove to be difficult because of these considerations. In fact, the linear programming approach provides a means of directly addressing many such problems.

There remains one area of difficulty in the direct application of linear programming to beamforming as discussed here. That is in dealing with large arrays of many elements. While, in principle, the technique

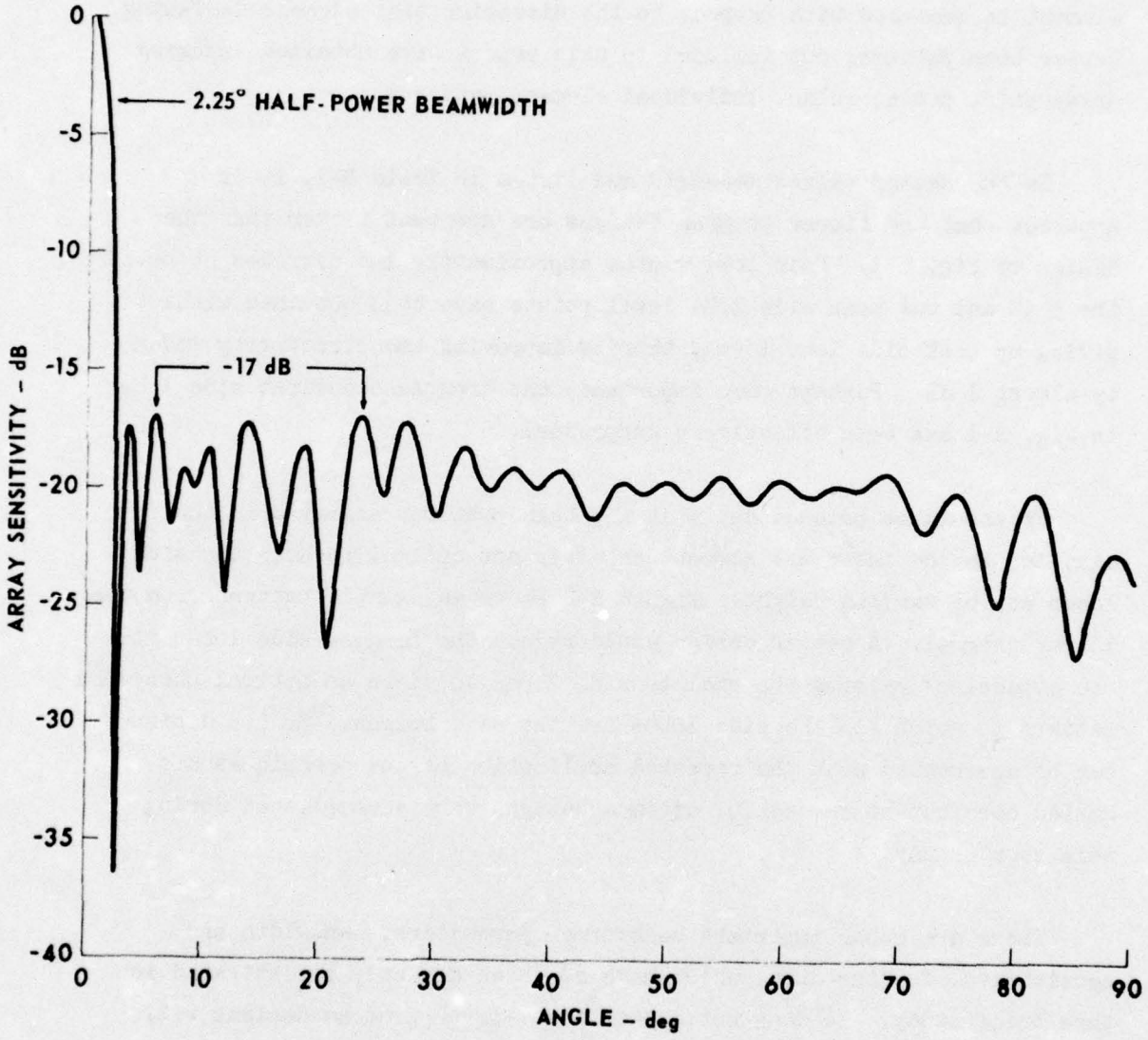

FIGURE B-2
AZIMUTHAL BEAM PATTERN
USING LINEAR PROGRAMMING COEFFICIENTS

ARL - UT
AS-76-57
DAS - DR
1 - 27 - 76

is independent of size, practical considerations limit the size of the arrays that may be handled to about 40 wavelengths radius and 250 elements. Perhaps larger arrays could be dealt with on the very large computers available today but the cost would be high. The patterns reported here for a 12.3 wavelength, 77-element array were generated in about 4 min each on a CDC 6600. The computer size and/or time requirements grow exponentially with problem size.

The solution to this difficulty lies not in larger and faster computers, but in a better algorithm to perform the optimizations. The linear program algorithm is probably not a very good technique for solving the beamformer problem; however it is readily available and therefore quite useful in an exploratory program. A really serious attempt at the optimization of large arrays of the type considered in this study will require a more fundamental look at optimization methods.

APPENDIX C

A SIZE AND COST COMPARISON

APPENDIX C

A SIZE AND COST COMPARISON

During the past several years ARL has been involved with either the specification, design, or construction of at least three small, high resolution sonars, whose application and requirements represent the solution to real, practical problems. Because of the applicability of these systems, they were selected for use in a realistic comparison with the new method.

The correlation method derives its advantage from the single fact that no time delay (delay lines) or phase shift networks are required. The beamformer cost is therefore reduced. In addition, because no practical delay line constraints are imposed, the entire diameter of a cylindrical array may be used as the aperture, resulting in either smaller arrays for the same beamwidth or higher resolution in the same sized arrays.

One should keep in mind that the three systems used for comparison are already compromises that are favorable to the delay line technique and size constraint. It is therefore fair to ask such questions as how the methods would compare if the angular resolution was doubled or the sector covered by preformed beams increased.

The first system used for comparison is called the Cylindrical Transducer (CT). It represents the experimental application of a cylindrical array to an existing sonar system. The array and beamformer simultaneously form 60 2° beams to cover 120° in azimuth, and are electrically switchable in 120° increments for a full 360° overall coverage. The total array diameter is 26 in. The beamformers use 60 delay lines costing about $70 each, for a total of about $4.2K. Each azimuthal beam is formed using 50 contiguous staves, for a total of 60 beams; this requires 3000 shading resistors costing about $300.

The application of the correlation beamformer to this system would use all the staves on the front half of the array for the aperture, thereby reducing the required array diameter to 17 in. However, 90 of the total 180 staves would contribute to each beam, increasing the number of shading resistors to 90x60=5400, costing about $540. No delay lines would be required, nor would additional staves or preamplifiers/filters. Therefore, the cost savings would be $4200-$240=$3960. The array size would be reduced to about 65% of the comparable CT array.

The second system used for comparison is called the VSS HAWAII. The array which is cylindrical and 19.5 in. in diameter, forms forty-five 2° beams covering a 90° sector. There is no requirement for additional sector coverage, so that only 86 staves/preamplifiers/filters are required. The VSS was implemented with 45 delay lines at about $50 each (about $2.25K). Since 42 staves contribute to each of 45 beams, the system uses 1890 shading resistors (about $189).

If a correlation beamformer uses a 180° sector of active elements that are contributing to each beam (an array size of 11.5 in.), and 45 beams are required, the total number of staves/preamplifiers/filters would have to be increased to 126. The VSS uses 86. The increased cost of preamplifiers/filters in the correlation implementation at about

$15 each would be $600. Also, with 84 staves contributing to each of 45 beams, 3780 resistors will be required, which cost more than the VSS implementation by about $190. However, the savings by not using delay lines is $2.25K. Therefore, the correlation beamformer could perhaps be constructed for about $1.46K less than the delay line implementation. Note also that the size is reduced 59%.

This system represents a difficult comparison because of the restricted requirements of sector coverage. If the requirement was to cover 360° with 2° beams, the same number of staves/preamplifiers/filters would exist in both implementations. The differences would then be a saving of $9K in delay lines and a factor of two increase in the number of resistors costing about $756, for a net saving of $8.244K. These cost savings depend almost linearly upon the required azimuthal coverage, with the savings being greatest at full coverage. On the other hand, the delay line method is cheapest if only one beam is formed.

The third comparison concerns the AN/WQS-1. This sonar array is cylindrical with a diameter of 14 in. and contains 54 staves covering approximately 170° on the cylinder. The AN/WQS-1 forms 40 beams each 3° wide covering a 120° azimuthal sector. The system contains 54 preamplfiers costing about $13 each ($702). Only 15 staves contribute to each of 40 beams, requiring 600 resistors ($60) and 40 delay lines at $50 each ($2K). The total cost attributable to the beamforming method is $2.76K.

The correlation method applied to this beam requirement can be accomplished by placing 100 staves over 300° of a cylinder whose diameter can be 5.8 in. compared to 14 in. for the AN/WQS-1. More preamplifiers and resistors, which will be required, will cost $1.54K. This represents a size savings of 41% and a cost savings of 44% ($1.22K).

Another way to compare the methods is to hold the size (14 in.), operating frequency, and cost ($2.76K) constant, and determine what resolution can be achieved over which sector of beam coverage by using the correlation method. The results of such computations show that beamwidths of 1.24° can be achieved on a 14 in. cylinder. Beams may be added to cover a 40° sector (32 beams) before the cost exceeds the $2.76K figure. If 120° coverage is required, then the cost would be $4.548K; for full 360° coverage using 1.24° beams, the cost would be $7.975K.

In summary, the correlation method is generally cheaper to apply and results in a smaller cylindrical array when compared to other methods. Depending primarily upon the sector coverage, the cost savings may be significant or insignificant; however, in all cases tested, the size reduction was nearly 50%.

APPENDIX D

SIGNAL-TO-NOISE RATIO ESTIMATES

APPENDIX D
SIGNAL-TO-NOISE RATIO ESTIMATES

During a progress meeting in April 1975 concerning the comparative advantages of the correlation beamformer versus a phase shift beamformer (delay line implemented), the subject of processing gain or signal to thermal noise ratio arose. A few quick calculations indicated that the S/N of the correlation beamformer would be 6 to 12 dB less than the phase shift implementation.

Upon returning from the meeting, a relatively quick analysis was conducted which was released as a technical letter. Both the cover letter (because it contains the summary) and the technical letter are reproduced here since they represent the total effort on S/N analysis conducted during this study.

Both the correlation method (called Dave's method) and the phase shift beamformer (called Bobby's method) were being compared for application to a specific requirement. The broadside line array, inserted as a standard, did not itself meet the system requirements, but served as a convenient reference.

THE UNIVERSITY OF TEXAS AT AUSTIN
APPLIED RESEARCH LABORATORIES

mailing address:
POST OFFICE BOX 8029
AUSTIN, TEXAS 78712

phone: (512) 836-1351

shipping address:
10000 FM ROAD 1325
AUSTIN, TEXAS 78758

29 April 1975
DAS:kk
Ser E-138

From: David A. Smith
Electroacoustics Division

To: Commanding Officer
Naval Coastal Systems Laboratory
Panama City, FL 32401
Attn: Don Folds (Code 773)

Subj: Report on Signal to Noise Ratio or Processing Gain Against Thermal Noise for Different Beamforming Techniques; Forwarding of

Encl: (1) "Signal to Noise Ratio or Processing Gain Against Thermal Noise for Different Beamforming Techniques," TL-EA-75-2 of 29 April 1975

Our conversation last Thursday concerning the relative performance of Bobby's phase shift beamformer and my replica-correlation beamformer has preyed on me since that time. As I recall, your opinion was that my method would result in Signal to Thermal Noise Performance between 6 and 12 dB poorer than Bobby's phase shift method.

Your argument, simple and elegant as it was, convinced me also, and I found myself agreeing on Friday, "certainly not 12 dB, but perhaps 6 to 4 dB loss!"

I have computed both signal to thermal noise ratios since my return home and find that, in fact, the difference between the two methods is 0.45 dB to my detriment. Enclosure (1) should enable you to come to the same conclusion.

I admit to some haste in this draft; however, several of my crew have checked these figures, and they appear to be in order. I'm sure you can understand my interest in correcting, as soon as possible, the assertion at the Friday meeting that my method was defficient in signal to noise ratio.

By the way, when compared to the broadside line array with equal aperture and equal element weights, it is true that my method (and Bobby's) compare unfavorably; however, the broadside line does not meet the specification. An equivalent line would contain 400 elements, and as shown in Section I of enclosure (1), the reference numbers are:

Signal Gain = 400
Noise Gain = 20
Signal/Noise Processing Gain = 20 ⇒ +26 dB

Section I of enclosure (1) outlines the ground rules and assumptions made in this analysis. It also solves the broadside line reference case for comparison purposes. Section II details the analysis for Bobby's method, and Section III computes the same number for my method. The results are given in the following table. In each case shown, the apertures are equivalent.

	BOBBY	DAVE	REFERENCE BROADSIDE LINE
NUMBER OF ELEMENTS PER BEAM	256	600	400
ARRAY SIGNAL			
Gain	190.92	153.89	400.00
Gain (dB)	+45.62	+43.74	+52.04
ARRAY NOISE			
Gain	12.76	10.83	20.00
Gain (dB)	+22.12	+20.69	+26.02
S/N RATIO			
Number	14.96	14.20	20.00
dB	+23.50	+23.05	+26.02

As you can see, my results indicate that although my method is less sensitive and exhibits less S/N than the reference case of the broadside line (which does not meet specs), both Bobby and I have the same problem. It seems to be the price paid with either method for meeting the required specifications. Please note the insignificant difference between the S/N ratios.

I appreciate your interest and criticism.

David A. Smith

David A. Smith

Copy To:

NCSL 101D (J. C. Anthony)
NCSL 190 (T. Haney)
NCSL 190 (A. Rolle)
NCSL 773 (H. Warner)
NAVSEA 03423 (F. Romano)
G. R. Barnard, ARL/UT
C. L. Wood, ARL/UT
R. H. Stokes, ARL/UT
B. F. Tupa, ARL/UT

bcc: Library, ARL/UT
Kent Mize, ARL/UT
Otto Friedrich, ARL/UT

THE UNIVERSITY OF TEXAS AT AUSTIN
APPLIED RESEARCH LABORATORIES

mailing address:
POST OFFICE BOX 8029
AUSTIN, TEXAS 78712

phone: (512) 836-1351

shipping address:
10000 FM ROAD 1325
AUSTIN, TEXAS 78758

29 April 1975
TL-EA-75-2

SIGNAL TO NOISE RATIO OR PROCESSING GAIN AGAINST THERMAL NOISE FOR DIFFERENT BEAMFORMING TECHNIQUES

David A. Smith

I. ARRAY GAIN
SIGNAL TO THERMAL NOISE RATIO

The purpose of this section is to identify and describe the ground rules for computation and comparison of the Array Signal Gain, the Array Thermal Noise Gain, and the Processor Signal to Thermal Noise Ratio for the two different processors under consideration and a standard broadside line array.

In one case the processor is a phase shift beamformer, which I will call Bobby's method. In the other case, the replica-correlation beamformer, which I will call Dave's method.

I will assume that each element in the array has identical receiving sensitivity and an identical thermal noise source. Further, for the present case I assume omnidirectional element patterns so that each element generates the same peak signal output voltage e_S when insonified with a standard sound field. The thermal noise voltage generated by each element is similarly e_N (an RMS noise).

I also assume that no additional noise is introduced by the processor itself, and that any channel bandwidth factor lowering the noise is assumed to be incorporated in e_N.

Now, the Signal Gain is a number which relates the processor output signal (peak) S to the peak element voltage e_S. It may be stated as either a numerical factor or in dB (20 log).

Enclosure (1) to
ARL ltr Ser E-138
of 29 April 1975

The Thermal Noise Gain is similarly the ratio of beamformer output noise N_o to the element output noise e_N. Both numbers are in RMS volts and are due only to thermal sources in each element.

The Signal to Noise Ratio is the ratio of peak signal to RMS thermal noise at the output of the processor to that ratio produced at the output of each element. That is, it is the processor's signal to noise ratio gain or Processing Gain against thermal noise.

In both processors, there exist a set of shading coefficients A_i which are used to scale the element output before summing or before phase shifting and summing.

Now, in general, the SIGNALS combine coherently; that is, we know the phase of each element's signal. Let the $i^{\underline{th}}$ element deliver $e_i(t)$ volts where $e_i(t)$ is the instantaneous output voltage when the peak is e_S. Long duration, co-sinusoidal signals are assumed so that

$$e_i(t) = e_S \cos[\varphi(t,i)] \tag{1-1}$$

If each element voltage $e_i(t)$ is scaled by A_i (the shading coefficient) and then summed over the M contributing elements, we have the processor output signal S. That is,

$$S = \sum_{i=1}^{M} A_i e_i(t). \tag{1-2}$$

In Bobby's case, the A_i contain phase shifts which correct for the elements position in the array. In Dave's case, the A_i are real numbers that represent the signal replica. These separate analyses appear in Sections II and III.

The Thermal Noise sources, each generating e_N (RMS volts), are combined in a Root Mean Square sense after scaling by A_i, because the individual phases are unknown and random. Therefore, the processor output noise N_o is

$$N_o = \left[\sum_{i=1}^{M} (A_i e_N)^2 \right]^{1/2} \qquad (1\text{-}3)$$

Again, separate analysis of the two methods appear in Sections II and III.

The element output signal to noise ratio or processor input signal to noise ratio is $\frac{e_S}{e_N}$. The processor output signal to noise is $\frac{S}{N_o}$. The Processing Gain is therefore $\frac{S}{e_S} \frac{e_N}{N_o}$

An Example

The standard reference case is the broadside line of M equal spaced elements of equal strength. Such a line would exhibit a farfield beam pattern like $\frac{\sin x}{x}$.

From Eq. 1-2, the signal is

$$S = \sum_{i=1}^{M} A_i e_i(t) \qquad (1\text{-}4)$$

For the broadside line with target in the farfield, all elements receive the same signal, and if t is selected so that the peak signal is measured, and equal strength shading means $A_i = 1$ for all i, we have

$$S = \sum_{i=1}^{M} 1 \; e_S \qquad (1\text{-}5)$$

or

$$\frac{S}{e_S} = \sum_{i=1}^{M} 1 = M \qquad (1\text{-}6)$$

From Eq. 1-3, the noise is

$$N_o = \left[\sum_{i=1}^{M} (A_i e_N)^2 \right]^{1/2} \tag{1-7}$$

Again $A_i = 1$, so that

$$N_o^2 = \sum_{i=1}^{M} 1\, e_N^2 = e_N^2 M \tag{1-8}$$

or $$\frac{N_o}{e_N} = \sqrt{M} \quad . \tag{1-9}$$

The Processing Gain against thermal noise, for this reference case, is therefore

$$\frac{S}{e_S} \frac{e_N}{N_o} = \frac{M}{\sqrt{M}} = \sqrt{M} \tag{1-10}$$

II. BOBBY'S METHOD

The Phase-Shift Processor

From Section I, Eq. 1-2, we have that the processor output signal S is

$$S = \sum_{i=1}^{M} A_i^* \, e_i(t) \tag{2-1}$$

where the A_i^* contains the phase shift information. Since from Eq. 1-1, $e_i(t) = e_S \cos [\varphi(t,i)]$,

$$S = \sum_{i=1}^{M} A_i^* \, e_S \cos [\varphi(t,i)] \tag{2-2}$$

But the complex part of A_i^* is designed to be just enough to bring each element output voltage in phase, so that

$$S = \sum_{i=1}^{M} A_i \, e_S \cos (\varphi(t)) \tag{2-3}$$

(where the A_1 are now real numbers), and if t is chosen to be the time of $\cos (\varphi(t)) = 1$, then we have

$$S = \sum_{i=1}^{M} A_i \, e_S \tag{2-4}$$

$$S = e_S \sum_{i=1}^{M} A_i \tag{2-5}$$

or $$\frac{S}{e_S} = \sum_{i=1}^{M} A_i \quad . \tag{2-6}$$

Now for the noise term from Eq. 1-3 we have

$$N_o = \left[\sum_{i=1}^{M} (A_i e_N)^2 \right]^{1/2} \tag{2-7}$$

The real part of A_i is retained and the phase shift dropped since the noise is still random with unknown phase. Equation 2-7 can be simplied so that

$$\frac{N_o^2}{e_N^2} = \sum_{i=1}^{M} A_i^2 \tag{2-8}$$

or $$\frac{N_o}{e_N} = \sqrt{\sum_{i=1}^{M} A_i^2} \tag{2-9}$$

Equations 2-6 and 2-9 show how the processing gain of the method depends only upon the values of the A_i.

Data Analysis

The values of Bobby's shading coefficients are functionally very complicated, and have been computed and the output listed on the CDC 3200 computer. The data extracted are noted "best" as of 26 April 1975. Table 2-1 indicates the heading information, and Table 2-2 lists the real part of the shading coefficients. One-half are listed, since the array is even symmetric.

TABLE 2-1

HEADING INFORMATION FOR "BEST" COEFFICIENTS

Number of Elements	256
Frequency	300 kHz
Array Radius	36 inches
Stave Height	1 in.
Stave Width	0.150 in.
Stave Spacing	0.010 in.
Total Angular Width	64.94 deg.
Velocity of Sound	58,267.6 in/sec

TABLE 2-2

BEST ALS COEFFICIENT AS OF 26 APRIL 75

1	2	3	4	5	
.99998	.99998	.99957	.99916	.99875	5
.99793	.99711	.99630	.99507	.99385	10
.99262	.99100	.98937	.98774	.98572	15
.98369	.98166	.97925	.97683	.97441	20
.97161	.96880	.96600	.96282	.95964	25
.95646	.95291	.94936	.94581	.94190	30
.93800	.93409	.92984	.92559	.92134	35
.91675	.91217	.90759	.90268	.89778	40
.89287	.88766	.88245	.87724	.87174	45
.86625	.86075	.85497	.84920	.84342	50
.83739	.83136	.82532	.81905	.81278	55
.80650	.80000	.79351	.78701.	.78031	60
.77360	.76690	.76001	.75312	.74623	65
.73917	.73211	.72505	.71784	.71063	70
.70343	.69609	.68875	.68141	.67396	75
.66651	.65906	.65152	.64398	.63644	80
.62882	.62121	.61360	.60593	.59826	85
.59060	.58289	.57519	.56749	.55978	90
.55206	.54434	.53663	.52892	.52120	95
.51351	.50582	.49812	.49047	.48281	100
.47516	.46756	.45996	.45236	.44484	105
.43731	.42979	.42235	.41491	.40747	110
.40014	.39280	.38547	.37825	.37103	115
.36381	.35673	.34965	.34256	.33562	120
.32868	.32174	.31496	.30817	.30139	125
1.01625	1.73111	2.44598			128

A program was written for the HP-65, the purpose of which was to calculate the values represented in Eq. 2-6 for $\frac{S}{e_S}$, and Eq. 2-9 squared for the value $\left(\frac{N_o}{e_N}\right)^2$.

The results of the computation with the special program was:

$$\frac{S}{e_S} = 95.46042 \tag{2-10}$$

$$\left(\frac{N_o}{e_N}\right)^2 = 81.40017 \tag{2-11}$$

$$M = 128 \tag{2-12}$$

Because 256 elements will be used and the array is even symmetric, the values were multiplied by 2 and the square root of $\left(\frac{N_o}{e_N}\right)^2$ was obtained.

$$\frac{S}{e_S} = 190.92 \tag{2-13}$$

$$\frac{N_o}{e_N} = 12.76 \tag{2-14}$$

$$M = 256 \tag{2-15}$$

In order to check the computations, a standard program for the HP-65 was used (Mean, Standard Deviation, Standard Error - STD-02A). Equation 2-6 can be rewritten in terms of the average $A_i = \bar{A}$ as

$$\frac{S}{e_S} = M\bar{A} \; . \tag{2-16}$$

Further, Eq. 2-9 can be recast in terms of the average $A_i = \bar{A}$ and the standard deviation of $A_i = \sigma_{\bar{A}}$ as follows:

$$\frac{N_o}{e_N} = \sqrt{\sigma_{\bar{A}}^2 (M-1) + M \bar{A}^2} \qquad (2\text{-}17)$$

Thus by computing $\bar{A}$ and $\sigma_{\bar{A}}$, one can evaluate $\frac{S}{e_S}$ and $\frac{N_o}{e_N}$.

The values resulting from this check computation are as follows:

$$\bar{A} = 0.74578 \qquad (2\text{-}18)$$

$$\sigma_{\bar{A}} = 0.28350 \qquad (2\text{-}19)$$

$$M = 256 \qquad (2\text{-}20)$$

Therefore, from Eq. 2-16, we have

$$\frac{S}{e_S} = M\bar{A} = 190.92 \ , \qquad (2\text{-}21)$$

and by Eq. 2-17, we have

$$\frac{N_o}{e_N} = 12.76 \ . \qquad (2\text{-}22)$$

These values will be seen to agree with the previous results.

In summary, I present

Array Signal Gain (Bobby's Method)

$$\frac{S}{e_S} = 190.92 \Rightarrow +45.62 \text{ dB} \qquad (2\text{-}23)$$

Array Noise Gain (Bobby's Method)

$$\frac{N_o}{e_N} = 12.76 \Rightarrow +22.12 \text{ dB} \qquad (2\text{-}24)$$

Processing Gain (Bobby's Method)

$$\frac{S}{e_S}\frac{e_N}{N_o} = 14.96 \Rightarrow +23.50 \text{ dB} \qquad (2\text{-}25)$$

III. DAVE'S METHOD

The Replica-Correlator Processor

From Section I, Eq. 1-2, we have that the processor output signal S is

$$S = \sum_{i=1}^{M} A_i e_i(t) \tag{3-1}$$

where the A_i are real numbers and no phase shift is implied. Since from Eq. 1-1,

$$e_i(t) = e_S \cos [\varphi(t,i)], \tag{3-2}$$

the value of S becomes

$$S = \sum_{i=1}^{M} A_i e_S \cos [\varphi(t,i)]. \tag{3-3}$$

Now, in Dave's Method, the A_i can be written as

$$A_i = \cos [2\pi R(1-\cos \alpha_i)] \cos^2 \alpha_i \tag{3-4}$$

where R is the array radius in wave lengths and α_i is the pointing angle to the $i^{\underline{th}}$ element. If the elements are spaced Q wavelengths apart on the cylinder,

$$\alpha_i = \frac{iQ}{R}.$$

So

$$A_i = \cos \left[2\pi R\left(1-\cos\left(\frac{iQ}{R}\right)\right)\right] \cos^2\left(\frac{iQ}{R}\right) \tag{3-5}$$

Now the signal $e_S \cos(\varphi(i,t))$ is of the same form as part of the A_i; that is, if t is selected so that

$$e_S \cos\left[\varphi(i=0, t=t_o)\right] = e_S \tag{3-6}$$

then the signal at the $i^{\underline{th}}$ element is

$$e_i = e_S \cos\left[2\pi R\left(1-\cos\left(\frac{iQ}{R}\right)\right)\right] \tag{3-7}$$

If we substitute Eqs. 3-5 and 3-7 into Eq. 3-3, we have that

$$S = \sum_{i=1}^{M} e_S \cos^2\left[2\pi R\left(1-\cos\left(\frac{iQ}{R}\right)\right)\right]\cos^2\left(\frac{iQ}{R}\right). \tag{3-8}$$

Let

$$Al_i = \cos\left[2\pi R\left(1-\cos\left(\frac{iQ}{R}\right)\right)\right] \tag{3-9}$$

and

$$A2_i = \cos\left(\frac{iQ}{R}\right), \tag{3-10}$$

and rewrite Eq. 3-8 as

$$\frac{S}{e_S} = \sum_{i=1}^{M} (Al_i A2_i)^2 \tag{3-11}$$

Now for the noise factor, from Eq. 1-3 we have

$$N_o = \left[\sum_{i=1}^{M} (A_i e_N)^2\right]^{1/2} \tag{3-12}$$

or

$$\left(\frac{N_o}{e_N}\right)^2 = \sum_{i-1}^{M} A_i^2 \tag{3-13}$$

But from Eqs. 3-4 and 3-9, 3-10 we have

$$\left(\frac{N_o}{e_N}\right)^2 = \sum_{i=1}^{M} (A1_i A2_i^2)^2 \quad . \tag{3-14}$$

Data Analysis

Since simple functional forms exist for $A1_i$ and $A2_i$, a FOCAL program was written for the PDP-8 to evaluate Eq. 3-11 and the square root of Eq. 3-14. The program listing is presented in Table 3-1.

For the case of 601 elements spaced 0.5236 λ apart on 180°of a 100 λ radius cylinderical array, the results are as follows:

Array Signal Gain (Dave's Method)

$$\frac{S}{e_S} = 153.89 \Rightarrow +43.74 \text{ dB}$$

Array Noise Gain (Dave's Method)

$$\frac{N_o}{e_N} = 10.83 \Rightarrow +20.69 \text{ dB}$$

Processing Gain (Dave's Method)

$$\frac{S}{e_S}\frac{e_N}{N_o} = 14.21 \Rightarrow +23.05 \text{ dB}$$

AD-A033 113 TEXAS UNIV AT AUSTIN APPLIED RESEARCH LABS F/G 17/1
THE CORRELATION BEAMFORMER -- A METHOD OF BEAM CONTROL WITHOUT --ETC(U)
OCT 76 D A SMITH N61339-74-C-0031
UNCLASSIFIED ARL-TR-76-2-REV NL

3 OF 3
AD A033113

END
DATE FILMED
2-77

TABLE 3-1

```
C-FOCAL, 1971

01.05 C ADDISON SIG. & NOISE FACTORS
01.10 S P=3.14159
01.40 A R,N,S,!!!
01.70 S Y=2*P*R

02.10 S SG=0;S NO=0
02.30 F I=-N,N;S X=I*S/R;D 3;D 4
02.40 S NS=FSQT(NO)
02.50 S SN=SG/NS
02.60 T 2*N+1,SG,NS,SN,!!!;Q

03.10 S A1=FCOS(Y*(1-FCOS(X)))
03.20 S A2=FCOS(X)

04.10 S SG=SG+A1*A1*A2*A2
04.20 S NO=NO+(A1*A2*A2)↑2
*
```

INPUTS WERE R=100 N=300 (M IN TEXT = 2N+1) ELEMENT SPACING S(Q IN TEXT) = 0.5236.

REFERENCES

1. Walter Welkowitz, "Directional Circular Arrays of Point Sources," J. Acoust. Soc. Am. 28, 362-366 (1956).

2. T. T. Taylor, "Design of Line-Source Antennas for Narrow Beamwidth and Low Side Lobes," IRE Trans. on Antennas and Propagation, pp. 16-28, January 1955.

3. C. L. Dolph, "A Current Distribution for Broadside Arrays Which Optimizes the Relationship Between Beam Width and Side-Lobe Level," Proc. of the IRE on Waves and Electrons, pp. 335-348, June 1946.

4. R. C. Spencer, "Fourier Integral Methods of Pattern Analysis," Report 762-1, Radiation Laboratory, Massachusetts Institute of Technology, Cambridge, Massachusetts (January 1946).

5. Henry J. Bickel, "Real-Time Spectrum Analysis," J. Sound and Vib., 14-20 (March 1971).

6. C. L. Temes, "Sidelobe Suppression in a Range-Channel Pulse-Compression Radar," IRE Trans. on Military Electronics, pp. 162-169, April 1962.

7. D. G. Tucker and B. K. Gazey, Applied Underwater Acoustics (Pergamon Press, New York, 1966), Chapter 6.

8. Bernard D. Steinberg, "Comparison Between the Peak Sidelobe of the Random Array and Algorithmically Designed Aperiodic Arrays," IEEE Trans. on Antennas and Propagation, pp. 366-370, May 1973.

9. Michael Kump, David A. Smith, and Robert M. Adams, "Multiple Factor Selection Technique for Ceramic Transducer Elements," Applied Research Laboratories Technical Report No. 75-68 (ARL-TR-75-68), Applied Research Laboratories, The University of Texas at Austin, Austin, Texas (6 January 1976).

10. Bruce O. Moses and David A. Smith, "Acoustic Receive Beamforming Experiments Using a Cylindrical Array with Real Shading Coefficients," Applied Research Laboratories Technical Report No. 74-56 (ARL-TR-74-56), Applied Research Laboratories, The University of Texas at Austin, Austin, Texas (19 December 1974).

October 1976

DISTRIBUTION LIST FOR
ARL-TR-76-2 (Revised)
FINAL REPORT UNDER CONTRACT N61339-74-C-0031, Task 0003
29 November 1973 - 31 December 1975
UNCLASSIFIED

Copy No.

Commanding Officer
Naval Coastal Systems Laboratory
Department of the Navy
Panama City, FL 32401

1 - 3 Attn: Code 112.2
4 - 13 Code 112.6
14 A. L. Rolle
15 J. L. Bealor
16 Don Folds

Commander
Naval Sea Systems Command
Department of the Navy
Washington, DC 20362

17 Attn: C. E. Fox
18 R. Smith, Code 663CB
19 C. D. Smith, Code 06H1
20 W. L. Thompson
21 A. Breece, Code 661C-12
22 R. Snuggs, Code 660F-5
23 M. T. Giwer, Code 660E-23
24 V. Graves, Code 06H4-3
25 W. Brandon, Code 06H4-42
26 LCDR D. F. Bolka, Code 06H2
27 J. E. Neely, Code 06H1-1
28 M. C. Hansen, Code 06HB
29 E. J. McKinney, Code 0342
30 F. J. Romano, Code 03423
31 B. Welch, Code 03424
32 Roy Heaney, Code 661T
33 D. H. Bennet, Code PMS-406B

Commander
Naval Undersea Center
Department of the Navy
San Diego, CA 92132

34 Attn: J. R. Reardon, Code NUC-35601
35 H. W. Volberg
36 R. A. McLennan, Code NUC 256
37 D. L. Carson, NUC-302
38 Mike Kolar, NUC 6512

Distribution List for ARL-TR-76-2 (Cont'd)

Copy No.

Officer-in-Charge
New London Laboratory
Naval Underwater Systems Center
Department of the Navy
New London, CT 06320
39 Attn: H. Newman
40 W. R. Schumacher
41 W. Konrad

Commanding Officer
Newport Laboratory
Naval Underwater Systems Center
Department of the Navy
Newport, RI 02840
42 Attn: T. M. Fitzgerald

Director
Naval Research Laboratory
Department of the Navy
Washington, DC 20375
43 Attn: John Munson
44 L. Van Buren

Commanding Officer
Naval Surface Weapons Center
White Oak Laboratory
Department of the Navy
Silver Spring, MD 20910
45 Attn: Bill Rust
46 Joe Mobley

Commanding Officer
Naval Facilities Engineering Command
Department of the Navy
200 Stovall Street
Alexandria, VA 22332
47 Attn: P. Cave, Code NAVFAC-032C

Commanding Officer
Naval Air Systems Command
Department of the Navy
Washington, DC 20361
48 Attn: L. E. Wheat, NAVAIR-5305A

Distribution List for ARL-TR-76-2 (Revised) (Cont'd)

Copy No.

49 Office of the Chief of Naval Material
Department of the Navy
Washington, DC 20360
Attn: CDR R. K. Hastie, NAVMAT 0314

50 Superintendent
Naval Postgraduate School
Monterey, CA 93940
Attn: Librarian (Code 2124)

51 Commanding Officer
Naval Electronic Systems Command
Department of the Navy
Washington, DC 20362
Attn: W. Kamminga, NAVELEX-3203

52 Commander
Naval Ship Engineering Center
Department of the Navy
Center Building, Prince George's Center
Hyattsville, MD 20782
Attn: F. Hill, NAVSEC 6126

Chief of Naval Research
Department of the Navy
Arlington, VA 22217
53 Attn: R. Obrochta, Code ONR-222
54 M. Blizard, ONR-212

55 Commanding Officer
Naval Air Development Center
Department of the Navy
Warminster, PA 18974
Attn: Bill Parigian

56 Naval Research Laboratory
Underwater Sound Reference Division
P.O. Box 8337
Orlando, FL 32806
Attn: Joe Blue

Distribution List for ARL-TR-76-2 (Rev.) (Cont'd)

Copy No.

57 Catholic University
Electrical Engineering Department
620 Michigan Avenue, NE
Washington, DC 20017
Attn: Dr. H. F. Harmuth

58 Defense Advanced Research Projects Agency
Tactical Technology Office
1400 Wilson Blvd.
Arlington, VA 22209
Attn: CAPT H. Cox

59 - 70 Commanding Officer and Director
Defense Services Administration
Defense Documentation Center
Cameron Station, Building 5
5010 Duke Street
Alexandria, VA 22314

71 Office of Naval Research
Resident Representative
Room No. 582, Federal Building
Austin, TX 78701

72 Electroacoustics Group, ARL/UT

73 Electroacoustics Division I, ARL/UT

74 Computer and Marine Sciences Group, ARL/UT

75 Signal Physics Division, ARL/UT

76 Sonar Research Group, ARL/UT

77 Sonar Research Division III, ARL/UT

78 Sonar Engineering Group, ARL/UT

79 Sonar Engineering Division I, ARL/UT

80 Sonar Engineering Division II, ARL/UT

81 Sonar Development Division, ARL/UT

82 Underwater Systems Division, ARL/UT

Distribution List for ARL-TR-76-2 (Revised) (Cont'd)

Copy No.	
83	Garland R. Barnard, ARL/UT
84	Loyd D. Hampton, ARL/UT
85	Kent M. Mize, ARL/UT
86	Bruce O. Moses, ARL/UT
87	C. Richard Reeves, ARL/UT
88	Jack A. Shooter, ARL/UT
89	David A. Smith, ARL/UT
90	Reuben H. Wallace, ARL/UT
91	Library, ARL/UT
92-100	Reserve, ARL/UT